UNIVERSITY OF CALIFORNIA SAN DIEGO

Fracture and adhesion of liquid crystal elastomers

A Dissertation submitted in partial satisfaction of the requirements
for the degree Doctor of Philosophy

in

Materials Science and Engineering

by

Raja Annapooranan

Committee in charge:

Professor Shengqiang Cai, Chair
Professor Jinhye Bae
Professor Nicholas Boechler
Professor Darren Lipomi

2024

The Dissertation of Raja Annapooranan is approved, and it is acceptable in quality and form for publication on microfilm and electronically.

University of California San Diego

2024

TABLE OF CONTENTS

LIST OF FIGURES

ACKNOWLEDGEMENTS

First and foremost, I would like to thank Professor Shengqiang Cai for his support as my PhD advisor over the last six years. His extensive knowledge and his kind mentoring helped me develop a passion for learning new things and solving challenging problems. He gave me a lot of freedom and encouragement to explore problems that I felt passionate about and was patient with me when I made mistakes. I feel very lucky and privileged to have worked with him.

Secondly, I would like to thank my committee members, Professor Jinhye Bae, Professor Nicholas Boechler and Professor Darren Lipomi for their valuable suggestions to my research projects and advice on the academic journey.

Thirdly, I would like to thank the previous and current members of my lab group, Dr. Chihyung Ahn, Dr. Xudong Liang, Dr. Somaye Jafari, Dr. Qiguang He, Dr. Zhijian Wang, Dr. Yue Zheng, Dr. Zhaoqiang Song, Dr. Yang Wang, Dr. Zijun Wang, Dr. Nada F. Qari, Gaoweiang Dong, Chenghai Li, Robert J. Chambers, Ram Hemanth Yeerella, Fangchen Zhao, Devyansh Agarwal and Sunil Suresh Jeyakumar. The group members made sure that the lab was a fun and pleasant place to work, taught each other new things and contributed to brainstorming new ideas. I hope the future lab members will carry forward this team spirit.

Finally, I would like to thank my girlfriend (Krithika), my parents (Dr. S. Annapooranan and. N. Meenatchi), my sister (A. Siva Sankari), my family members and my friends. Their constant support and love pushed me through all the challenges I faced. Finishing this PhD would have been impossible without them.

I would like to extend my gratitude to John, Anthony, Flea and Chad for their music that uplifted my spirits and helped me push through several unsuccessful polymer chemistry experiments. I am also very thankful for my pet dog Alfie for being a constant source of happiness.

Chapter 2, in full, is a reprint of the material as it appears in Annapooranan, R.; Cai, S. Thermally Induced Self-Rupture of a Constrained Liquid Crystal Elastomer. *Engineering Fracture Mechanics* **2022**, *269*, 108584. The dissertation author was the primary investigator and first author of this paper.

Chapter 3, in full, is a reprint of the material as it appears in Annapooranan, R.; Wang, Y.; Cai, S. Highly Durable and Tough Liquid Crystal Elastomers. *ACS Applied Materials & Interfaces* **2022**, *14* (1), 2006–2014. The dissertation author was the primary investigator and first author of this paper.

Chapter 4, in full, is a reprint of the material as it appears in Annapooranan, R.; Suresh Jeyakumar, S.; J. Chambers, R.; Long, R.; Cai, S. Ultra Rate-Dependent Pressure Sensitive Adhesives Enabled by Soft Elasticity of Liquid Crystal Elastomers. *Advanced Functional Materials* **2024**, *34* (1), 2309123. The dissertation author was the primary investigator and first author of this paper.

Chapter 5, in part is currently being prepared for submission for publication of the material. Annapooranan, R.; Yeerella, R.H.; Chambers, R. J.; Li, C.; Cai, S.; Enhanced adhesion of liquid crystal elastomers on rough surfaces. The dissertation author was the primary researcher and author of this material.

VITA

2017 Bachelor of Engineering in Materials Science and Engineering, Anna University, Chennai, India

2019 Master of Science in Materials Science and Engineering, University of California San Diego

2024 Doctor of Philosophy in Materials Science and Engineering, University of California San Diego

PUBLICATIONS

1. **Annapooranan, R**.; Suresh Jeyakumar, S.; J. Chambers, R.; Long, R.; Cai, S. Ultra Rate-Dependent Pressure Sensitive Adhesives Enabled by Soft Elasticity of Liquid Crystal Elastomers. *Advanced Functional Materials* **2024**, *34* (1), 2309123.
2. **Annapooranan, R**.; Wang, Y.; Cai, S. Harnessing Soft Elasticity of Liquid Crystal Elastomers to Achieve Low Voltage Driven Actuation. *Advanced Materials Technologies* **2023**, 2201969.
3. **Annapooranan, R.**; Cai, S. Thermally Induced Self-Rupture of a Constrained Liquid Crystal Elastomer. *Engineering Fracture Mechanics* **2022**, *269*, 108584.
4. **Annapooranan, R**.; Wang, Y.; Cai, S. Highly Durable and Tough Liquid Crystal Elastomers. *ACS Applied Materials & Interfaces* **2022**, *14* (1), 2006–2014.
5. Wang, Z.; Dong, Y.; **Annapooranan, R**.; Li, C.; Chambers, R.; Cai, S. PVC Gel-Based Electro-Adhesion on Extremely Rough Surfaces. *Applied Materials Today* **2024**, *38*, 102189.
6. Herard, N.; Wang, Z.; **Annapooranan, R**.; Qian, K.; Chiu, P.-H.; Lawrence, B. D.; Nataraj, L.; Henry, T.; Cai, S.; Boechler, N. Push, Snap, Pull, and Buckle: A Material Design Framework Enabled by Cooperating Active and Geometrically Nonlinear Passive Microstructures. *Materials & Design* **2023**, *236*, 112432.

7. Li, C.; He, Q.; Wang, Y.; Wang, Z.; Wang, Z.; **Annapooranan, R**.; Latz, M. I.; Cai, S. Highly Robust and Soft Biohybrid Mechanoluminescence for Optical Signaling and Illumination. *Nature Communications* **2022**, *13* (1), 3914.
8. Q. He, Z. Wang, Y. Wang, Z. Wang, C. Li, **Annapooranan. R**, J. Zeng, R. Chen, S. Cai. Electrospun Liquid Crystal Elastomer Microfiber Actuator. *Science Robotics* **2021**, *6* (57), eabi9704.
9. Elumalai, V.; Rathinavel, S.; **Annapooranan, R**.; Ganapathikrishnan, M.; Sangeetha, D. Phosphonated Mesoporous Silica Based Composite Membranes for High Temperature Proton Exchange Membrane Fuel Cells. *Journal of Solid State Electrochemistry* **2019**, *23* (6).
10. Elumalai, V.; **Annapooranan, R**.; Ganapathikrishnan, M.; Sangeetha, D. A Synthesis Study of Phosphonated PSEBS for High Temperature Proton Exchange Membrane Fuel Cells. *Journal of Applied Polymer Science* **2018**, *135* (10), 45954.

ABSTRACT OF THE DISSERTATION

Fracture and adhesion of liquid crystal elastomers

by

Raja Annapooranan

Doctor of Philosophy in Materials Science and Engineering

University of California San Diego, 2024

Professor Shengqiang Cai, Chair

Elastomeric materials, characterized by their elasticity and energy dissipation capabilities, are crucial in everyday life. Over the years, the development of elastomers with novel properties is driven by the growing demand for materials that can meet the increasingly complex and specific requirements in automotive, aerospace, medical, structural and industrial applications and enable new applications such as soft robotics and flexible electronics. Liquid crystal elastomer is one such material system that combines liquid crystals with rubbery polymers, which gave rise to several unique properties such as anisotropic elasticity, stimuli responsiveness and actuation, energy

dissipation, photoelasticity and reversible adhesion. Since materials need to withstand multiple cycles of mechanical loading and exposure to thermal fields in real world applications, it is important to understand the rate and temperature dependent properties of liquid crystal elastomers, which will result in the development of robust materials and reliable engineering structures.

In this dissertation, we first explore the rate and temperature dependent fracture properties of liquid crystal elastomers and develop predictions of the temperature of self-rupture for various geometries. Secondly, we develop an interpenetrating network strategy to improve the high temperature fracture and fatigue properties of liquid crystal elastomers, while preserving their actuation properties. Then, we develop a pressure sensitive adhesive using liquid crystal elastomers and explore the ultra-high rate dependence of adhesion energy. Finally, we study the enhanced adhesion of liquid crystal elastomers on various rough surfaces. We hope that the understanding of the fracture and adhesive properties of liquid crystal elastomers and the strategies developed to further improve these properties using materials chemistry will translate to real world in solving critical challenges in medical technology, robotics, automotive, aerospace and industrial applications

Chapter 1 Introduction

1.1 Background

Elastomers are polymer materials commonly known for their elasticity, are comprised of long crosslinked molecules, which are generated by the polymerization of smaller molecules or repeating units called monomers. These long molecules by themselves form a viscous liquid which on crosslinking or curing form a three-dimensional network structure[1]. Under zero external stress, these thermally fluctuating chains possess a random coil configuration with high entropy. On applying an external stress, the chains become more aligned which causes a reduction in entropy. Following the laws of thermodynamics, the entropy of an isolated system always increases. Therefore, an entropic restoring force provides the origin for the elasticity or the tendency of elastomers to return to their original shape. The combination of entropic elasticity and the long polymer molecules with intermolecular friction or viscosity, gives rise to the viscoelastic properties of elastomers that are dependent on temperature and time. [2]

There are archeological evidences for the use of natural rubber in Latin America dating back to 1600 BC.[3] Today, elastomers are ubiquitous in everyday life with applications such as automobile tires, seals, gaskets, medical devices, vibration dampers, conveyor belts, consumer goods, adhesives and so on. Therefore, the understanding the physical properties of elastomers can improve the durability of existing materials and lead to the development of elastomers with novel properties, which in turn can pave way for new applications such as soft robotics, artificial muscles, flexible electronics, bio-compatible implants, energy harvesting etc [4].

1.2 Liquid crystal elastomers

Liquid crystals are rod like molecules which can flow like a liquid but also exhibit some orientational alignment like a crystalline solid. Liquid crystals are known for their anisotropic or direction dependent properties and are widely used in display technologies. Liquid crystal elastomers (LCE) are synthesized by combining liquid crystal molecules into an elastomeric polymer network.[5] This combination endows LCE with unique properties such as anisotropic elasticity, shape memory, birefringence, photoelasticity and so on, out of which thermomechanical actuation and energy dissipation have generated great interest in the recent times. [6]

An actuator is a device that converts input signal, in the form of energy, into output work, in the form of force and displacement. There is a great demand for novel actuators in medical devices, robotics and wearable devices, that are lightweight, versatile and safe for human interaction.[4] The traditional types of actuators including hydraulic, pneumatic, electromagnetic etc, can be bulky, hard to miniaturize and might not be safe. On the other hand, soft actuators consisting of polymer materials, are compliant like the human muscle and can respond to various external stimuli such as heat, light, electric and magnetic fields[7]. Liquid crystal elastomer is a leading candidate of soft actuators, owing to the large reversible actuation, work capacity, specific power and programmable deformation under heating and cooling cycles[8]. Heating LCE changes it from an anisotropic nematic state to an isotropic state, which results in reversible actuation. In real world applications, liquid crystal elastomers will be subjected to cyclic loads and heating-cooling cycles as a thermomechanical actuator. Under static and cyclic loading of elastomers, the presence of any small defects or cracks can lead to decreased performance over time or even result in

catastrophic failure. Therefore, it is important to understand the temperature dependent fracture properties of liquid crystal elastomers, for designing robust soft actuators for various applications.

Due to their viscoelastic properties, elastomers are used in vibration attenuation, noise reduction, impact absorption and seismic dampers for buildings[9,10]. When elastomers are subjected to loading, they can dissipate a fraction of the input mechanical energy due to friction between the polymer chains[11]. The viscoelastic energy dissipation is frequency and temperature dependent, therefore the elastomers must be carefully designed based on the application criterion. One widely used technique to improve the damping abilities of elastomers, is to add fillers like silica and carbon black, which further enhance chain friction. But the addition of fillers can lead to other properties such as increased stiffness and processing difficulties which might not be suitable for some applications[12]. Therefore, various combinations of materials and structural designs are constantly being explored for damping. Elastomeric adhesives, also rely on energy dissipation for providing robust adhesion between two substrates. [13]

Liquid crystal elastomers have shown excellent energy dissipation under mechanical loading, for a wide range of temperature and frequencies[14,15]. The enhanced dissipative properties arise from the viscosity due to rotation of liquid crystal mesogens in addition to the polymer chain friction, which manifests as a large hysteresis area in the stress-strain curve. Over the past few years, various studies have explored the benefits of using liquid crystal elastomers for damping and vibration attenuation[16,17]. Due to compatibility with 3D printing, various structures have been fabricated using LCEs to further enhance the dissipative capabilities[18]. Since the dissipative properties of LCE are dependent on temperature, heating up LCE above the nematic transition temperature can change it into an isotropic elastomer with lower dissipation[19]. In the context of

adhesion, this large change in viscous dissipation has been recently harnessed to develop switchable adhesives triggered by temperature and light[20,21].

1.3 Dissertation structure

The objective of my dissertation is to understand the fracture and adhesive properties of liquid crystal elastomers and use materials chemistry to further enhance these properties. This dissertation is organized as follows :

Chapter 1 introduces the background of elastomeric materials and an overview of liquid crystal elastomers. In Chapter 2, we probe the rate and temperature dependent fracture properties of LCE and make predictions for the temperature of self-rupture of LCE. In Chapter 3, we describe an interpenetrating network strategy, to improve the high temperature fracture and fatigue properties of LCE. In Chapter 4, we study the adhesives developed using liquid crystal elastomers that show an anomalously high-rate dependence. In Chapter 5, we study the adhesion of liquid crystal elastomers on very rough surfaces. Chapter 6 summaries the dissertation and provides outlooks for future works.

Chapter 2 Thermally induced self-rupture of a constrained liquid crystal elastomer

2.1 Introduction

Inspired by the compliance and resilience of animal muscles, there has been a substantial surge in the development of various soft actuators recently [22–26]. Liquid crystal elastomer (LCE) is one such soft actuating material with several fascinating properties. LCEs can be reversibly actuated by different stimuli like heat and light, exhibit large actuation strains and work density [6,27] , can be 3D printed into complex geometries [28,29] and in some cases are re-processible and reprogrammable [30–32]. These promising advancements endow LCE with great potential in applications such as artificial muscles, soft robots, biomedical and biomimetic devices [33–37].

In LCEs, rod-shaped liquid crystal mesogens are covalently bonded to polymer chains, resulting in a crosslinked elastomeric network, while preserving some of the liquid crystalline properties. Using the two-step method [38–41], a crosslinked LCE with the mesogens aligned uniformly along a direction can be obtained, which is also defined as a "monodomain LCE". The thermally driven actuation of a LCE is due to the nematic to isotropic transition, where the polymer chains transform from an anisotropic to an isotropic conformation on heating [42,43].

When used as a thermally driven soft actuating material, LCEs are subjected to various mechanical loads and heating, to generate work. A free-standing LCE sample can contract on heating, but in the applications, the LCE actuators are often subjected to a mechanical load, or the deformation is nearly constrained with large actuation stress being generated by the LCE sample. As a result, the LCE often ruptures by its own actuation stress (as shown in Figure 2.1) or the external load. Therefore, understanding and predicting the fracture behavior of LCEs at different temperatures is critical for their applications.

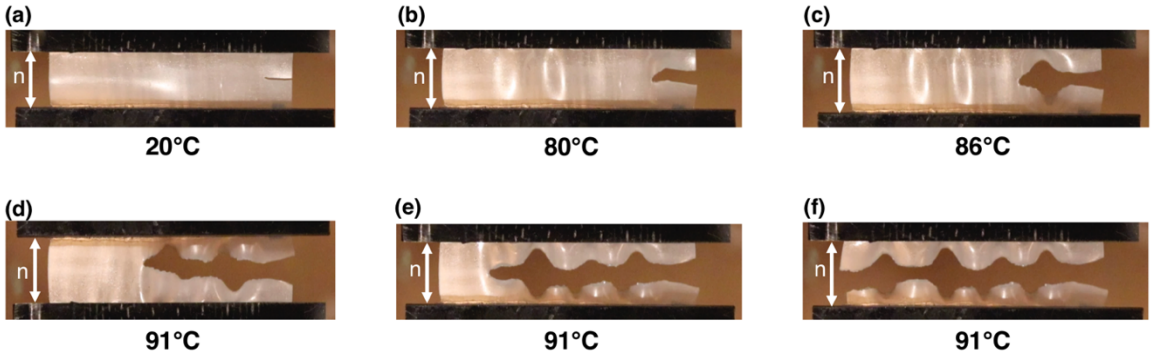

Figure 2.1 : Photographs of the thermally induced self-rupture of a monodomain liquid crystal elastomer sample with a precut. The displacement of the sample was fixed and the precut sample was subjected to a temperature increasing from 20°C to 91°C, with a ramp rate of 0.1°C/s. The vertical arrow indicates the mesogen alignment direction (n). Note, at lower rates of heating, complete rupture happens at a narrower temperature range.

In this work, to investigate the fracture of monodomain LCEs, we measure the fracture toughness of monodomain LCE at different temperatures and different strain rates using pure shear test. We observed that the fracture energy of LCE decreases drastically at higher temperatures and at lower loading rates. Such measurements enabled us to quantitatively predict the thermally induced self-rupture of a constrained monodomain liquid crystal elastomer.

2.2 Methods

2.2.1. Chemicals

1,4-Bis-[4-(3-acryloyloxypropyloxy)benzoyloxy]-2-methylbenzene (RM257) (Wilshire Technologies; 95%) , 2,2′-(ethylenedioxy) diethanethiol (EDDET; Sigma-Aldrich; 95%), pentaerythritol tetrakis (3-mercaptopropionate) (PETMP; Sigma-Aldrich; 95%), (2-

hydroxyethoxy)-2- methylpropiophenone (HHMP; Sigma-Aldrich; 98%), dipropylamine (DPA; Sigma-Aldrich; 98%), were used as received without further purification.

2.2.2 Synthesis of Liquid crystal elastomers (LCEs)

LCEs were synthesized following the two-stage reaction from previous literature [38]. Liquid crystal monomer RM257 (10.975 g, 18.6 mmol) was dissolved in Toluene at 85°C. To this mixture, EDDET (3.076 g, 16.9 mmol), PETMP (0.244 g, 0.5 mmol), DPA (0.038 g, 0.4 mmol) and HHMP (0.077 g, 0.3 mmol) were added, which corresponds to a mol % ratio of RM257/EDDET/PETMP = 104%/94.4%/5.6%. Then the mixture was poured in a glass mold and left for 24 hours at room temperature for the first stage crosslinking reaction to conclude. Then the loosely crosslinked LCE film was placed in an oven at 85°C for 12 hours to evaporate the solvent. Finally, the loosely crosslinked LCE film was uniaxially stretched to a strain of ε=100%, and placed under an ultraviolet lamp (365 nm, 100W) for 15 minutes to complete the second stage crosslinking reaction of the excess acrylate groups (4%) from RM257 and obtain a monodomain LCE film. In all the mechanical tests, the LCE samples were prepared such that the liquid crystal mesogens (monodomain) were aligned along the direction of the applied tensile load. The nematic to isotropic transition temperature (T_{NI}) of this LCE is reported to be 75-80°C [38].

2.2.3 Measurement of fracture energy of LCE at different temperatures

We conducted the mechanical tests using TA instruments Electroforce 3300 with a 250 lbf load cell and a temperature chamber. When a free-standing LCE sample of height H_O is heated to a temperature T, the sample contracts along the mesogen alignment direction, and the

corresponding strain is defined as the actuation strain as denoted by $\varepsilon_a(T)$. If an LCE sample is fixed between the grippers of the tensile tester and heated, the contraction is restricted, and it can generate actuation stress of 100-500 kPa. Therefore, at a given temperature T, prior to the test, the sample height is decreased by the corresponding actuation strain to begin the tensile test at a stress-free state.

To measure the fracture energy of LCE, we adopted the pure shear test [44–50]. In this method, two rectangular LCE samples (~10mmx 50mm) were glued on to acrylic plates (Figure 2.2). An edge crack (length=$2*H_o$, ~20mm) was created in the precut sample using a sharp razor blade. At a fixed temperature, the precut sample was subjected to a monotonically increasing tensile load and the critical strain at which the sample ruptured (ε_c) was noted. Then, a pristine LCE sample was also subjected to a monotonically increasing tensile load until failure. Strain (ε) is defined as $\varepsilon = (h-H(T))/H(T)$, where h is the height of the sample in the deformed state and H(T) is the height of the sample in a stress-free state at that temperature.

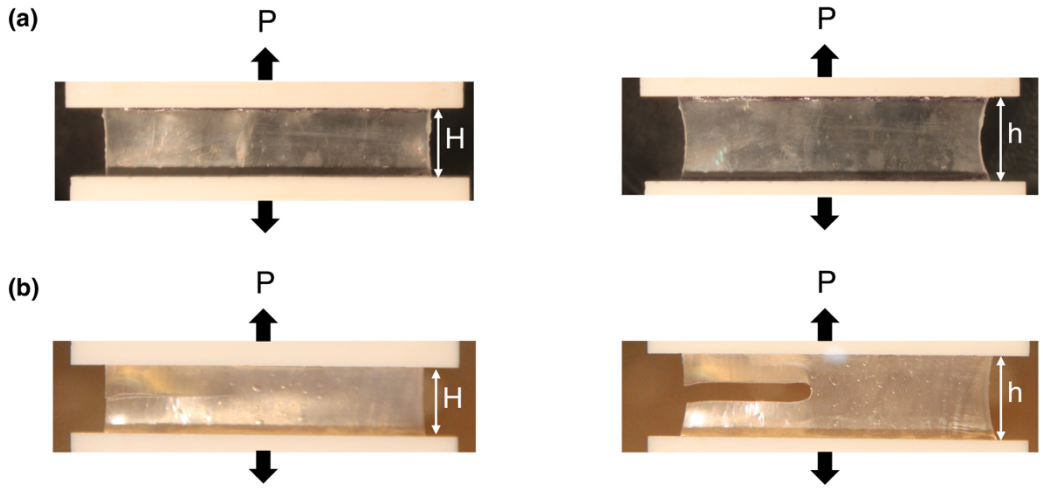

Figure 2.2: Pure shear test of monodomain LCE for measuring its fracture energy at a constant temperature. The figures on the left show the configuration of the LCE in free standing state and the figures on the right show the deformed configuration. (a) Photos of pristine LCE sample, (b) Photos of LCE sample with a precut. Strain (ε) is defined as ε = (h-H)/H.

The fracture energy Γ can be calculated as

$$\Gamma = W(\varepsilon_C) \times H \tag{1.1}$$

where W is the external work density, which is obtained by integrating the stress-strain curve of the pristine samples between ε=0 to ε=ε_c, (ε_c is the critical strain at rupture for the precut samples) and H is the height of the samples in a stress-free state. This test was performed at different temperatures (20,40,50,70,90°C) and strain rates (0.5 s^{-1}, 0.01 s^{-1}, 0.001 s^{-1}, 0.0001 s^{-1}).

For visualization purposes, the data from the tensile tests were smoothed using "smoothdata" function with 'sgolay' option on MATLAB (R2021a) to generate the stress-strain curves.

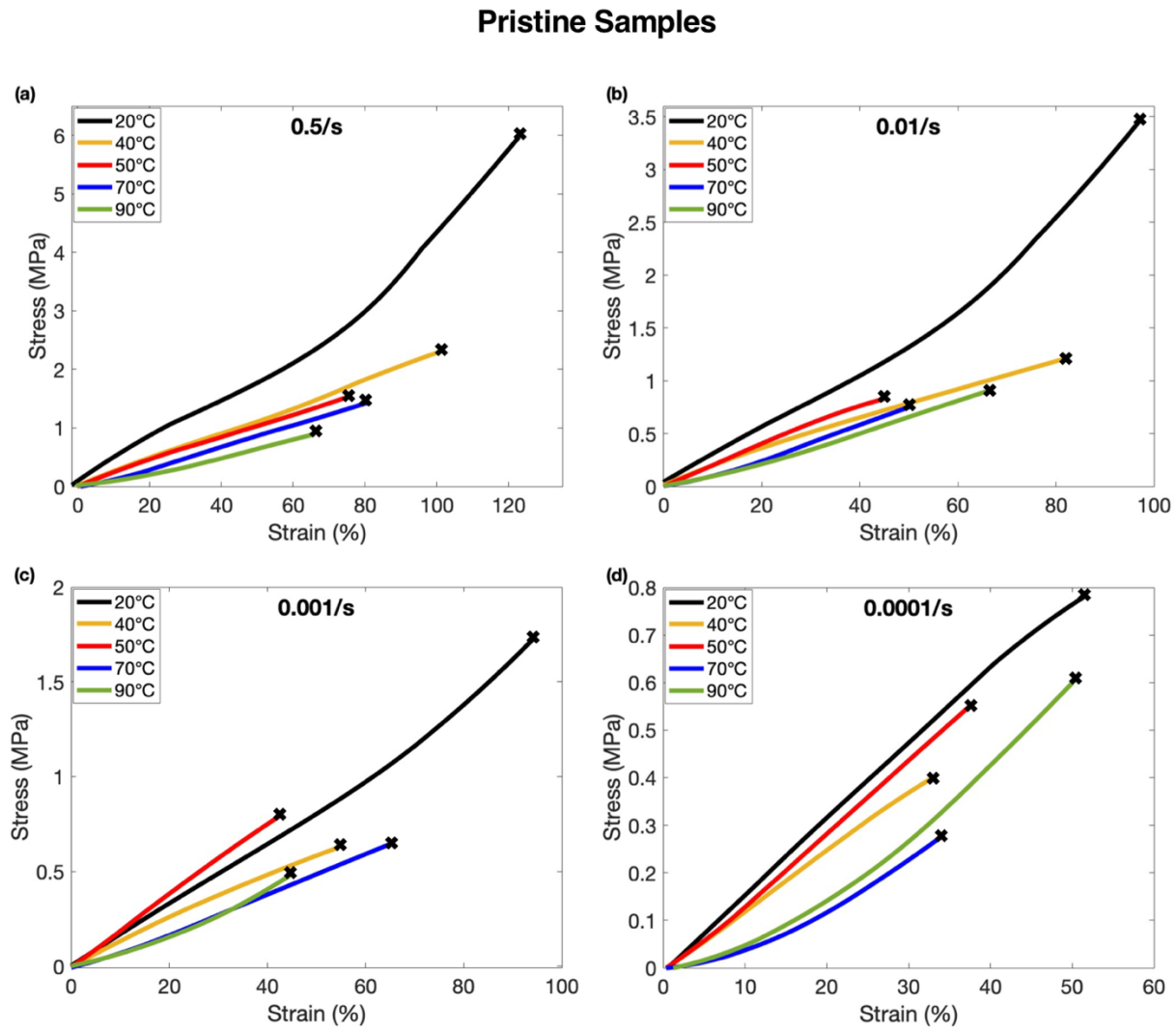

Figure 2.3: Stress-strain curves of pristine LCE samples subjected to pure shear loading at different temperatures (20°C, 40°C, 50°C, 70°C and 90°C) and at loading rates of (a) 0.5 s^{-1}, (b) 0.01 s^{-1}, (c) 0.001 s^{-1} and (d) 0.0001 s^{-1}. The black crosses at the end of the curves (x) indicate rupture.

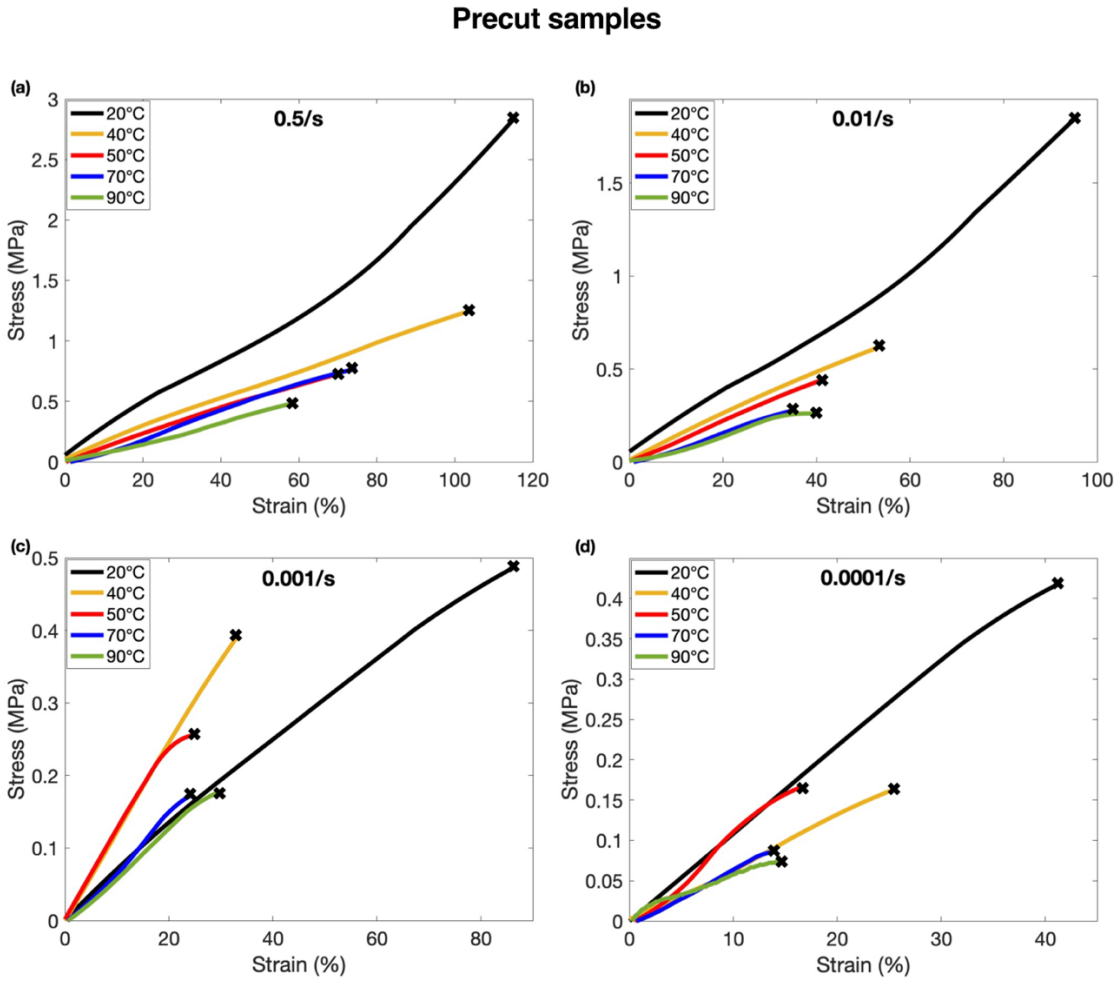

Figure 2.4: Stress – strain curves of LCE samples with precut subjected to pure shear loading at different temperatures (20°C, 40°C, 50°C, 70°C and 90°C) and at loading rates of (a) 0.5 s^{-1}, (b) 0.01 s^{-1}, (c) 0.001 s^{-1} and (d) 0.0001 s^{-1}. The black crosses at the end of the curves (x) indicate rupture.

It is to be noted that there are still quite a few fundamental debating questions regarding the fracture in viscoelastic solids. We do not try to address those fundamental problems in this paper. The original Rivlin and Thomas analysis [51] assumed that the material is hyperelastic without viscosity. However in practice, it not uncommon that the original analysis was extended and used similar ways to measure rate-dependent fracture energy of viscoelastic materials[44–46]. It is important to note that in the Rivlin-Thomas analysis, W is the strain energy density of the material

which is the same as external work density. However, for a viscoelastic material, the W in the equation is external work density, which is not the same as strain energy density. Despite this, the measured fracture energy of a viscoelastic material based on pure shear testing method is often a material constant.

2.2.4 Heating induced self-rupture of a constrained LCE

In this test, rectangular LCE samples (pure shear) with five different heights (H_o = 5,7.5,10,12.5 and 15mm) and an edge crack (length=2*H_o) were used. The samples held between tensile testing grippers inside a temperature chamber, without any applied pre-strain. The sample was then subjected to a temperature ramp from 20°C to 100°C at a rate of 0.01°C/s with its boundary being constrained (iso-strain) as shown in Figure 2.1. The temperature at which the sample catastrophically ruptured due to the actuation stresses was measured.

2.3 Results and Discussion

2.3.1 Dependence of Fracture energy and Rupture strain on Strain rate and Temperature

Figure 2.3 shows the tensile stress-strain curves for pristine LCE samples at different strain rates and temperatures. At a constant temperature, the stress at rupture of the pristine sample generally decreased when the loading rate was reduced from 0.5 s^{-1} to 0.0001 s^{-1}.

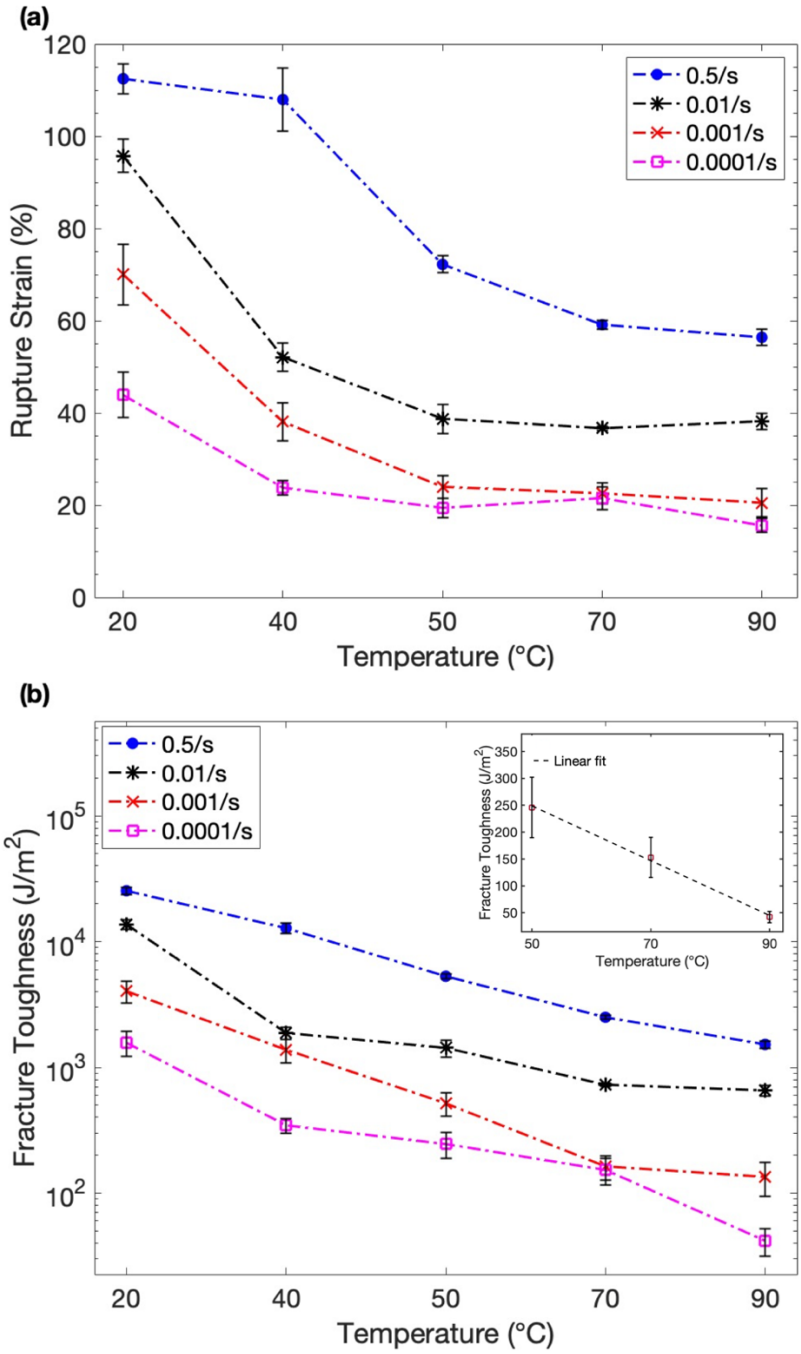

Figure 2.5: (a) Rupture strain (ε_c) of precut LCE samples and (b) Fracture toughness of LCE, at different temperatures (20°C, 40°C, 50°C, 70°C and 90°C) and loading rates (0.5 s^{-1}, 0.01 s^{-1}, 0.001 s^{-1} and 0.0001 s^{-1}). The solid markers denote the mean value of three samples and error bars represent one standard deviation. (b) Inset : Linear fitting of fracture energy data (loading rate : 0.0001 s^{-1}) between 50-90°C. Equation of linear fit $\Gamma(T)=A\times T+B$ where A = -5.0962 $J.m^{-2}.°C^{-1}$, B = 503.51 $J.m^{-2}$.

For the precut samples (Figure 2.4 and Figure 2.5a), the strain at which the samples catastrophically ruptured also dropped with increase in temperature or decrease in loading rate. This resulted from the dramatic reduction of the fracture energy of LCEs at high temperatures and low loading rates. Figure 2.5b summarizes the fracture energy of LCE, which decreased from 25.37 kJ/m^2 at 20°C and a strain rate of 0.5 s^{-1} to 41.82 J/m^2 at 90°C and a strain rate of 0.0001 s^{-1}. The dependence of fracture energy of LCE on the temperature and strain rate agrees well with that of most elastomers [47–49,52,53]. Previous studies have shown that an LCE can exhibit strong viscoelasticity, resulting from the mesogen rotation and the sliding between polymer chains [15,19,54,55]. The main reason for such rate and temperature dependence of the fracture energy is the reduction of viscoelastic dissipation of the elastomer at high temperature and low strain rate [47,53].

As seen in Figure 2.5b, at 90°C the fracture energy of LCE drops from 1570.51 J/m^2 at 0.5 s^{-1} to 41.82 J/m^2 at 0.0001/s rate. The fracture energy at the highest measured temperature and lowest strain rate (41.82 J/m^2) is in the same order as the threshold fracture energy (50-100 J/m^2) predicted by the Lake-Thomas model and observed in several elastomers [47,49,56]. Compared to the fracture energy of natural rubber (~ 10000 J/m^2)[45] and skeletal muscles (~2490 J/m^2)[57], one can notice that LCE is quite tough at room temperature, but it becomes very brittle at high temperature with small strain rate. Therefore, our results indicate that for the application of LCE as thermally actuating material, it requires toughening mechanisms for enhancing its fracture toughness above the nematic to isotropic transition temperature (T_{NI}), to prevent unexpected failure.

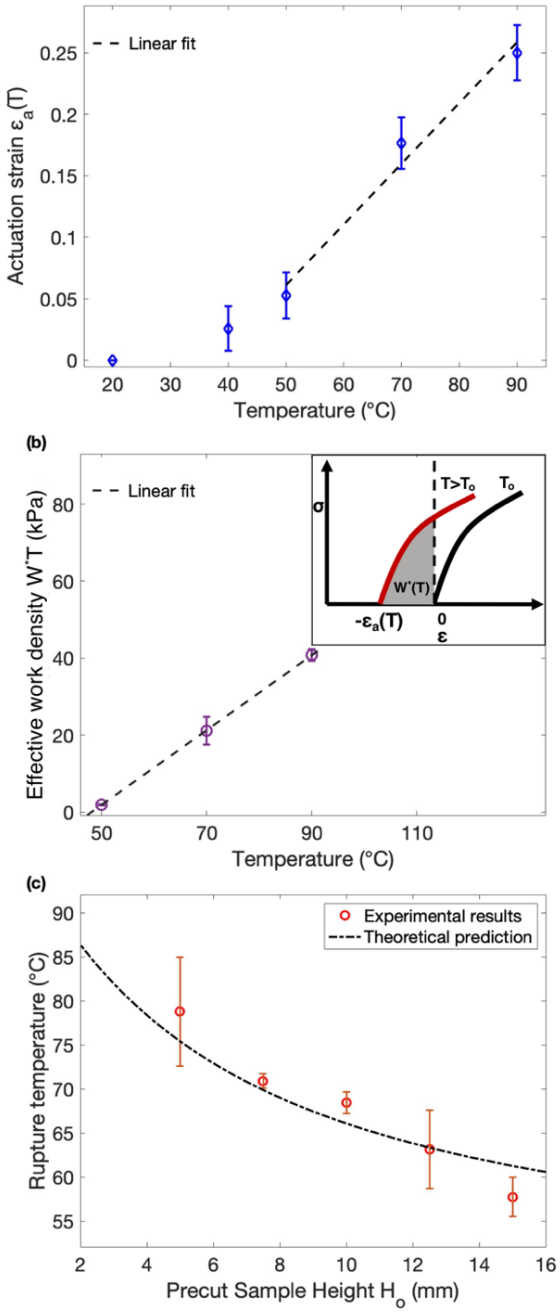

Figure 2.6: (a) Actuation strain $\varepsilon_a(T)$ of LCE at various temperatures with a linear fit, where $\varepsilon_a(T)=(H_o–H(T))/H(T)$, H_o is the height of the sample at room temperature and H(T) is the free-standing height of the sample at temperature T. The range of temperature for the linear fit is 50-90°C. The equation of linear fit is $\epsilon_a(T) = C\times T+D$, C = 0.00493 °C^{-1} and D = -0.18569. (b) Temperature dependent effective work density $W^*(T)$ between 50-90°C, with a linear fit. Equation of linear fit is $W^*(T)=E\times T+F$; where E = 971.47 Pa.°C^{-1}, F = 46682 Pa. (c) The temperature of thermally induced self-rupture of precut LCE samples of height H_o (5-15mm). The solid markers denote the mean experimental result of three samples and error bars represent one standard deviation. The dashed black line represents the theoretical predictions.

2.3.2 Self-rupture of a constrained LCE

When a free-standing LCE sample is heated to a temperature T, one can observe the contractile actuation strain ($\varepsilon_a(T)$) along the monodomain direction. On the other hand, if the displacement of an LCE sample is fixed and then heated to temperature T, the contraction is constrained. As a response, actuation stress is generated in the LCE sample. The increase of the actuation stress together with the reduction in the fracture energy at high temperatures (Figure 2.5b), cause the rupture of the constrained precut LCE sample as shown in Figure 2.1.

Figure. 2.6C shows the temperature of self-rupture for precut LCE samples with different heights (5-15mm). Given that the fracture energy of an elastomer is independent of specimen geometry, we can predict the critical temperature, at which the constrained LCE with different dimensions ruptures. For a displacement constrained precut LCE sample of height H_o at room temperature, its energy release rate (G) at an elevated temperature T can be given as:

$$G(T)=W^{*}(T)\times H(T) \tag{1.2}$$

where H(T) is the height of the LCE sample at temperature T in the free-standing state such that $H(T)=H_0/(1+\epsilon_a(T))$ with $\epsilon_a(T)$ the actuation strain as the offset in the stress-strain curve shown in the inset of Fig.6b. The actuation strain of LCE at different temperatures is shown in Figure 2.6a. Inset of Figure 2.6b shows the schematics for the determination of the temperature dependent effective work density $W^{*}(T)$ at different temperatures, where T_0 is the room temperature. For a given temperature $T>T_0$, the stress-strain curve of pristine LCE is offset by the actuation strain $\varepsilon_a(T)$ of LCE at that temperature. The corresponding $W^{*}(T)$ is obtained by integrating the stress-

strain curve between strain $\varepsilon=-\varepsilon_a(T)$ to $\varepsilon=0$ and $W^*(T)$ is the shaded area in grey. When the energy release rate reaches the fracture energy of LCE, namely, $G(T)=\Gamma(T)$, the LCE sample ruptures, where $\Gamma(T)$ is the fracture energy of the LCE measured at the lowest strain rate (0.0001 s^{-1}) shown in Figure 2.5b. We obtain the function $\Gamma(T)$, $\epsilon_a(T)$ and $W^*(T)$ by a linear fit of the experimental results between 50°C and 90°C in Figure 2.5b, Figure 2.6a and 2.6b respectively. The fitting functions are $\Gamma(T)=A\times T+B$; $\epsilon_a(T)= C\times T+D$, $W^*(T)=E\times T+F$; where A = -5.0962 $J.m^{-2}.°C^{-1}$, B = 503.51 $J.m^{-2}$, C = 0.00493 $°C^{-1}$ and D=-0.18569, E = 971.47 $Pa.°C^{-1}$, F = 46682 Pa.

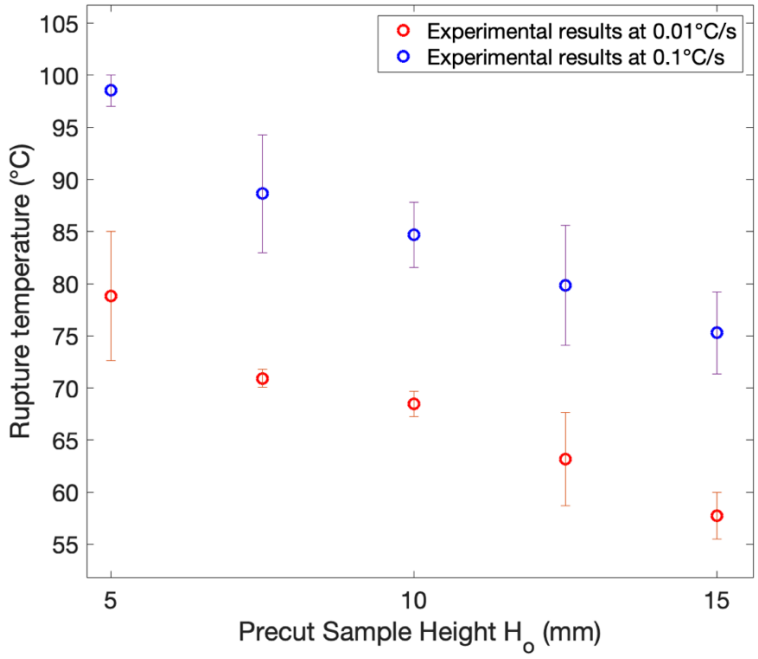

Figure 2.7: The temperature of thermally induced self-rupture of precut LCE samples of height H_o (5-15mm) at two temperature ramp rates : 0.01°C/s (Red) and 0.1°C/s (Blue). The solid markers denote the mean experimental result of three samples and error bars represent one standard deviation.

With a given H_0, the fitting equations above and the equation (1.2) allow us to predict the critical temperature T at which the LCE ruptures. The comparison between the prediction and the experimental measurements are shown in Figure 2.6c, which shows good agreement. For the

temperature ramp rate of 0.01°C/s, the average strain rate corresponds to approximately 0.00005 s^{-1}. Hence, we used the fracture energy measured at the lowest loading rate (0.0001 s^{-1}) to predict the rupture temperature, since the viscous effects are minimal at this loading rate. For higher rates of heating, the fracture energy corresponding to an appropriate higher loading rate can be used to predict the rupture temperature. The theoretical predictions and experimental results of the self-rupture temperature of precut LCE samples at a higher heating rate (0.1°C/s) is given in the Figure 2.7 and 2.8. In this work, we ignored the effect of the wavy configuration on the stress state in the sample, since the wavy crack morphology only becomes obvious after the crack extends through the elastomer (as seen in Figure 2.1). These results can help one to choose the appropriate geometry for designing structures using LCE that can reliably perform in a certain temperature range.

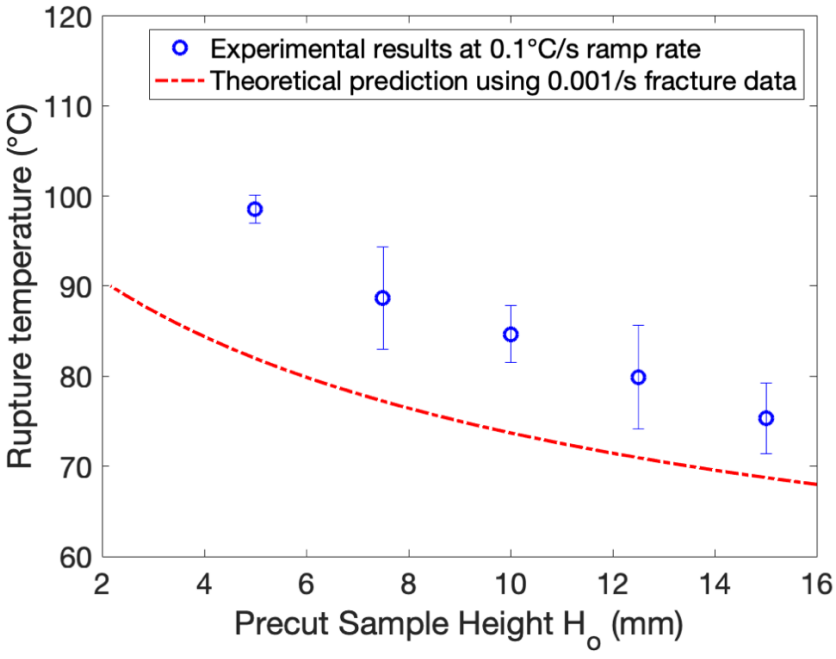

Figure 2.8: The temperature of thermally induced self-rupture of precut LCE samples of height H_o (5-15mm) at a heating rate of 0.1°C/s. The solid markers denote the mean experimental result of three samples and error bars represent one standard deviation. The dashed red line represents the theoretical predictions using 0.001 s^{-1} fracture data.

2.4 Conclusion

In this chapter, we systematically explore the fracture properties of liquid crystal elastomers at different temperatures and loading rates. LCE, being a viscoelastic material, shows rate and temperature dependent fracture behavior. At high loading rates and low temperatures, LCE is a tough elastomer. But once it is heated above the isotropic transition temperature, the viscous dissipation effects are minimized, leading to lowered fracture energy. Using the measured fracture energy, we can predict the rupture temperature under self-actuation stress for monodomain LCE. We believe that the results from this article can be used in designing LCE structures for various applications. The results also shine a light on the need to incorporate toughening mechanisms that can improve the fracture properties of LCEs at high temperatures.

Acknowledgements

Chapter 2, in full, is a reprint of the material as it appears in Annapooranan, R.; Cai, S. Thermally Induced Self-Rupture of a Constrained Liquid Crystal Elastomer. *Engineering Fracture Mechanics* **2022**, *269*, 108584. The dissertation author was the primary investigator and first author of this paper.

Chapter 3 Highly durable and tough liquid crystal elastomers

3.1 Introduction

Liquid crystal elastomer (LCE) is an emerging soft actuating material, that has garnered a lot of attention over the past few years. LCEs are synthesized by covalently bonding rod-shaped liquid crystal monomers in a flexible polymer network. The long-range orientational order of liquid crystal molecules or mesogens, combined with the elasticity of the polymer network results in the unique properties of LCE. Using different stimuli like heat and light, LCEs can undergo reversible and programmable actuation with large actuation strains and work densities [6,43,58]. Various surface alignment techniques allow LCEs to be patterned in a precise molecular order to produce complex deformations [59] and different types of aligned LCE structures can be fabricated using 3D printing techniques [28,60,61]. Introducing dynamic covalent bonds into the polymer networks, allows LCEs to be reprocessible and reprogrammable [30–33,62]. The unique thermo-mechanical properties, combined with the advancement in the fabrication techniques, has made LCE an emerging candidate for soft robots [35,37], artificial muscles [26,27,34], micromechanical systems [63,64], biomedical [36] and wearable devices [65].

Thermally actuated LCEs can be synthesized by the two-step method, where mechanical stretch is used in the alignment of the mesogens, resulting in a highly anisotropic "monodomain LCE" [38]. On heating a monodomain LCE above the nematic to isotropic transition temperature, the polymer chains transform from an anisotropic to an isotropic conformation, causing notable macroscopic deformation, which is reversible on cooling [42]. When used as a thermal actuator, LCE can be subjected to numerous heating-cooling cycles and prolonged cyclic mechanical loading [63]. It has been often observed in the experiments that LCE can be ruptured by externally applied

mechanical load or heat induced stresses. A recent work has shown that LCE is tough at room temperature, but the fracture energy of LCE decreases severely with increasing temperatures [66]. Nevertheless, in practical applications, LCE should have adequate high temperature fracture and fatigue properties to reliably perform as an actuating material for multiple cycles.

There have been significant advancements to improve the fracture and fatigue properties of soft materials like elastomers and hydrogels recently [48,67,68]. While the intrinsic fracture energy of elastomers is usually in the order of 10-100 J/m^2, substantial toughening has been possible due to the introduction of various dissipative mechanisms. For example, viscoelasticity of polymer network can dissipate energy during crack extension, which contributes to the fracture energy of the elastomer [10,50]. However, such viscous dissipation decreases with the increase of environmental temperature. The addition of fillers have been also used to significantly improve the tearing energy of elastomers, at the expense of increased stiffness [49]. Addition of nanofibers to hydrogels can result in mechanical energy dissipation through fiber pull-out and fracture [69]. By controlling the macromolecular architecture, for example, high-functionality crosslinks can create tough hydrogels, as the shorter polymer chains can fracture and dissipate energy [70]. A high degree of entanglements created by long polymer chains have been shown to improve toughness, strength and fatigue properties of gels. [71]

Among the different toughening techniques, interpenetrating polymer networks (IPN) have proven to be versatile for enhancing the fracture energy while maintaining the stretchability of the networks. The double network tough hydrogels, developed first by Gong and coworkers [72], used the rupture of the pre-stretched first network to dissipate mechanical energy, while the longer second network maintained the extensibility. The double network hydrogels also exhibited a fatigue threshold higher than 400 Jm^{-2} [44]. Followed by this work, various other IPN and semi-IPN

have been used for fabricating tough hydrogels and elastomers, using covalent and ionic crosslinks [45,73]. Although a recent work has shown that IPN can improve the tensile strength of LCE [74], it is unknown how IPN may enhance the fracture toughness and fatigue of LCE.

When it comes to using IPN to enhance the mechanical properties of a soft actuating material like LCE, it is important to consider the following requirements 1) The compliance of the network should be maintained to not impede actuation, namely, high stiffening should be avoided, 2) Easy alignment of mesogens during synthesis should be possible, i.e the second network cannot be too brittle to be completely ruptured during mesogen alignment using mechanical stretch. Keeping the above challenges in mind, we use the IPN strategy to synthesize Double network LCE (DNLCE), using an acrylate LCE network and a non-LCE polyurethane (PU) network. Polyurethane was chosen as the second network for its softness, large stretchability, and the easily tunable crosslinking chemistry. Compared to the single network LCE (SNLCE), the DNLCE samples show improved high temperature fracture energy and resistance to fatigue crack growth, while retaining the actuation properties. This simple technique allows for the fabrication of LCE actuators that are tough and can reliably perform at high temperatures for greater number of cycles.

3.2 Methods

3.2.1 Chemicals

1,4-Bis-[4-(3-acryloyloxypropyloxy)benzoyloxy]-2-methylbenzene (RM257) (Wilshire Technologies; 95%) , 2,2′-(ethylenedioxy) diethanethiol (EDDET; Sigma-Aldrich; 95%), (2-hydroxyethoxy)-2- methylpropiophenone (HHMP; Sigma-Aldrich; 98%), dipropylamine (DPA; Sigma-Aldrich; 98%), N-N-Dimethylformamide (anhydrous DMF; Sigma-Aldrich; 99.8%), 4,4'-

Methylenebis(phenyl isocyanate) (MDI; Fisher Scientific; 98%), Trimethylolpropane (TMP; Sigma-Aldrich 97%), Poly(propylene glycol) (PPG; Sigma-Aldrich; average Mn ~2,000); were used as received without further purification.

3.2.2 Synthesis of polydomain Single network Liquid crystal elastomer (SNLCE)

LCE oligomer was synthesized by the Michael addition reaction between liquid crystal monomer RM257 and the chain extender EDDET, which was then UV crosslinked to obtain polydomain LCE. RM257 (10 g) was dissolved in 10 ml of DMF. Then, the chain extender EDDET (2.692 g), catalyst DPA (0.03447 g) and photoinitiator HHMP (0.06406 g) were added to this mixture and stirred at room temperature for 12 hours, to obtain the LCE oligomer. The oligomer was degassed and poured in a glass mold and placed under a UV lamp (365 nm, 100 W) for 15 minutes to get a partially crosslinked LCE, which was then left in an oven at 85°C for 24 hours to evaporate the solvent. Finally, the LCE film was placed under UV lamp for 60 minutes to ensure complete crosslinking.

3.2.3 Synthesis of Single network Polyurethane elastomer (PU)

Polyurethane elastomer was synthesized by the reaction between monomers (MDI), chain extender (PPG) and crosslinker (TMP). MDI (5g), PPG (18.789 g) and TMP (0.947 g) were dissolved in 25 ml of anhydrous DMF and stirred at 65°C for 2 hours under nitrogen atmosphere. The mixture was degassed, poured in a glass mold and placed in an oven at 85°C for 48 hours to evaporate the solvent and ensure complete crosslinking.

3.2.4 Synthesis of Double network Liquid crystal elastomer (DNLCE)

LCE oligomer was prepared using RM257 (10 g, 41.811 mol%), EDDET (2.692 g, 36.314 mol%), catalyst DPA (0.03447 g, 1.215 mol%) and photoinitiator HHMP (0.06406 g, 0.658 mol%) in a three necked flask. To the LCE oligomer, PU network reagents : MDI (1.115g, 10.96 mol%), PPG (4.19 g, 5.156 mol%) and TMP (0.211 g, 3.877 mol%) were added. This reaction mixture was stirred at 78°C for 5 hours under nitrogen atmosphere, as the PU network slowly begins to crosslink. Then the mixture was degassed, poured in a glass mold and placed under a UV lamp (365 nm, 100 W) for 30 minutes to crosslink the LCE network. Then the mold was placed in an oven at 85°C for 48 hours to evaporate the solvent and ensure complete crosslinking of the PU network. Finally, the film was placed under the UV lamp for 60 minutes to ensure complete crosslinking of the polydomain LCE network. The ratio between PPG and TMP was modified to vary the crosslinking density of the PU networks, but the proportion of LCE network reagents (80 mol%) and PU network reagents (20 mol%) was kept constant throughout the study.

3.2.5 Fabrication of monodomain LCE samples

To prepare the monodomain LCE samples, two-step UV crosslinking of the acrylate LCE network was used. In case of SNLCE, the LCE oligomer with the photoinitiator was degassed and poured in a mold. Then the first UV crosslinking step was performed for 30s, followed by placing the sample in the oven at 85°C for 48 hours for solvent evaporation. Finally, the partially crosslinked SNLCE film was stretched to $\lambda_p = 2$ and placed under a UV lamp for 60 mins to completely crosslink the SNLCE network in the monodomain state.

In case of DNLCE, the LCE oligomer with the photoinitiator was mixed with the PU precursors and stirred for 5 hours at 78°C. Then the reaction mixture was degassed and poured in

a mold. The first UV crosslinking step was performed for 100s, followed by placing the sample in the oven at 85°C for 48 hours for allowing the complete thermal crosslinking of the PU network. Then the partially crosslinked DNLCE film was stretched to $\lambda_p = 2$ and placed under a UV lamp for 60 mins to crosslink the DNLCE network in the monodomain state.

3.2.6 Uniaxial tensile tests

We conducted the uniaxial tensile tests and cyclic loading-unloading tests using Universal Mechanical Testing System (5965 Dual Column Testing System, Instron) with a 5-kN load cell and a temperature chamber. Pristine rectangular samples (height = 5 mm, width = 50mm) were glued on to acrylic plates and were held between the tensile grippers. The applied stretch (λ) is defined as $\lambda = h/H$, where H is the height of the sample in the undeformed state and h is the height of the sample in the deformed state. The loading rate of 0.005 s^{-1} was used for the tests.

3.2.7 Thermal Analysis

We used dynamical mechanical analyzer (RSA-G2, TA Instruments) to obtain the Storage modulus and loss tangent of the samples. Rectangular samples (10x5x0.5 mm) were held between tensile grippers. A strain oscillation (0.5%) was applied onto the sample at 1 Hz, while the temperature was ramped between -50°C and 150°C at a ramp rate of 20°C/min.

We conducted the DSC measurements using Discovery DSC250 (TA Instruments) in a nitrogen atmosphere. The samples were sealed in aluminum pans and the measurements were performed at a heating rate of 2°C/min between the temperature -20°C to 150°C.

3.2.8 Fracture energy

To determine the fracture energy of the LCE samples, we used the pure shear test method [45,51] using Universal Mechanical Testing System (5965 Dual Column Testing System, Instron) with a 5-kN load cell and a temperature chamber. In this method, two rectangular samples (height = 5 mm, width = 50mm) were glued on to acrylic plates (Figure 3.1). In one of the samples, an edge notch (~10mm) was created using a sharp razor blade. The precut sample was subjected to a monotonic tensile load and the critical stretch at which the sample ruptured (λ_c) was noted. Then a pristine DNLCE sample was also subjected to a monotonic tensile load until failure. The fracture energy (Γ) is given by

$$\Gamma = W(\lambda_C) * H \tag{2.1}$$

where $W(\lambda_c)$ is the strain energy density, which is obtained by integrating the stress-stretch curve of the pristine samples between $\lambda=1$ to $\lambda=\lambda_c$, and H is the height of the sample in the undeformed state. This test was performed at different temperatures (20, 50 and 90°C) and at a strain rate of 0.005 s^{-1}. Note that the fracture energies were measured for the LCEs in the polydomain state.

3.2.9 High temperature fatigue crack growth

We conducted the high temperature fatigue experiments [75] using TA instruments Electroforce 3300 with a 250 lbf load cell and a temperature chamber at 90°C. We used two rectangular samples (height = 10 mm, width = 50mm), one pristine sample and one precut sample with an edge notch (Figure 3.1). The precut sample was subjected to cyclic loading between $\lambda=1$ to $\lambda = \lambda_{max}$ at a strain rate of 0.1 s^{-1}. A digital camera (Canon Rebel T4i) was used to record photos during the crack extension of the precut sample. A custom MATLAB program was used to

determine the crack extension Δc from the photos. The crack length extension Δc was then plotted versus the cycle number (N) and the slope (dC/dN) was calculated. The pristine sample was also subjected to cyclic loading between λ=1 to λ = λ_{max}. The energy release rate (G) can be calculated from

$$G=W(\lambda_{max})*H \tag{2.2}$$

where W(λ_{max}) is the strain energy density, which is obtained by integrating the loading stress-stretch curve of the pristine samples between λ=1 to λ= λ_{max}, and H is the height of the sample in the undeformed state. This experiment was repeated for different values of λ_{max}. Note that the fatigue crack growth experiment was performed for the LCEs in the polydomain state.

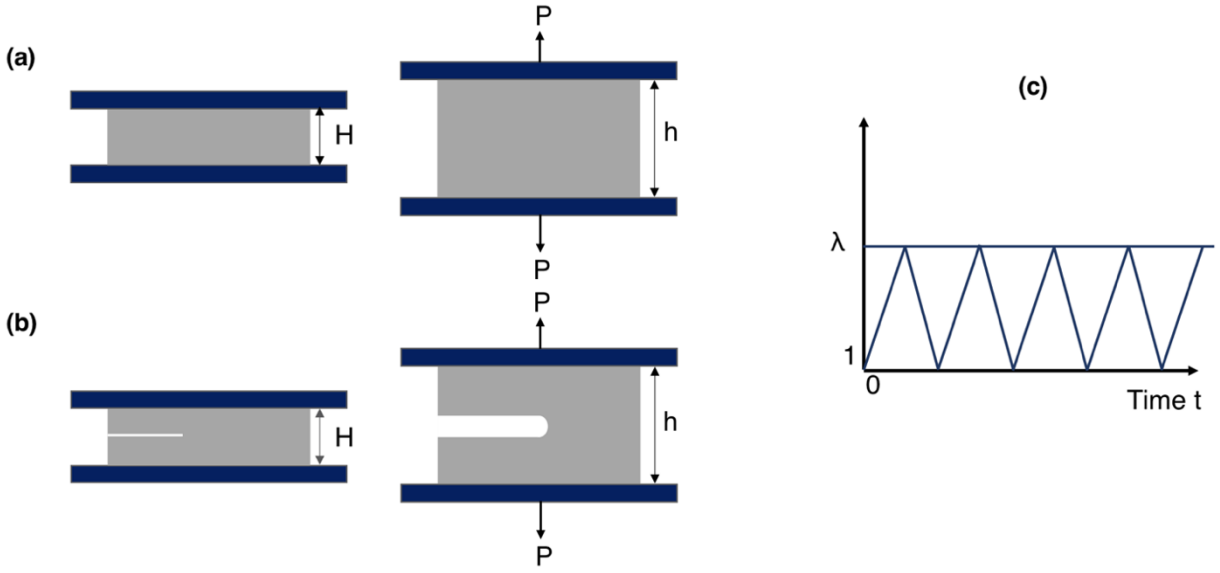

Figure 3.1: Schematics of a LCE pure shear specimen used in the fracture and fatigue experiments; (a) Pristine sample in undeformed state (left) and deformed state (right); (b) Precut sample in undeformed state (left) and deformed state (right); (c) The applied loading profile used for the fatigue experiments.

3.2.10 Actuation stress and strain measurement

The actuation stress of SNLCE and DNLCE was measured using a dynamical mechanical analyzer (RSA-G2, TA Instruments). Rectangular monodomain SNLCE and DNLCE samples (10x5x0.5 mm) were held between tensile grippers and heated from 25° to 180°C at a ramp rate of 20°C/min. The corresponding actuation stress generated by the LCE samples were measured.

The actuation strains of SNLCE and DNLCE was measured by attaching one end of the rectangular sample to an acrylic plate, which was held between the tensile grippers inside a temperature chamber. The other end of the sample was subjected to a small load (stress = 0.05 MPa) to keep the sample taut. The temperature of the chamber was increased from 25°C to 160°C and the deformation in the sample was observed using a digital camera. The actuation strain was calculated using the following equation

$$\text{Actuation strain } (\%) = \frac{(H_O - H_T)}{H_O} \times 100 \tag{2.3}$$

where H_O is the height of the sample at room temperature and H_T is the height of the sample at high temperature T.

3.3 Results and Discussion

For preparing the interpenetrating polymer networks (IPN), we adopt a one-pot simultaneous polymerization method utilizing two orthogonal crosslinking reactions. The double network LCE (DNLCE) is composed of a diacrylate LCE network and a non-LCE polyurethane (PU) network, as shown in Figure 3.1a. To prepare the LCE network, first an LCE oligomer is synthesized using the Michael addition between the acrylate liquid crystal monomer RM257 and the thiol chain

extender 2,2′-(ethylenedioxy) diethanethiol (EDDET) [28]. Typically, the ratio of liquid crystal monomer to chain extender is chosen such that a non-equimolar excess (1.15:1) of acrylate moieties exist with respect to the thiol groups. Facilitated by a photoinitiator (HHMP), the excess acrylate end groups of the oligomer can be UV photocrosslinked to form the LCE network. On the other hand, the PU network is thermally crosslinked, using a monomer 4,4'-Methylenebis(phenyl isocyanate) (MDI), chain extender Poly(propylene glycol) (PPG) and a tri-functional crosslinker Trimethylolpropane (TMP) (Figure 3.2). An equimolar ratio (1:1) is maintained between the monomer (MDI) and polyols (PPG + TMP). The isocyanate groups react readily with the polyols to form urethane links. By controlling the ratio between PPG and TMP, we can tune the crosslinking densities and the mechanical properties of the PU network. Due to the orthogonal chemistries, the LCE oligomer can be mixed with the PU reagents to simultaneously polymerize the LCE and PU networks and obtain double network LCE (DNLCE). The proportion of LCE network reagents (80 mol%) and PU network reagents (20 mol%) was kept constant throughout the study.

The newly crosslinked LCE samples have no global order in the absence of any mechanical pre-stretching and are known to be in the polydomain state. When the polydomain LCE samples are uniaxially stretched, the liquid crystal mesogens are aligned in the direction of stretch and the sample changes to a monodomain state. For the fracture and fatigue experiments in this study, polydomain SNLCE and DNLCE samples are used for comparison. Figure 3.2 shows the mechanism of toughness enhancement, using a precut DNLCE sample subjected to loading. Due to the reduction of bulk dissipation mechanisms at high temperatures (above the nematic to isotropic transition, >80°C), the fracture of SNLCE proceeds by the scission of polymer chains right in front of the crack tip, where the stress concentration is large. In case of DNLCE at high

temperature, the entanglement between the two networks results in the enlargement of the process zone. The rupture of the stiffer LCE network causes dissipation of strain energy over a larger part of the sample, while the extensible PU network maintains the integrity of the elastomer. This reduces the stress concentration at the crack tip and leads to a high fracture energy. [76]

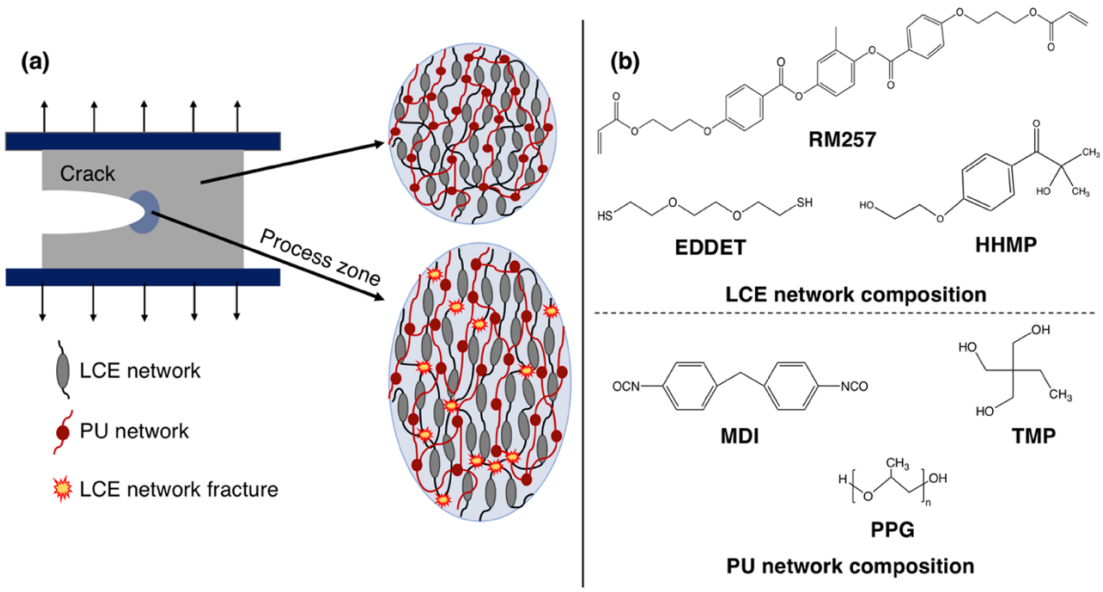

Figure 3.2: (a) Illustration of the toughening mechanism in Double network LCE (DNLCE). In the process zone near the crack tip, significant amount of energy is dissipated by the rupture of the stiff LCE network, leading to enhanced fracture energy of DNLCE compared to single network LCE (SNLCE). (b) Chemical compositions of the LCE network and the PU network, used in the synthesis of DNLCE.

Figures 3.3 a-c show the tensile stress-stretch curves of pristine SNLCE, PU and DNLCE pure shear samples at three different temperatures and a strain rate of 0.005 s^{-1}. The PU networks are soft, stretchable and the tensile properties of pristine PU remains mostly unchanged at all the temperatures: its tensile strength is about 0.15 MPa and stretch at rupture is between 2.4-2.8. At 20°C, the stress-stretch curve for SNLCE exhibits an initial linear part, then followed by a plateau, where mesogen reorientation takes place, followed by a stiffening regime. The stress-stretch curve

for DNLCE at 20°C is qualitatively similar to SNLCEs, but has a higher failure stretch. On heating from 20°C to 90°C, the tensile stress and failure stretches of pristine SNLCE samples drop dramatically. SNLCE becomes less stretchable compared to PU at 90°C. On the other hand, the DNLCE samples have failure stretches higher than SNLCE at the three testing temperatures, while the tensile strength of DNLCE samples are comparable or even higher than SNLCE. At 90°C, the SNLCE and DNLCE samples also have similar values of elastic modulus (~0.7 MPa) at small deformation.

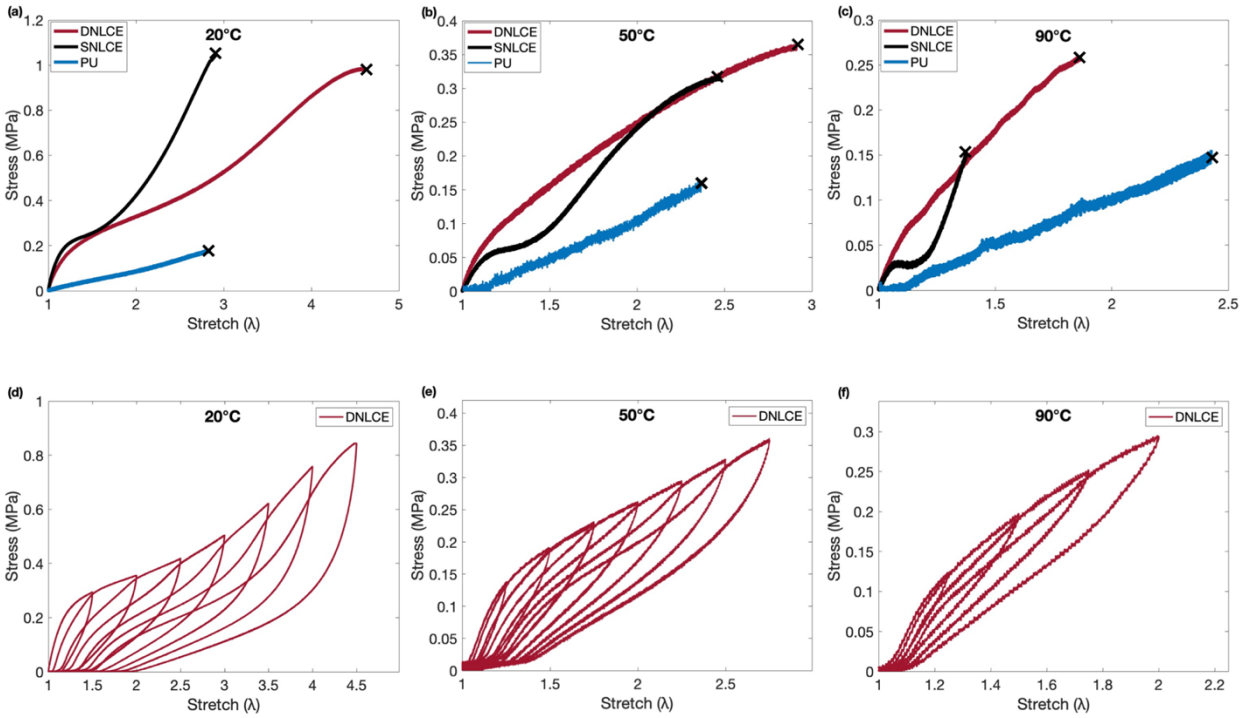

Figure 3.3: (a)-(c) Stress-stretch curves of pristine DNLCE, SNLCE and PU pure-shear samples subjected to uniaxial tensile loading at (a) 20°C, (b) 50°C and (c) 90°C. The crosses at the end of the curves represent rupture. (d)-(f) Stress-stretch curves of pristine DNLCE samples subjected to a cycle of loading and unloading of varying maximum stretch at (d) 20°C, (e) 50°C and (f) 90°C. The loading rate is 0.005 s^{-1}.

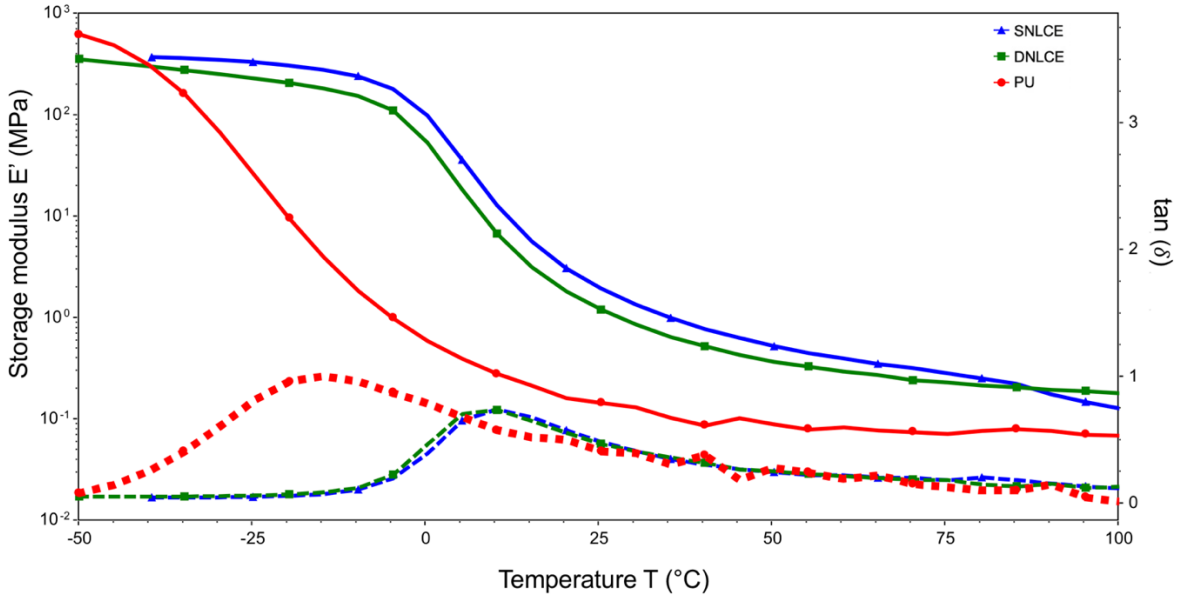

Figure 3.4: Dynamic mechanical analysis (DMA) results of SNLCE (Blue), DNLCE (Green) and PU (Red), performed at 0.5% strain oscillation at 1 Hz. Solid lines: Storage modulus; Dotted lines: Tan delta.

Figures 3.4 show the results from Dynamic Mechanical Analysis (DMA) of the three polymers. The glass transition temperature obtained from the peak of the loss tangent curve is 10.3°C for SNLCE, 10.4°C for DNLCE and -15°C for plain PU, which shows that the addition of PU networks did not drastically change the glass transition temperatures of DNLCE compared to that of SNLCE. Figure 3.5 shows the results from the differential scanning calorimetry (DSC) experiments on the three polymers. As seen in the DMA experiment we could only observe one peak corresponding to glass transition for DNLCE in the DSC traces suggesting that the two networks are miscible[77]. Similar to previous studies[38,78], it is hard to detect the nematic-to-isotropic phase transition temperature of crosslinked LCE from the DSC results.

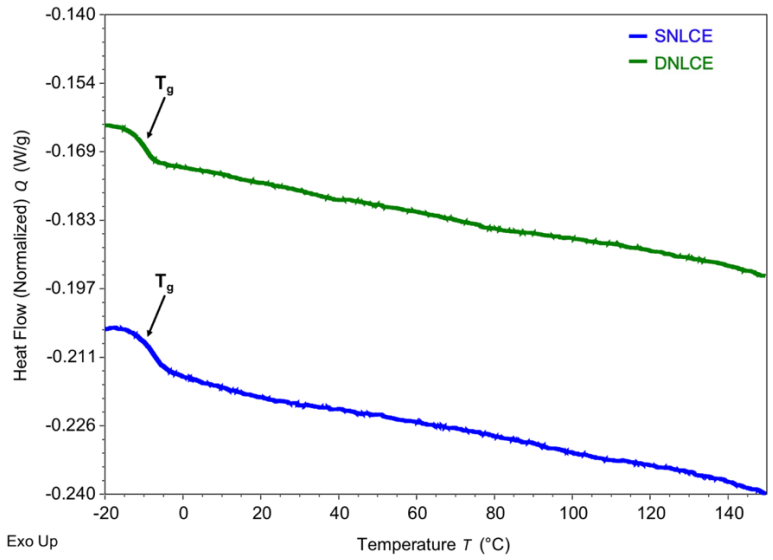

Figure 3.5: Differential Scanning Calorimetry (DSC) results for SNLCE (Blue) and DNLCE (Green), obtained at a heating rate of 2°C/min.

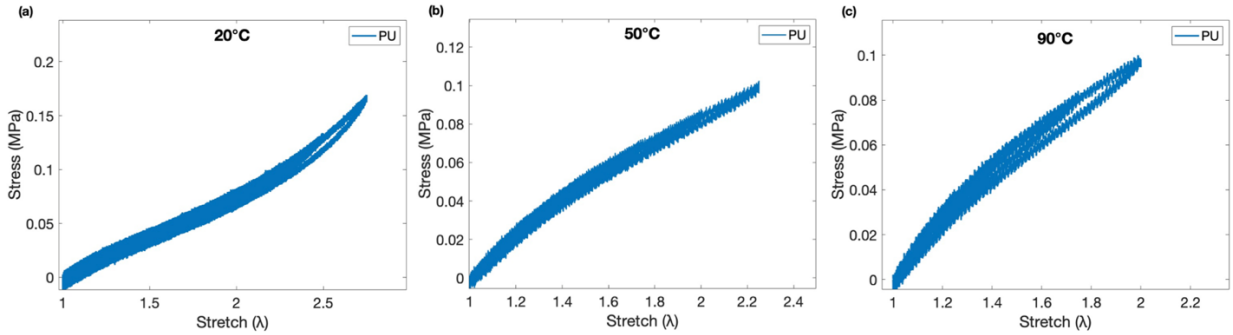

Figure 3.6: Stress-stretch curves of pristine PU pure shear samples subjected to a cycle of loading and unloading of varying maximum stretch at (a) 20°C, (b) 50°C and (c) 90°C. The loading rate is 0.005 s^{-1}.

Additionally, on heating to 150°C, we do not observe any dramatic decrease in the storage modulus of DNLCE and PU in the plateau region, hinting that there is no depolymerization of PU networks within the range of actuation temperatures[79]. We also do not observe any endothermic wells corresponding to depolymerization in the DSC results at 150°C. It is noted that at temperature above 220°C, depolymerization of PU may occur[80].

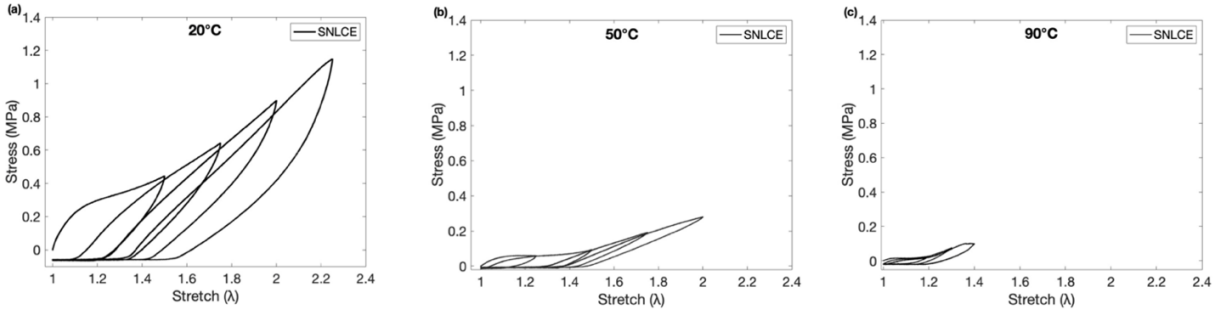

Figure 3.7: Stress-stretch curves of pristine SNLCE pure shear samples subjected to a cycle of loading and unloading of varying maximum stretch at (a) 20°C, (b) 50°C and (c) 90°C. The loading rate is 0.005 s^{-1}.

Figures 3.6 and 3.7 show the cyclic loading-unloading curves of pristine PU and SNLCE. For all the three temperatures, PU is nearly perfectly elastic with negligible hysteresis. The hysteresis of SNLCE decreases with the increase of the temperature, due to the reduction of viscoelastic dissipation in the network [54]. Such trend is consistent with that of many elastomers [56]. Figures 3.3 d-f show the cyclic loading-unloading curves of pristine DNLCE samples at three different temperatures. The DNLCE samples show significant hysteresis, observed by the area between the loading and unloading curves in Figures 3.3 d-f. Similar to SNLCE, there is a decrease in the hysteresis area for DNLCE as the temperature is increased. SNLCE and DNLCE samples also show some residual stretch on unloading.

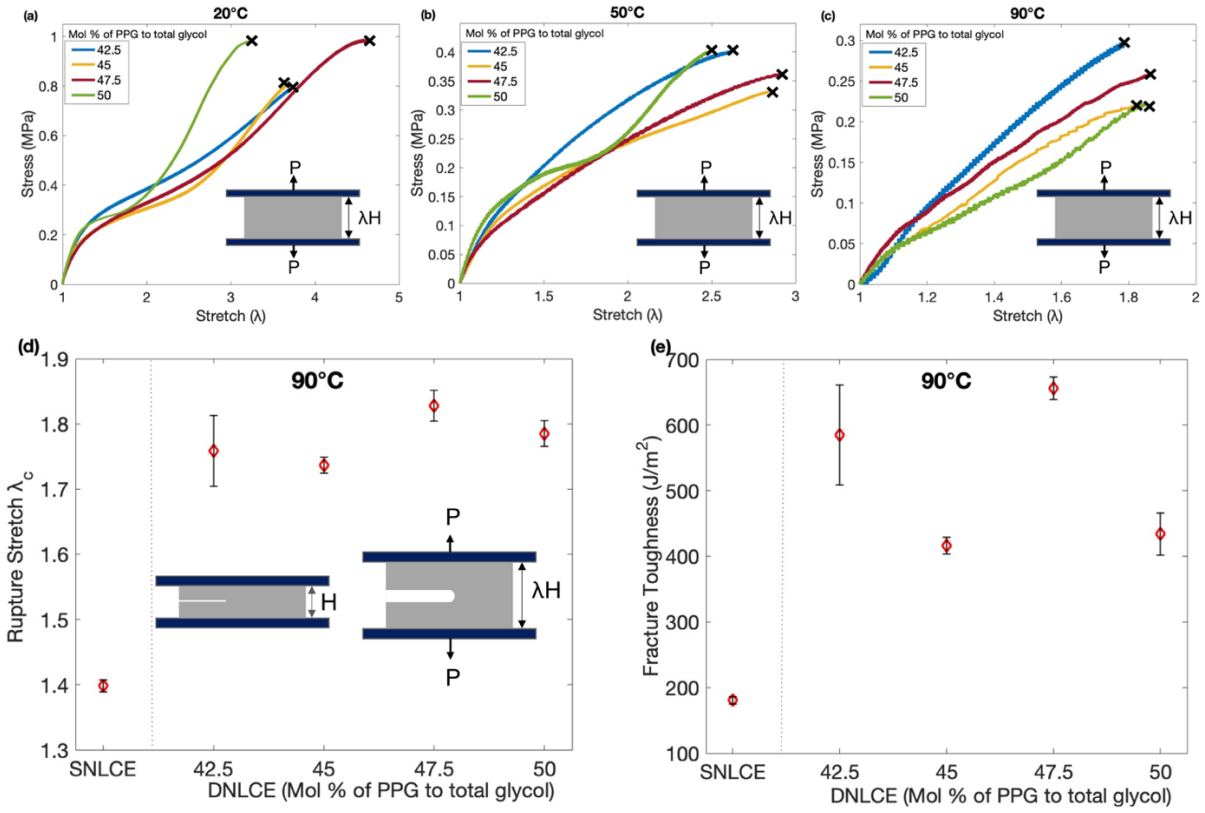

Figure 3.8: (a)-(c) Stress-stretch curves of DNLCE samples of various compositions of the PU network at (a) 20°C, (b) 50°C and (c) 90°C. Varying the ratio of the PPG and TMP in the PU composition results in networks of different crosslinking densities. The crosses at the end of the curves represent rupture. (d)-(e) Fracture properties of SNLCE and DNLCE samples at high temperature (90°C). (d) Critical stretch (λ_c) at rupture and (e) Fracture toughness (Γ), for precut SNLCE sample and DNLCE samples of varying compositions measured using pure shear test method at 90°C. Error bars represent one standard deviation (n=3). The loading rate is 0.005/s.

It is also noted that on increasing the applied stretch under cyclic loading-unloading, softening (known as the Mullins effect) is observed for DNLCE. The softening can be observed for stretches lower to or equal to the maximum stretch previously applied, but once the maximum stretch has been exceeded, the response becomes comparable to the monotonic tensile curve. Similar softening in hydrogels, have been attributed to irreversible damage from fracture [81]. Cyclic softening is also observed for SNLCE samples (Figures 3.7), which may arise from the network heterogeneities and uneven chain lengths, due to the free-radical UV polymerization. When the

sample is stretched, the shorter chains may rupture and cause the softening. To quantitatively understand the contribution of PU network to the improvement of fracture properties of DNLCEs, we change the ratio between the polyols in the PU system and compare their mechanical properties, as shown in Figures 3.8 a-c. By modifying the ratio between the glycol spacer (PPG) and the triol crosslinker (TMP), we can control the crosslinking density and the stretchability of the PU network. The stiffness of the PU network increases with the amount of TMP, which in turn determines how the load is transferred between the LCE and PU network, thereby resulting in different overall mechanical properties. For the pristine samples of the different compositions of DNLCE (Figures. 3.8 a-c), the initial stiffness is comparable, and the failure stretch is higher compared to that of SNLCE at the three testing temperatures.

The pure shear test method was used to measure the fracture energy of SNLCE and DNLCE, using a pair of pristine and precut samples at a loading rate of 0.005 s^{-1}. For a certain ratio of PPG:TMP (47.5:52.5), the fracture energies were found to be the highest at all the testing temperatures (Figure 3.9) and this composition was used throughout the study. At room temperature (20°C), the fracture energies of SNLCE (7092.69 Jm^{-2}) and of DNLCE (8551.80 Jm^{-2}), are comparable to the fracture energy of tough elastomers like Natural rubber (~10000 Jm^{-2}) [49].

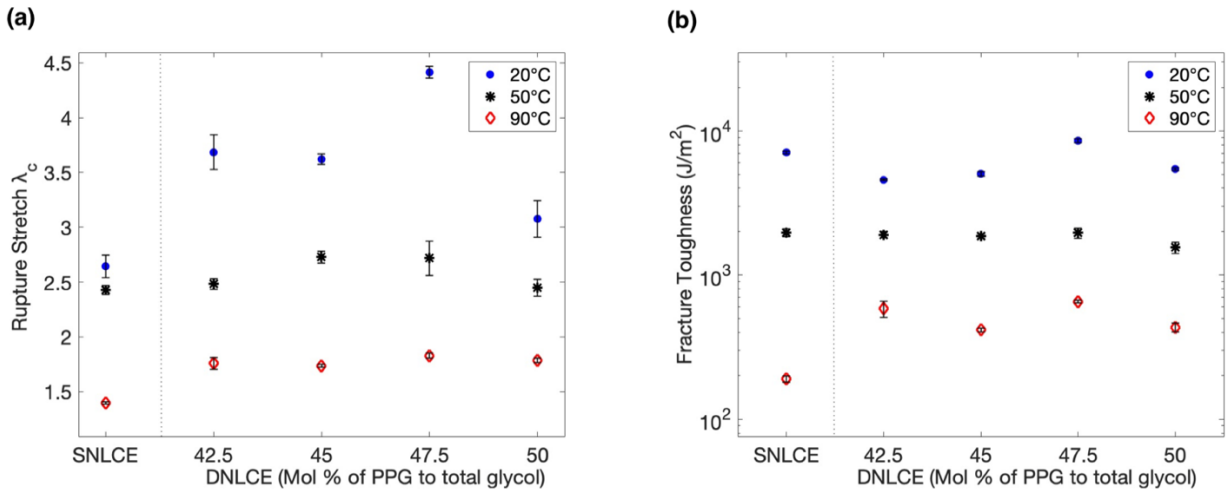

Figure 3.9: Fracture properties of SNLCE and DNLCE samples at three different temperature (20,50 and 90°C). (a) Critical stretch (λ_c) at rupture of precut samples and (b) Fracture energy (Γ) for SNLCE sample and DNLCE samples of varying compositions measured using pure shear test method. Error bars represent one standard deviation (n=3).

The large fracture energy of SNLCE arises from viscoelastic dissipation caused by mesogen rotation and the sliding of polymer chains [54]. Since these bulk dissipation mechanisms are suppressed at high temperatures, there is a dramatic decrease in the fracture energy of SNLCE. At 90°C (Figures 3.8 d-e), the rupture stretch of precut samples (λ_c) and the fracture energy (Γ) of DNLCE (λ_c~1.8, Γ=655.69 Jm^{-2}) are much higher compared to that of SNLCE (λ_c~1.4, Γ=180.70 Jm^{-2}). In addition to the dissipation caused by the enlarged damage zone of the LCE network during crack extension, the hydrogen bonds between the polyurethane chains can also contribute to the overall toughening. [82,83]

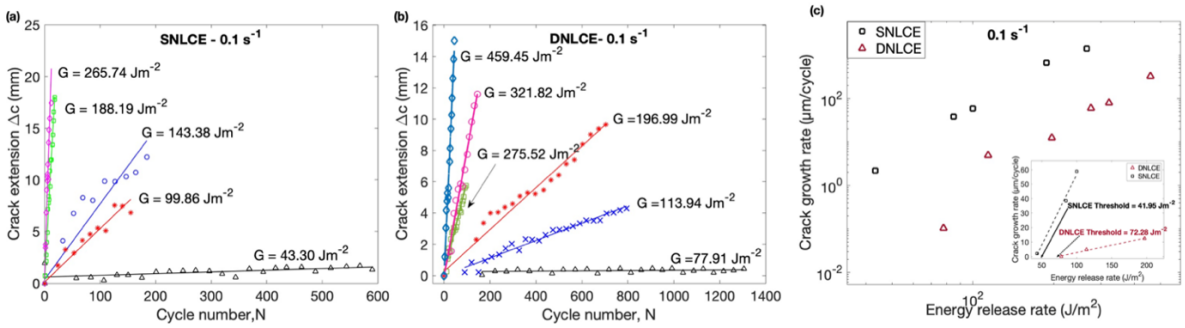

Figure 3.10: High temperature fatigue fracture of SNLCE and DNLCE samples (90°C). Crack extension with cycles at different energy release rates (G) for (a) SNLCE samples (b) DNLCE samples (c) Crack growth per cycle (dc/dN) as a function of the energy release rate (G) for SNLCE and DNLCE samples at 90°C. Inset : Determination of fatigue threshold by extrapolation. Fatigue threshold for SNLCE is 41.95 Jm^{-2} and for DNLCE is 72.28 Jm^{-2}. The loading rate is 0.1 s^{-1}.

A thermally actuating material like LCE is typically subjected to various mechanical loads and temperatures and is expected to function for many numbers of cycles. Though several elastomers and hydrogels have high toughness, they are typically prone to fatigue failure [44,84–87] . Figure 3.1 shows the schematics of the fatigue crack growth experiment. A precut sample of pure shear geometry was subjected to cyclic loading between $\lambda = 1$ to λ_{max} and the crack extension was recorded using a digital camera (Figure 3.11), which was plotted versus the cycle number (N) in Figures 3.10a and 3.10b, from which the crack growth rate (dC/dN) was calculated. Then a pristine sample was subjected to the same number of cycles between the similar stretches and the applied energy release rate (G) was calculated. Figure 3.10c shows the crack growth rate of SNLCE and DNLCE samples for various applied energy release rates. For the similar applied energy release rates, the crack growth rate is significantly lower for the DNLCE samples compared to SNLCE samples, thereby resulting in the increased high temperature fatigue life.

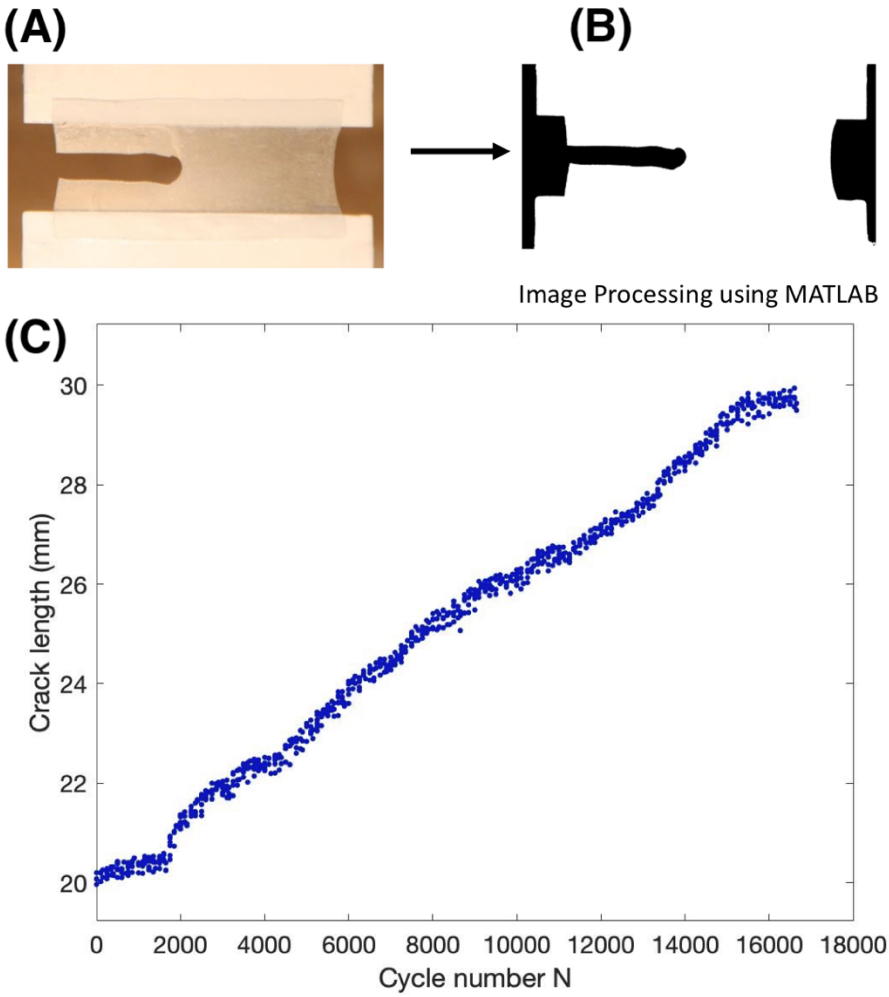

Figure 3.11: Crack growth in a precut LCE specimen subject to fatigue test; (a) Photograph of a precut-SNLCE sample with a precut taken using a digital camera; (b) The photo was converted to black and white, to measure the crack length using a custom MATLAB code; (c) Example - Crack length measurement is shown as a function of cycle number N, at room temperature.

The fatigue threshold is defined as the critical energy release rate above which fatigue fracture can take place and below which the material can be cyclically loaded without causing crack growth and rupture. It has been elucidated that toughening mechanisms based on covalent bond rupture can play a role in improving the fatigue threshold, while non-covalent mechanisms cannot, though both mechanisms can enhance the fracture toughness quite considerably [85]. At 90°C, the fatigue threshold of DNLCE was measured to be 72.28 Jm^{-2}, while the fatigue threshold of SNLCE is 41.95 Jm^{-2} at a strain rate of 0.1 s^{-1} (Figure 3.10 c, Inset). The fatigue threshold of SNLCE is close to the threshold value of fracture energy, as predicted by the Lake-Thomas model for various elastomers [47,49,88]. Due to their viscoelastic nature, the mechanical properties of LCEs show strain rate dependence [54]. As seen in Figure 3.12, at a higher strain rate of 0.5 s^{-1}, the fatigue crack growth rate is slightly lowered at the same energy release rates for both SNLCE and DNLCE. At 0.5 s^{-1}, the fatigue threshold of DNLCE was measured to be 131.22 Jm^{-2}, while the threshold for SNLCE was 36.25 Jm^{-2}. In a recent work on double-network elastomers with covalent bonds, strain hardening using a stiff first network and the resulting stabilization of the damage zone has been shown to considerably improve the fatigue threshold [89]. This shows that judicious fine tuning of the mechanical properties of the networks, allows substantial improvement of the fatigue and fracture properties.

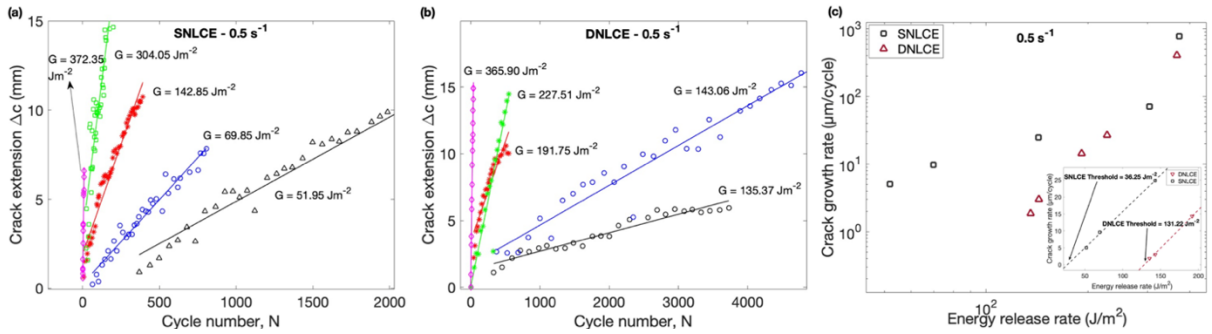

Figure 3.12: High temperature fatigue fracture of SNLCE and DNLCE samples (90°C). The loading rate is 0.5 s^{-1}. Crack extension with cycles at different applied energy release rates (G) for (a) SNLCE samples (b) DNLCE samples (c) Crack growth per cycle (dc/dN) as a function of the energy release rate (G) for SNLCE and DNLCE samples at 90°C. Inset : Determination of fatigue threshold by extrapolation. Fatigue threshold for SNLCE is 36.25 Jm^{-2} and for DNLCE is 131.22 Jm^{-2}.

For applications as a soft actuator, LCE is expected reversibly deform under the application of heat. To actuate a polydomain LCE, the mesogens need to be aligned along a director using a mechanical load, to get a monodomain LCE. We can also generate reversible actuation without any preload, by fixing the monodomain using additional UV crosslinking. In case of SNLCE, a monodomain LCE can be prepared by loosely UV-crosslinking the LCE oligomer (30s), then pre-stretching the loosely crosslinked network (λ_p = 2) to align the mesogens, followed by UV crosslinking (60 mins) to fix the monodomain. In case of DNLCE, the oligomer can be mixed with the PU precursors, followed by partial UV crosslinking (90s) of the acrylate LCE network. Once the PU network is allowed to form completely (48 hours of heating at 85°C), the DNLCE samples can be pre-stretched (λ_p = 2) and UV-crosslinked (60 mins) to align and fix the monodomain. Figure 3.13a shows the actuation stress generated by the LCE samples with fixed displacement and subjected to a temperature ramp from 20°C to 180°C.

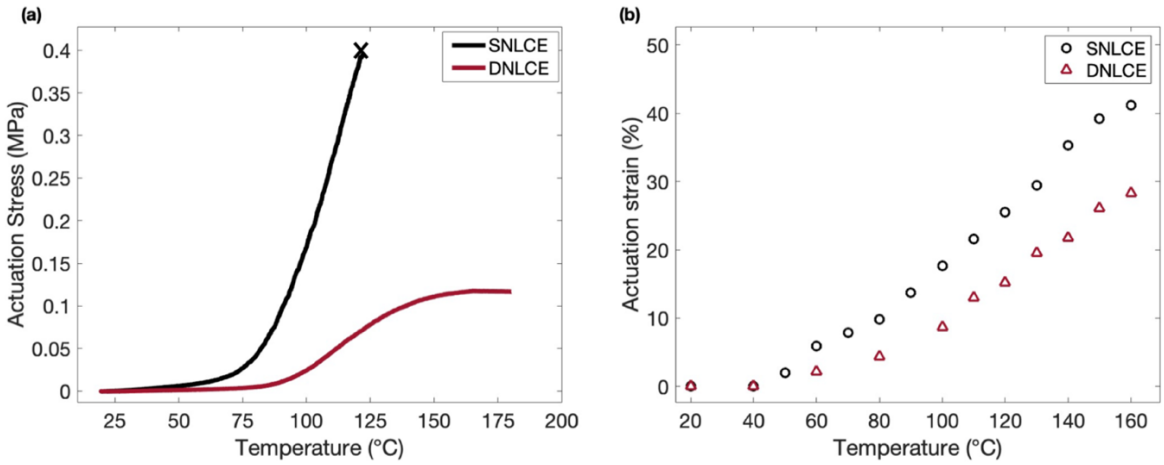

Figure 3.13: Thermal actuation properties of single network and double network LCE. (a) Actuation stress of monodomain SNLCE and DNLCE samples, crosslinked with an applied pre-stretch $\lambda_p = 2$. The samples were subjected to a temperature increasing from 20°C to 180°C with a ramp rate of 20°C/s. Note that the SNLCE sample ruptured at 122°C (indicated by the cross), while the DNLCE sample did not rupture at the end of the measurement at 180°C. (b) Actuation strains (%) of monodomain SNLCE and DNLCE samples in a free standing state and subjected to a temperature increasing from 20°C to 160°C.

At the same applied pre-stretch ($\lambda_p = 2$), DNLCE sample showed an actuation stress of 0.11 MPa while SNLCE samples showed an actuation stress of 0.39 MPa. The presence of interpenetrating and crosslinked PU network warrants a slightly higher pre-stretch for DNLCE to get an actuation stress comparable to that of SNLCE. The optimization of the actuation stress was not the objective of this study, which can be possibly improved by increasing the applied pre-stretch and adjusting the mol % of PU network reagents. Figure 3.13 b shows the actuation strains generated in monodomain SNLCE (41%) and DNLCE (29%) in free standing states. This shows that the IPN strategy can be used to improve the high temperature fracture and fatigue properties of LCE while preserving the actuation properties.

3.4 Conclusion

Here we report a method to enhance the high temperature fracture and fatigue properties of liquid crystal elastomers using interpenetrating networks. LCEs in general have poor high temperature fracture properties, due to diminished viscoelastic dissipation mechanisms. We show that by incorporating a soft and stretchable PU network, and tuning the crosslinking density, the overall fracture energy of DNLCE at high temperature can be significantly enhanced. The entanglement of the LCE and PU networks and the covalent bond breakage on loading can result in significant energy dissipation. Since the PU network doesn't show much mechanical deterioration with increasing temperature compared to the LCE network, a fracture energy of 655 Jm^{-2} is achieved for DNLCE at 90°C. Compared to SNLCE, the high temperature fatigue crack growth is also reduced significantly in DNLCE. The extensible PU network also allows us to apply mechanical stretch to align the mesogens, thereby retaining the actuation properties of LCE.

While entanglement and bond breakage can toughen DNLCE to an extent and delay fatigue crack growth, it does not eliminate fatigue fracture. Incorporating dynamic covalent bonds such as Diels alder chemistry [90], can enable reformation of the broken network by the application of heat, thereby restoring the fracture properties to an extent and significantly increasing the fatigue life. Further understanding of the effects of entanglements and phase separation in IPN, can lead to the development of mechanically robust materials. We hope that the results of this study can pave way for the creation of soft thermally actuating materials that are tough and fatigue resistant at various temperatures.

Acknowledgements

Chapter 3, in full, is a reprint of the material as it appears in Annapooranan, R.; Wang, Y.; Cai, S. Highly Durable and Tough Liquid Crystal Elastomers. *ACS Applied Materials & Interfaces* **2022**, *14* (1), 2006–2014. The dissertation author was the primary investigator and first author of this paper.

Chapter 4 Ultra Rate-Dependent Pressure Sensitive Adhesives Enabled by Soft Elasticity of Liquid Crystal Elastomers

4.1 Introduction

Pressure sensitive adhesive (PSA) is one of the most widely used non-structural adhesives in automotive and biomedical devices, electronic manufacturing and in consumer products such as packaging tapes, post-it notes and labels. PSA is typically a thin layer of viscoelastic polymer that can be used to adhere the surfaces of various materials using a light pressure, without the requirement of solvents or heat to activate adhesion[48,91]. Compared to other adhesives, PSAs offer advantages such as their easy application, clean residue free removal, compatibility with versatile materials and they could be customizable for both short and long-term usage. Generally any polymer system can be used to fabricate a PSA, as long as they satisfy the following criteria, 1) a low glass transition temperature to ensure rubbery phase in applications, 2) a low shear modulus that enables conforming to various surfaces without a large gain in strain energy, 3) elasticity to avoid flow or creep under long durations of application, 4) some tack for quick bonding and 5) viscoelasticity for energy dissipation on debonding[48,92]. These properties can be fine-tuned to an extent by controlling polymer architecture and crosslinking or by using additives like tackifiers and plasticizers, but the interdependence of the properties makes the materials design challenging. PSAs are traditionally prepared using acrylics, silicones, natural rubber and styrene-based block copolymers, with each family of materials having certain pros and cons for specific applications[93]. As PSAs are becoming ubiquitous, developing PSAs using polymers with special properties can enable novel applications.

Liquid crystal elastomer (LCE) is a class of functional materials, fabricated by the combination of liquid crystal monomers or mesogens with crosslinked polymer networks[94–96,5]. The interaction between the liquid crystal molecules results in a local ordering, which in combination with rubbery networks, yields distinctive features such as stimuli responsive actuation and non-linear elasticity under mechanical loading (soft elasticity)[95–98]. The readers can refer to a recent textbook and review articles for more information on LCE [41,99,100]. The unique actuation properties of LCE have been explored in various studies for applications in soft robotics, biomedical devices etc.[36,63,101–103] On the other hand, soft elasticity is observed in the uniaxial tension of LCE, as a plateau of constant low stress for a large deformation arising from the rotation of liquid crystal mesogens with little increase in the elastic energy[5,104–106]. Hence compared to a routine elastomer, LCEs show enhanced viscoelastic dissipation emerging from the inter-mesogen interaction in addition to the friction of typical polymer networks. These interactions have been exploited in various applications such as impact attenuation and frequency dependent mechanical damping[14,16–18]. LCEs show a pronounced temperature dependence of the nematic order and become an isotropic elastomer on heating beyond a critical transition temperature. This corresponds to the dramatic reduction of viscoelastic dissipation on heating, which is evident from the reduction of hysteresis and fracture energy[15,19,54,107,108]. Since adhesion is intricately related to viscoelasticity, the temperature dependence of LCE has been explored in developing "switchable" adhesives in recent studies[20,21,109,110]. In a theoretical study, Corbett and Adams reported the differences in the tack energy of LCEs with various nematic director orientations and the isotropic phase, highlighting a mechanism for reversible adhesion[20]. Cui and co-workers reported an array of LCE micropillars and attributed the tunable adhesion to the change in the height of micropillars driven by thermal actuation[109]. Only in the recent reports, the link between viscoelasticity of LCE

and adhesion was introduced and explored in detail.[21,110] The adhesive force of LCE measured using a probe-tack test was correlated to the loss tangent from DMA, both of which dramatically decreased on heating beyond the nematic to isotropic transition temperature. Moreover, this dynamic adhesion was found to be reversible over multiple heating and cooling cycles.[21,110] Dynamic adhesion of LCE has also been achieved using light as a stimulus, by the introduction of azobenzene moieties in the LCE network which undergo trans-cis isomerization under radiation and disrupt the nematic order[111–113]. While probe tack experiments have been mostly used to study the adhesive properties of LCE, peel test remains an important characterization method for adhesives due to its resemblance to real-world applications of PSAs and therefore the usefulness of the measured peeling force[114]. A recent work by Guo et al, explored the adhesion of LCE PSAs using Probe-tack, 90 degree peeling and lap shear tests[115]. Their results show that the adhesion of LCE depends significantly on the contact time, which is attributed to the nematic director reorientation and the slow relaxation of local stress. Although the work of adhesion for most of the PSAs are known to show rate and temperature dependence, a systematic study of the peeling of LCE PSAs and comparison with other PSAs has not been reported. Such a comparison can lead to deeper insights on leveraging the unusual properties of LCE for future designs of novel PSAs.

In this work, we fabricated a pressure sensitive adhesive using LCE and systematically performed peeling tests at various rates and temperatures, where we observed regimes of steady state peeling and unstable stick slip peeling. Compared to most PSAs in the literature, LCE adhesive exhibits extreme rate and temperature dependence of adhesion energy which is correlated to the dynamical mechanical properties and large strain behavior of LCE enabled by soft elasticity. Time temperature superposition was applied to the measured adhesion energy and a master peel

curve was generated spanning rates beyond experimental limits. Our results further reveal the unique properties of LCE compared to existing PSAs and will act as a guide for developing LCE based novel pressure sensitive adhesives in the future.

4.2 Methods

4.2.1 Materials

1,4-Bis-[4-(3-acryloyloxypropyloxy)benzoyloxy]-2-methylbenzene (RM257; Wilshire Technologies; 95%) , bisphenol A dimethacrylate (BPA, Sigma-Aldrich 98%), 2,2′-(ethylenedioxy)diethanethiol (EDDET; Sigma-Aldrich; 95%), pentaerythritoltetrakis(3-mercaptopropionate) (PETMP; Sigma-Aldrich; 95%), (2-hydroxyethoxy)-2-methylpropiophenone (HHMP; Sigma-Aldrich; 98%), dipropylamine (DPA; Sigma-Aldrich; 98%), Tetrahydrofuran (THF; Sigma Aldrich; 99%), Dimethylformamide (DMF; Sigma Aldrich; 99.8%), N,N,N′,N″,N‴-Pentamethyldiethylenetriamine (PMDETA,Sigma Aldrich' 99%) were used as received without further purification. PET backing film (75 μm thickness) was obtained from McMaster Carr.

4.2.2 Synthesis of LCE and BPA adhesives

The adhesives were synthesized using Michael addition reaction between acrylate and thiol monomers in presence of an amine catalyst based on previous literature, with minor modifications. Liquid crystalline monomer RM257 (10 g, 16.98 mmol) was dissolved in THF (3.15 g) at 85°C. To this mixture, EDDET (3.019 g, 16.64 mmol), PETMP (0.1037 g, 0.169 mmol) were added and

stirred. This corresponds to a mol % ratio of RM257/EDDET/PETMP = 100%/ 98%/2.5%. Finally, a solution of DPA (0.03441 g, 0.34 mmol) diluted in THF (1:50 by volume) was added, which was followed by stirring and degassing. Then the mixture was cast on PET films (25 mm wide) using a thin film applicator to obtain a final adhesive thickness of 50 μm. The PET films with the adhesives were left at room temperature for 48 hours and in an oven at 80°C and under vacuum overnight to completely remove the solvent. To prepare the BPA adhesives, the same procedure was used with the following ratio of the reagents: BPA (10 g, 27.4 mmol), EDDET (4.902 g, 26.89 mmol), PETMP (0.3458 g, 0.7 mmol) with the mol % ratio of BPA/EDDET/PETMP = 100%/ 95%/5% and 0.425g of PMDETA was used as the catalyst. To prepare the bulk samples for oscillatory and tensile testing, a glass mold was used and DMF was used as a solvent, to obtain uniform crosslinking through the bulk. BPA samples with 5 mol% crosslinking were used throughout the study to make comparisons with the crosslinked LCE adhesive. At this crosslinker ratio, BPA forms a poorly crosslinked polymer with a similar storage modulus to LCE. This way, we compare two adhesives with very similar small strain rheological properties, but with significant differences in the rate dependent adhesion. Such comparison method of using polymers with slightly different crosslinker content has been adopted in recent studies of mechanical energy dissipation of LCE and BPA elastomers[17], and in comparing the rate dependent adhesion of acrylic polymers[116].

4.2.3 Peel testing (180°) of adhesives

We performed the 180° peel test following the ASTM D3330 test procedure with some modifications. We used a Universal mechanical testing system (5965 Dual column testing system, Instron) fitted with a 5-kN load cell and a temperature chamber. The adhesive with the PET backing layer was bonded to a stainless-steel substrate using a weighted roller (4.5 lbs.) and was

allowed to remain for ten minutes inside the temperature chamber, to obtain a uniform temperature. The steel substrate was fixed to the bottom gripper and the tapes were peeled by the top gripper moving at a constant rate, from which we can obtain the steady state peel force (F). The energy release rate is given by G = 2*F/b, where b is the width of the tape (0.025 m). Under steady state peeling, the energy release rate G is equal to the work of adhesion Γ. According to the ASTM standard, the peeling rate is 5 mm/s. To gain more insight into the rate dependent behavior of LCE PSA, this experiment was repeated at various temperatures (-20°C – +90°C) and rates (0.5,1,5,10,50 mm/s).

4.2.4 Mechanical characterization of adhesives

Uniaxial tensile testing was conducted on the Instron tensile tester, using rectangular samples (height: 20 mm, width: 10 mm) which were stretched at a constant rate. The applied stretch (λ) is defined as λ = h/H, where H is the height of the sample in the undeformed state and h is the height of the sample in the deformed state. The nominal stress was calculated by dividing the force by the original cross-sectional area of the sample. The equivalent strain rates were calculated by multiplying the strain rates at different temperatures by the corresponding shift factor a_T, obtained from the DMA. The rheological characterization of the adhesives was conducted using the Discovery HR-3 Rheometer (TA Instruments) using a 20-mm steel parallel plate geometry. The oscillatory tests were conducted for a frequency range of 0.1 - 10 Hz and a temperature range of 0-50°C. Dynamic mechanical analysis tests were conducted on RSA-G2 (TA Instruments) using uniaxial tensile mode, with rectangular samples (height: 10 mm, width: 5 mm). The DMA tests were conducted for a frequency range of 0.01 - 10 Hz and temperature range of -20 to +90°C. The thickness of the samples used for all the mechanical characterization was ~0.5 mm.

4.3 Results and Discussion

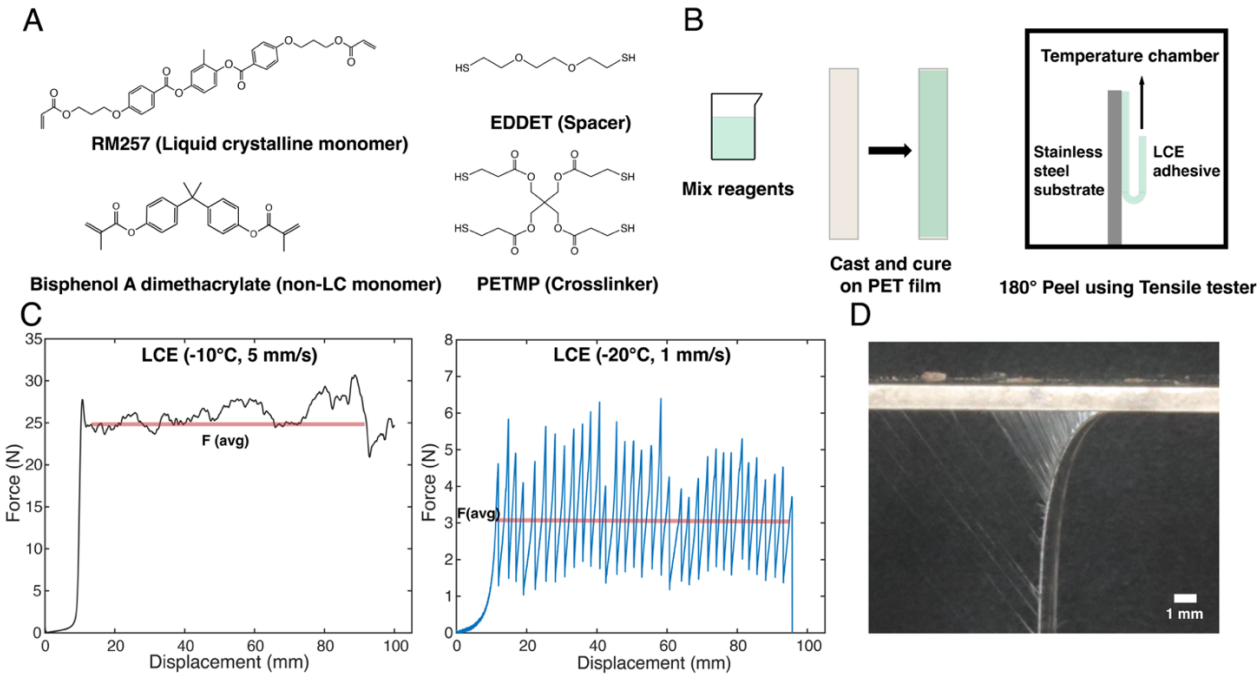

Figure 4.1: A) Chemical structures of the reagents used in the synthesis of the pressure sensitive adhesives. B) Schematic showing the fabrication of the adhesive on an inextensible PET backing film and 180° peel test with temperature control. C) Force displacement curves obtained from the peel tests, showing steady-state peeling (left) and stick-slip peeling (right). D) Photograph of the peeling front of LCE PSA peeled from a stainless-steel substrate using a hanging weight, showing fibrillation.

Figure 4.1 A shows the chemical reagents for the synthesis of the adhesives using Michael addition reaction between acrylate monomers and thiol spacers and crosslinkers in presence of an amine catalyst[38]. Two different monomers RM257 and Bisphenol A dimethacrylate (BPA) were chosen for comparison since RM257 is a liquid crystal monomer and BPA shows no liquid crystallinity[17]. Comparing these two materials could give a better insight by separating the contribution of liquid crystal mesogens and the polymer networks to viscoelastic dissipation and

adhesion. The reagents were mixed, cast on an inextensible PET backing layer, and allowed to crosslink at room temperature, followed by solvent removal. To perform a 180° peel test, the adhesives were bonded to a stainless-steel substrate and were pulled at a constant rate using a tensile tester fitted with a temperature chamber (Figure 4.1 B). More details of the experiment are provided in the experimental section. Figure 4.1 C shows the two types of force displacement curves obtained from the peel test for various combinations of peel rate and temperature. The curve on the left corresponds to steady-state peeling and the curve on the right corresponds to stick-slip peeling. The stick-slip peeling is associated with unstable crack propagation with complex dependence on rate, temperature, system inertia, material properties and loading control[114]. In both the cases, the average peel force (F) was used to calculate the work of adhesion (Γ) as $\Gamma = 2F/b$, where b is the adhesive width (0.025 m). Figure 4.1 D shows a snapshot from a 90° peeling of LCE PSA from a stainless-steel substrate using a hanging load. Despite the thickness of the LCE adhesive being ~50 µm, the formation of fibrils that are hundreds of µm long, points to the role played by large non-linear deformations in adhesion.

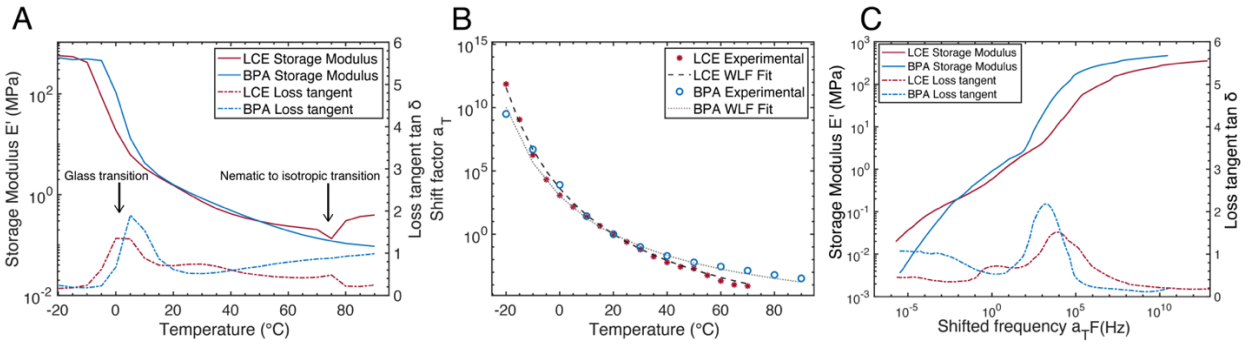

Figure 4.2: A) DMA temperature sweep of LCE and BPA polymers in uniaxial tension mode at 10 Hz, showing the curves of storage modulus (E') and loss tangent (tan δ). B) Horizontal shift factors a_T for LCE and BPA adhesives at various temperatures, with a best fit calculated using the WLF model. C) DMA Master curve of the storage modulus and loss tangent of LCE and BPA polymers, obtained by time temperature superposition of the results obtained at various temperature and frequencies.

The viscoelastic properties of the adhesives play an important role in the peel performance. Dynamical mechanical analysis experiments can provide the storage (E') and loss modulus (E") of the adhesives. The storage modulus (E') plays a crucial role in the bonding process, since the adhesive should be soft enough to conform to a surface and the elastic energy stored at the adhesive interface should not exceed the work of adhesion. On the other hand, the loss tangent, which is the ratio of (E"/E'), represents the energy dissipation of the adhesive during the debonding process. Typically, the peak of loss tangent corresponds to a material transition such as glass transition, which can lead to enhancement in the adhesion energy. Hence fine tuning these physical properties using chemical crosslinking and additives like tackifiers are crucial for the performance as a pressure sensitive adhesive[48]. Figure 4.2A shows the DMA temperature sweep of LCE and BPA bulk samples, performed at 10 Hz and 1% strain. Both LCE and BPA show comparable values of storage modulus at room temperature. From the peak of the loss tangent, we can define the glass transition temperatures of LCE to be ~ 0°C and of BPA to be ~10°C. BPA also shows an increasing loss tangent at higher temperatures, which indicates that it is an uncrosslinked (or very loosely crosslinked) polymer as compared to LCE. More discussion on the crosslinking of the adhesives is provided in the experimental section. For thermorheologically simple viscoelastic materials, we can generate a master curve of storage modulus and loss tangent at a reference temperature (T_{ref}) using the time temperature superposition principle [11,117]. The results from the oscillatory experiments at different frequencies and temperatures can be shifted horizontally on the frequency axis using a shift factor a_T, to obtain a master curve. Figure 4.2B shows the shift factors at various temperatures and the fitting according to the Williams-Landel-Ferry model (Equation 4.1).

$$log_{10}\, a_T = -C_1 * \left(\frac{T - T_{ref}}{C_2 + T - T_{ref}}\right) \quad (4.1)$$

This yielded the constants C_1 = 9.66 and C_2 = 73.38 K for LCE and C_1 = 7.56 and C_2 = 70.16 K for BPA at a T_{ref} = 20°C. Figure 4.2C shows the DMA master curve for LCE and BPA at a T_{ref} = 20°C, which spans a wide range of testing frequencies beyond the typical experimental limits. Note that the WLF superposition does not apply for the storage modulus of LCE across the nematic-isotropic transition, which occurs at ~75°C [16,17,21,110]. Therefore, an upper limit of 70°C was used in the construction of the master curve for LCE. Both LCE and BPA exhibit high values of loss tangent (tan δ >1) at rates corresponding to peeling (100-1000 Hz). BPA exhibits a higher peak value of loss tangent (~2), while LCE shows a much broader loss tangent curve, indicating energy dissipation across a wider range of strain rates. Typically, adhesives exhibit unstable crack growth in the glassy region of high strain rates to right of the loss tangent peak, and stable crack growth in the rubbery region of low strain rates to the left of the peak.[114]

Since most of the PSAs are very loosely crosslinked, the dynamic properties are typically evaluated by applying oscillatory shear strains using a rheometer. Likewise, we can obtain the complex shear modulus $G^* = \sqrt{G'^2 + G''^2}$, from the storage (G') and loss shear modulus (G") of LCE and BPA from a rheometer. The shear modulus of both LCE and BPA adhesives is less than 0.3 MPa at 1 Hz, which ensures good contact during the bonding process, as put forth by the Dahlquist criterion[118,119]. Similar to DMA, we can apply time temperature superposition for the results from the oscillatory rheological experiments. The Cox-Merz rule allows us to relate the steady-state and oscillatory experiments $G(\omega^{-1}) = G(t)$ and therefore we can transform the results to time domain [120] (Figure 4.3). Fitting a power law equation to the complex shear modulus curve ($G \sim t^{-\beta}$) yields an exponent of β ~ 0.4 for both LCE and BPA in the range of rates

corresponding to peeling. This has similarities to the observations from previous studies that polymers can exhibit similar properties under small strain measurements, but their large strain behavior can lead to dramatic differences in their adhesion properties[116].

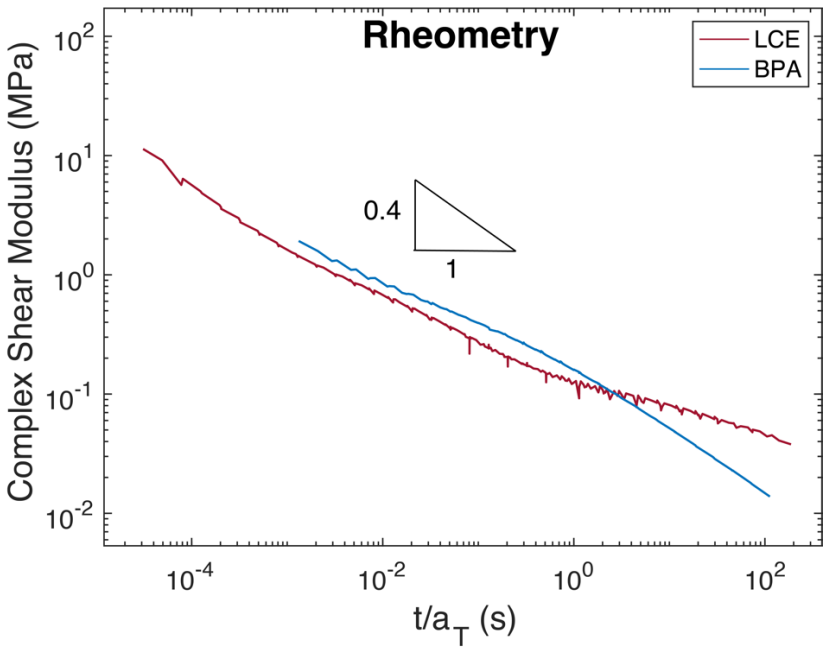

Figure 4.3: Master curve of the complex shear modulus (G*) constructed from the time temperature superposition of complex shear modulus obtained at various temperatures and frequencies. The complex shear modulus shows an approximate time dependence of $G \sim t^{-\beta}$, with $\beta \sim 0.4$ for both LCE and BPA at the time scales corresponding to the peel test.

Figure 4.4 shows the work of adhesion of LCE and BPA, measured from the peel experiments performed at various temperature and a peel rate of 5 mm s^{-1}. At low temperatures (-20°C – 0°C), the adhesion energy of LCE is higher compared to BPA and reaches a maximum of ~ 2.1 kJ/m^2 at 0°C. On further increasing the temperature, the LCE adhesive shows a rapid decrease in the adhesion energy, to 500 J/m^2 at 10°C and 120 J/m^2 at room temperature. On the other hand, BPA shows a maximum adhesion energy of 2.1 kJ/m^2 at 10°C and 760 J/m^2 at room temperature. The temperature corresponding to the peak adhesion energy of LCE and BPA could be related to the respective glass transition temperatures, as seen in Figure 4.2A. On increasing the temperature by 10°C from T_g, LCE shows a 75% decrease in the adhesion energy, compared to BPA which

shows a 55% decrease from the peak value. While viscous dissipation is known to decrease with heating in all polymers[56,121], the nematic to isotropic transition of the liquid crystal mesogens could additionally contribute to the steeper drop in the adhesion energy of LCE[21,54,110]. The applicability of time-temperature equivalence to LCE PSA, hints the role played by bulk dissipation in the extreme rate dependence of LCE adhesives.

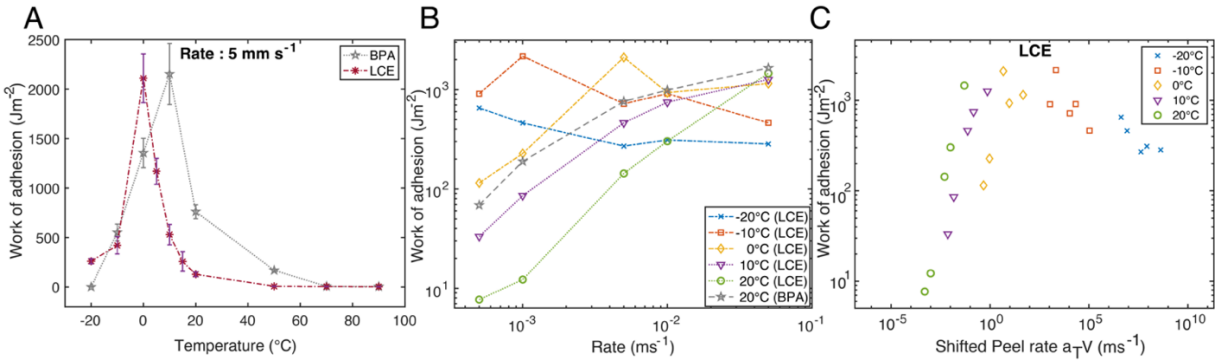

Figure 4.4: A) Work of adhesion of LCE and BPA adhesives measured from the peeling tests at a peel rate of 5 mm s^{-1} and a temperature range of -20°C to +90°C. B) Work of adhesion of LCE and BPA adhesives measured from peeling tests at various rates and temperatures. C). Master peel curve of LCE obtained by the time temperature superposition of work of adhesion results of peel experiments at various rates and temperatures shown in Figure 4.3B.

Figure 4.4B shows the work of adhesion of LCE at various rates and temperatures. At temperatures above the glass transition, the adhesion energy of LCE (Γ) shows a strong dependence on the rate (V). Fitting the room temperature adhesion energy with a power law $\Gamma \sim V^n$, yields an exponent of n~1.17 for LCE, compared to n~0.62 for BPA, though both LCE and BPA showed similar power law dependence of the complex shear modulus, obtained from linear viscoelastic measurements (Figure 4.3). The results of LCE and BPA show similarities to the results from a previous study on the peeling of two acrylic polymer PSAs, where the polymers showed comparable linear rheological properties but one of the polymers showed significant strain

stiffening compared to the other. [116,122] The adhesion energy of the polymer with strain stiffening showed a stronger rate dependence compared to the loosely crosslinked polymer. By applying time temperature superposition, the results from the peel experiments can also be shifted horizontally using the shift factors a_T obtained from DMA, yielding a peel master curve across various rates at a $T_{ref} = 20°C$ (Figure 4.4C). The master curve obtained from superposition, qualitatively resembles the peel master curves of various PSAs in literature, showing a positive slope in the regimes of cohesive failure at low to intermediate rates and showing a negative slope of unstable interfacial failure at high rates. [117,123–125]

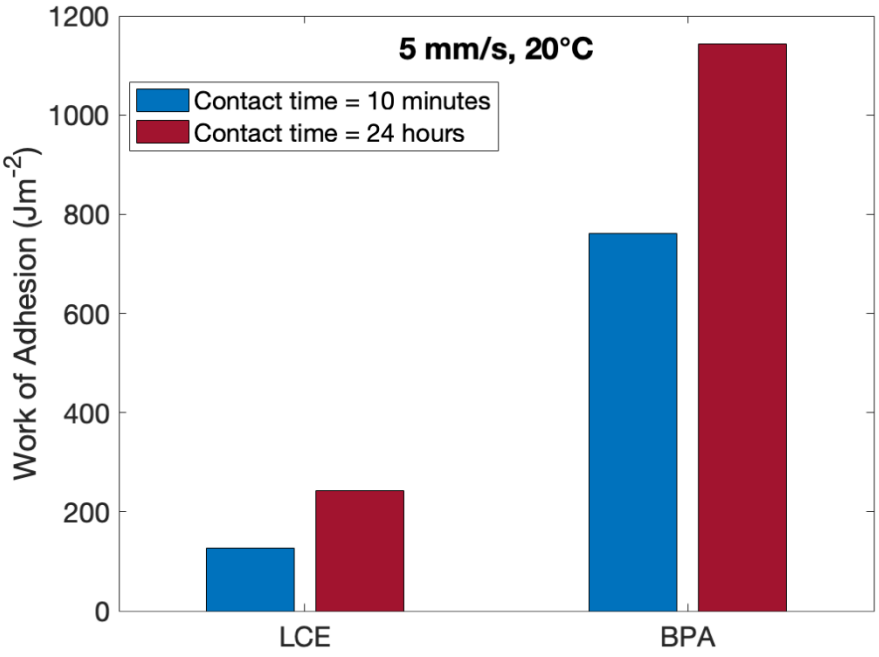

Figure 4.5: Bar graph showing the effect of contact time in the adhesion energy of LCE and BPA adhesives, for two contact times of 10 minutes and 24 hours at a peeling rate of 5 mm/s and at room temperature.

In previous reports, contact time has been found to significantly affect the adhesion strength of PSAs[126,127]. In this work, we performed the peel experiments after 10 minutes of adhering to the stainless-steel substrate, to allow uniform heating and cooling before the peel test. The effect of contact time to the adhesion energy of LCE is shown in Figure 4.5, which is similar to the results from a recent study on LCE adhesion[115].

Despite the similarities in the small-strain rheological and oscillatory properties, LCE and BPA exhibit remarkable differences in adhesion. Although there are several reports in the literature which offer significant insights towards viscoelastic adhesives, they are based on the assumption that the rate-dependent adhesion is governed by linear viscoelasticity, which is inconsistent with our experimental observation[128–130]. Indeed, the importance of nonlinear stress-strain behavior in the adhesion PSA has been recognized in the literature[48,116,117,130]. In the model proposed by Gent and Petrich[117], the work of adhesion (Γ) is given by

$$\Gamma = a \int_0^{\varepsilon(\sigma_c)} \sigma(\varepsilon, \dot{\varepsilon})\, d\varepsilon \tag{4.2}$$

where the integral denotes the work per unit volume to deform the PSA material to a critical stress (σ_c) under uniaxial extension and a is the thickness of the adhesive. Unlike theoretical models that treat the detachment of viscoelastic adhesives as a process of interface crack propagation [128,129], soft PSAs can undergo large stretch at the peel front and deform into an array of fibrils (Figure 4.1 D). Consequently, adhesion is dominated by the total work to stretch and break the fibrils under uniaxial extension. For example, a polymer which can undergo a large extension during the debonding stress can result in a greater work of adhesion compared to a polymer which stiffens at a much lower strain.

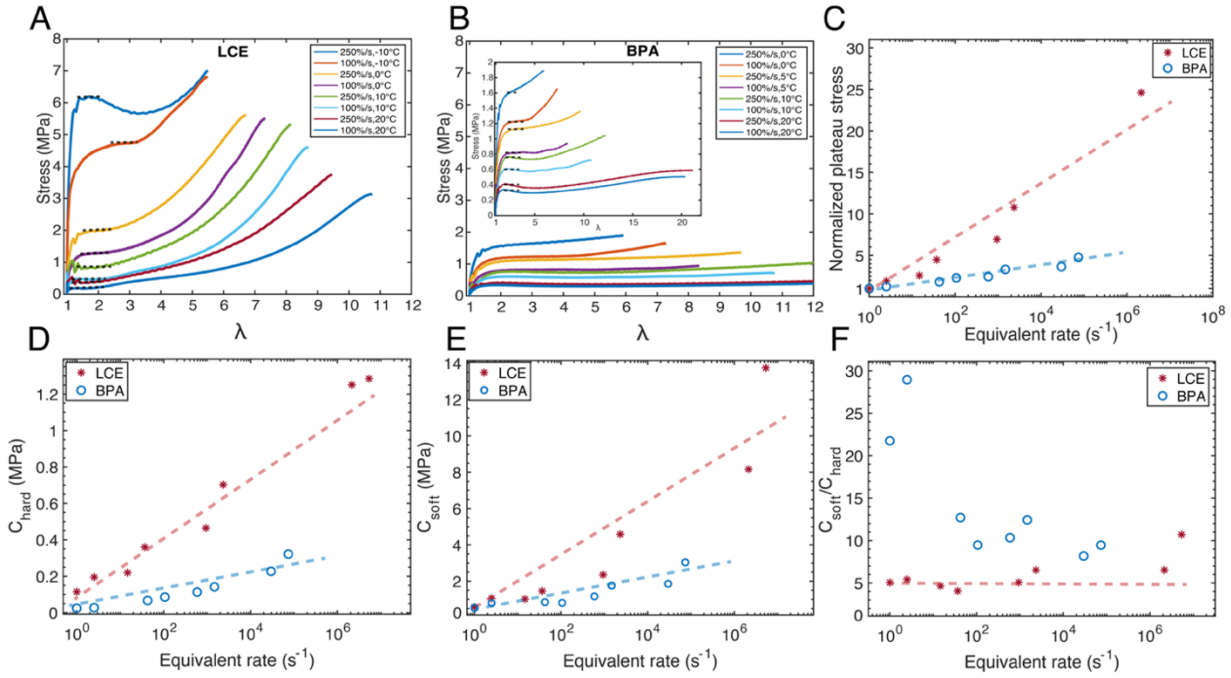

Figure 4.6: Uniaxial tensile stress-strain curves of A) LCE and B) BPA polymer at various strain rates and temperatures, showing a linear portion, plateau (dashed lines) and a strain stiffening regime. C) The magnitude of normalized plateau stress of LCE and BPA at equivalent strain rates. The plateau stress is normalized by the value at the equivalent rate of 1 s^{-1}. D) C_{hard} and E) C_{soft} values of LCE and BPA at various strain rates. The parameters C_{hard} and C_{soft} were obtained from the Mooney plot. F) The ratio of C_{soft} / C_{hard} at various strain rates. The dashed lines are guide for the eyes.

To probe the large strain behavior, bulk LCE and BPA samples were subjected to uniaxial tensile tests at rates of 1 s^{-1} and 2.5 s^{-1} and various temperatures (Figure 4.6A and 4.6B). The stress-strain curves of LCE and BPA show similarities across different rates, starting with a linear portion, followed by a plateau and finally a strain stiffening regime and failure, typical to PSAs[48,116,117]. Limited by the maximum velocity of the tensile tester, we performed tensile tests at higher equivalent strain rates by lowering the temperature down to T_g -10°C. The equivalent strain rates were calculated by multiplying the strain rate at a given temperature by the corresponding shift factor a_T, shown in Figure 4.2B[117]. The shift factors from the DMA experiments were used to calculate the equivalent rates for the uniaxial tensile experiments, since both the experiments

have similar loading modes and due to the better temperature control of our DMA instrument. With increasing strain rates, both LCE and BPA showed increase in the magnitude of the plateau stress (marked by dashed lines), increase in the failure stress and reduction of failure strains. For typical polymer networks at high strain rates, the lack of time for relaxation of entanglements results in stress buildup without showing the plateau stress[48,117,122]. In the case of LCE, even at high velocities, there is an increase in the plateau stress with comparatively high failure strain, resulting in drastic strain stiffening and a large work of rupture. The increase in the plateau stress with increasing rates is significantly higher for LCE compared to BPA (Figure 4.6C). We believe that similar dependence of modulus at high strain rates have been ascribed to non-equilibrium nematic effects, though LCE behaves like an isotropic elastomer at sufficiently low strain rates or equivalently at high temperatures[19,54].

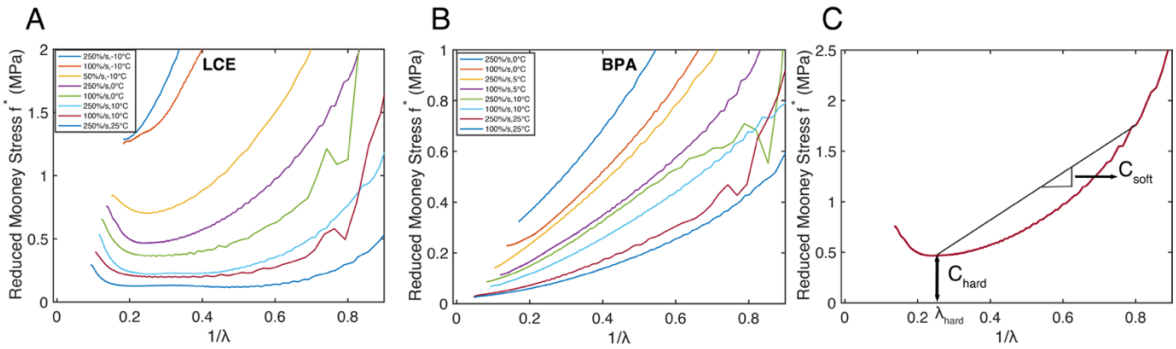

Figure 4.7: Mooney plot for A) LCE and B) BPA adhesives at various strain rates and temperatures. C) Example of a Mooney plot showing the estimation of the parameters C_{hard} and C_{soft}.

At increasing strain rates, the presence of a large plateau in the stress-strain curve and the increase in the magnitude of plateau stress, indicates that LCE adhesives can withstand large deformation without debonding. In both the adhesives, the use of low boiling point solvent (THF) in the casting might have possibly resulted in a slightly weaker crosslinking than their bulk counterparts. Still the differences in the stress-strain curves highlight the superior dissipation of

LCE at high strain rates, due to soft elasticity.

To gain more quantitative insights from the nonlinear large strain behavior, we can represent the tensile data using the Mooney plot of reduced stress f^* versus the inverse of stretch $1/\lambda$ (Figure 4.7A and 4.7B) [48,131–133]. The reduced stress is given by

$$f^* = \frac{\sigma}{\lambda - \lambda^{-2}} \tag{4.3}$$

where σ is the nominal stress and λ is the stretch. For a loosely crosslinked adhesive, the reduced stress decreases with increasing λ, due to the relaxation of entanglements, followed by a minimum and an increase of the reduced stress at large values of λ, corresponding to strain stiffening by permanent crosslinks. For an uncrosslinked adhesive, there is no increase in the reduced stress at large values of λ, resulting in flow. The Mooney plot of LCE resembles to that of a crosslinked polymer, while the Mooney plot of BPA resembles to that of an uncrosslinked polymer[48].

From the Mooney plot, we can separate the shear modulus 'μ', into two components C_{soft} and C_{hard} (Figure 4.7C). C_{soft} represents the contribution from the relaxation of temporary intermolecular interactions to strain softening, while C_{hard} represents the contribution of the permanent crosslinks, which do not relax, to strain hardening. Following the literature, C_{hard} is obtained from the reduced stress f* at the minimum and C_{soft} is obtained from the slope between the points [f*(0.8), 0.8] and [f^*_{min}, $1/\lambda_{hard}$], where λ_{hard} corresponds to the stretch value at the minimum. Figure 4.6D and 4.6E, show the C_{hard} and C_{soft} values of LCE and BPA adhesives at various strain rates respectively. C_{soft} and C_{hard} values of LCE show significant rate dependence

compared to BPA, similar to the normalized plateau stress (Figure 4C). The extreme rate dependence exhibited by LCE adhesives can be attributed to the contributions from the liquid crystal mesogens to both softening and stiffening components. Additionally, the ratio of C_{soft} / $C_{hard,}$ represents the balance between the adhesive's ability to dissipate and sustain stresses at large deformations. A large value of C_{soft} / C_{hard} means that the adhesive is likely to flow under high strains, while a very small value of C_{soft} / C_{hard} means that the adhesive is highly crosslinked and favors interfacial crack propagation. It has been reported in the literature that optimized commercial PSAs typically possess a value between 2-5[131–133]. Figure 4.6F, shows the values of C_{soft} / C_{hard} of LCE and BPA, at various strain rates. Despite showing a strong rate dependence of C_{soft} and C_{hard} values separately, the ratio of C_{soft} / C_{hard} for LCE remains close to 5, across a wide range of strain rates. This hints that LCE adhesives show a good balance between energy dissipation and load bearing.

Figure 4.8A compares the rate dependent work of adhesion during stable crack growth of LCE and BPA adhesives with other PSAs from literature, which includes commercially available PSAs such as 3M Scotch 600 or Scotch 3450 RD [116,117,122,124,134–139]. When fitted with a power law, $G \sim V^n$ yields an exponent value between n~0.1 to 0.6 for typical PSAs. Though the value for the BPA falls close to that range (n~0.62), LCE exhibits an abnormally high value (n~1.17). Following the Gent-Petrich model, the following observations can be made: 1.) For most of the typical PSAs under uniaxial tension, increasing the strain rate results in the stiffening and stress buildup at modest strains and the disappearance of any stress plateaus[48,117,122]. In the case of LCE, the plateau stress is evident even at high strain rates. Hence it is reasonable to assume that the debonding strain of the LCE adhesives does not decrease as much as the typical PSAs at higher strain rates.

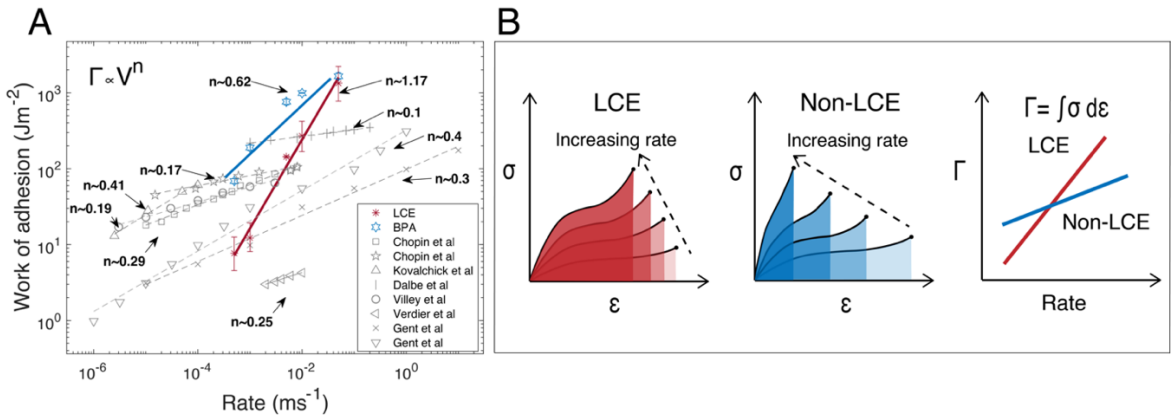

Figure 4.8: A) Comparison of the rate dependent adhesion of LCE (red asterisk) and BPA (blue star) adhesives, with different pressure sensitive adhesives from the literature, Chopin et al (custom made acrylic adhesive), Kovalchick et al (3M Scotch 3450S-RD), Villey et al (custom made acrylic adhesive), Dalbe et al (3M Scotch 600, from a modified substrate), Verdier et al (custom made PDMS adhesive) and Gent et al (Butadiene-styrene copolymers). The solid lines show a power law fit ($\Gamma \sim V^n$), with traditional PSAs showing values of exponent n~0.1-0.6, while LCE shows an anomalously high n~1.1. The error bars on the LCE and BPA data correspond to one standard deviation (n=3). B) Schematic showing the relationship between the uniaxial tensile properties and the difference in the rate dependent adhesion energies of LCE and other PSAs.

2.) Though BPA also shows a plateau stress at a range of strain rates, the increase in the magnitude of plateau stress of LCE is more significant for LCE compared to BPA (Figure 4C). Furthermore, in a typical polymer network, the C_{soft} and C_{hard} values from Mooney plot, correspond to softening due to the relaxation and stiffening due to the permanent crosslinks respectively. In the case of LCE, there is an additional contribution from the rotation of liquid crystal mesogens and their associated viscosity. The combination of the large plateau in the stress-strain curve, and the corresponding increase in the magnitude of plateau stress at high strain rates, likely results in the ultra-rate sensitivity of LCE adhesive, as illustrated by the schematic in Figure 4.8B. In the Gent - Petrich model[117], the work of adhesion (Γ) was predicted using the uniaxial stress-strain curves of the adhesives and a suitable debonding criterion for the upper limit of integration of Equation 4.2, such as a critical debonding stress. The more recent work of Chopin et al, used a debonding

criterion of rate dependent critical stretch, obtained from imaging the fibrils during peeling, to predict the adherence energy of acrylic PSAs[116]. Following these works, the prediction of adhesion energy using an assumption of constant debonding stress or a constant debonding strain was not valid for LCE, which can be due to complex stress states of the fibrillation process compared to simple uniaxial tension. Further imaging at the peel crack front to carefully determine the fibril peeling criterion at different rates and complementary information from probe-tack tests, could help obtain a more suitable upper limit of integration for Equation 4.2 and yield better predictions for LCE adhesives. [140,141]

Though the detailed quantitative predictions of the rate dependent adhesion demand further investigation, the extreme rate dependence of LCE's adhesion energy can be exploited for applications such as transfer printing, which is widely used in the fabrication of flexible electronic devices[142,143]. Here the rate dependent adhesion is desired for transferring and adhering thin layers of materials to various substrates. The rapid advancements in the chemistries of LCEs, allows fine tuning of the glass transition temperature, nematic to isotropic transition temperatures, inter-mesogen interactions and response to other stimuli like light[41,144,145]. By utilizing liquid crystal monomers like RM82, which exhibits crystallinity at room temperature or by spatially controlling the crosslink density using two-step UV crosslinking, we can introduce heterogeneity in the adhesive stiffness, which could lead to further enhancement of adhesion[146,147]. With the results from the current work and the progress in the field of LCEs and adhesion in general, there are lot of prospects for developing robust pressure sensitive adhesives for various novel applications[148–150].

4.4 Conclusion

Though the frequency and temperature dependent dissipation properties of liquid crystal elastomers have been explored in several recent studies, the systematic peel experiments of LCE PSA and comparison with other PSAs has not been reported. We show that pressure sensitive adhesives fabricated using liquid crystal elastomers exhibit significant temperature and rate dependence of adhesion energy, compared to the PSAs in literature. The rate and temperature dependence arises from soft elasticity and strong non-linear viscoelasticity of LCE enabled by inter-mesogen interaction and polymer chain friction. Time temperature superposition has been shown applicable for all the viscoelastic properties and adhesion energy of LCE. The advancements in the LCE chemistries can allow further fine tuning of adhesion properties, which can deliver functions typically inaccessible to traditional polymers, such as reversible and frequency dependent adhesion. We hope that the results from this study can lead to the development of novel PSAs and enable new applications of LCE.

Acknowledgements

Chapter 4, in full, is a reprint of the material as it appears in Annapooranan, R.; Suresh Jeyakumar, S.; J. Chambers, R.; Long, R.; Cai, S. Ultra Rate-Dependent Pressure Sensitive Adhesives Enabled by Soft Elasticity of Liquid Crystal Elastomers. *Advanced Functional Materials* **2024**, *34* (1), 2309123. The dissertation author was the primary investigator and first author of this paper.

Chapter 5 Enhanced adhesion of liquid crystal elastomers on rough surfaces

5.1 Introduction

Pressure sensitive adhesives (PSAs) are one of the widely used adhesives in engineering applications, which enable quick contact between various surfaces using a gentle pressure without requiring additional chemical reactions or stimuli such as heat or UV radiation[48,91,92]. PSAs consists of blending loosely crosslinked viscoelastic polymers such as natural rubber, acrylates, silicones and styrenic block copolymers, with additives to achieve a low shear modulus ($G < 10^5$ Pa) to create a good conformal contact on various substrates. Owing to their ease of application and compatibility with different materials, PSAs are used in household products such as tapes and in automotive, aerospace, electronics, and medical industry.[92] Depending on the application, the viscoelastic properties of PSAs are fine-tuned by formulating the polymer network, crosslinking, using additives such as tackifier, plasticizers and rheological modifiers. Despite the wide variety of synthetic and processing techniques, the complex interaction between the additives and the base polymer complicates the design of PSAs. [93,151] Due to their simplicity and versatility, there is an increasing demand for superior PSAs for existing and new applications.

The adhesive properties of various classes of PSAs have been studied using various standard testing methodologies such as peel, probe-tack and lap-shear tests, typically on smooth substrates such as glass or stainless steel[48]. Real world surfaces consist of various inherent irregularities or asperities ranging from hundreds of nm to microns that contribute to their roughness[152,153]. This led to the various studies on the effect of roughness on adhesion[154–157]. Roughness has been found to generally decreases the adhesion energy of PSAs as the presence of asperities can affect the effective contact area between the adhesive and the substrate [153,158]. While crosslinking a polymer adhesive endows it with strength and creep resistance over long durations,

the compliance of the polymer (1/modulus) is inversely related to the crosslink density. When the crosslinked adhesive makes contact over a rough surface with asperities, it deforms and gains elastic strain energy. This stored strain energy gets released during the adhesive debonding and drives crack growth, leading to poor adhesion strength[159]. The compliance of the polymer can be increased by reducing the crosslink density but will reach a limiting value for an uncrosslinked polymer due to chain entanglements[2]. Due to the paradox between compliance and strength, it is challenging to design adhesives that provide good bonding on rough surfaces[159,160]. Various strategies have been reported for overcoming this trade-off, such as swelling the polymer network with solvents, curing a liquid adhesive precursor, bottlebrush elastomers, supramolecular bonded gels, shape memory polymers and using structural designs[161–163]. Swelling a polymer with a solvent can lead to low modulus, but solvent leaching and interaction with the substrates are unfavorable in applications. A liquid precursor can sufficiently wet rough surfaces but requires additional chemical reaction for curing such as heat or UV radiation[93]. Bottlebrush elastomers can possess high compliance by using polymer architecture that favors disentanglement but can require complex synthesis[161,162,164]. Recently Wu et al proposed a supramolecular gel doped with an ionic liquid, which can conform to various substrates due to the inherent softness and show excellent adhesion due to intermolecular interactions and rate dependent phase separation[165]. Despite the high adhesion toughness, the ionogels are susceptible to humidity and creep, thereby limiting their applications. Due to their shape retaining ability under heating and cooling, shape memory polymers have been shown to adhere to rough surface in the soft rubbery state and debonding in the stiff glassy state[166]. However, the application of heat during the bonding process can be impractical for many applications. Hence, an adhesive that is soft enough to conform over

asperities without gaining a large strain energy and possess sufficient strength on debonding is highly desired.

Liquid crystal elastomers (LCEs) are a class of novel polymeric materials, which possess unique anisotropic properties such as non-linear viscoelasticity, soft elasticity and stimuli-responsiveness emerging from the combination of liquid crystal mesogens with elastomeric networks[5,9,41,94,95]. In addition to the chain friction in traditional polymer networks, the rotation of liquid crystal mesogens have been shown to result in the large energy dissipation of LCEs. These novel properties have been harnessed in various studies for applications as soft actuators, impact damping and, more recently in adhesion[16,21,110,115,167–169]. On heating beyond the nematic transition temperature, LCEs become an isotropic elastomer and show a pronounced decrease in viscoelastic dissipation[15,19,54,107,108]. This temperature dependence has been exploited for developing various reversible adhesives[20,21,110]. The disruption of nematic order can also be achieved using light as a stimulus in LCEs crosslinked with azobenzene functional groups, leading to dynamic adhesion triggered by radiation[112]. Under uniaxial tension, loosely crosslinked LCEs show pronounced ductility and a large deformation at a constant plateau stress, a property known as soft elasticity.[14,104–106] A recent study from our group showed that this unique non-linear stress strain behavior of LCE resulted in an abnormally high-rate dependence on peeling of LCE PSAs compared to traditional polymeric adhesives[169]. Guo et al showed that the adhesion strength of LCE adhesives under peeling and probe tack tests, increased significantly at long contact times[115]. This enhancement of adhesion was attributed to the relaxation of local stresses and the slow reorientation of the nematic domains, which has been reported in similar earlier studies. Therefore, in contrast to most traditional polymers, LCEs can simultaneously exhibit liquid like properties

due to soft elasticity which can be favorable for bonding to rough surfaces and solid-like properties due to crosslinking of polymer networks which provides strength on debonding.

In this study, we explore the adhesion of polydomain LCE on various rough surfaces using probe tack, lap shear and indentation experiments. We compare the results of LCE with that of a commercial acrylic foam tape (3M VHB 4910). We observe that on very rough surfaces, the adhesion of both LCE adhesive and the acrylic adhesive decreases. However, on increasing the contact time from 1 min to 1000 mins, the adhesion strength of LCE adhesive can be enhanced quite significantly on a very rough surface. We believe the underlying mechanism responsible for the observation is the long relaxation time scale and soft elasticity of LCE. This enables LCE to overcome the adhesion paradox faced by traditional polymer adhesives and broadens the scope of PSAs for more challenging real-world applications.

5.2 Methods

5.2.1 Materials

1,4-Bis-[4-(3-acryloyloxypropyloxy)benzoyloxy]-2-methylbenzene (RM257; Chemfish Japan; 98%), 2,2′-(ethylenedioxy)diethanethiol (EDDET; Sigma-Aldrich; 95%), pentaerythritoltetrakis(3-mercaptopropionate) (PETMP; Sigma-Aldrich; 95%), dipropylamine (DPA; Sigma-Aldrich; 98%), Butylated Hydroxytoluene (BHT; 99% Sigma-Aldrich) Toluene (Fisher Scientific; 99%), were used as received without further purification. 304 Stainless steel strips were obtained from McMaster Carr and 304 Stainless steel balls were obtained from Uxcell, Amazon.

5.2.2 Synthesis of LCE adhesive

Polydomain LCE adhesive was synthesized using Michael addition reaction between acrylate capped liquid crystal monomer (RM257), thiol spacer (EDDET) and thiol crosslinker

(PETMP) in presence of an amine catalyst (DPA). Liquid crystalline monomer RM257 (15 g, 25.48 mmol) was dissolved in Toluene (4.725 g) at 85°C. To this mixture, EDDET (4.529 g, 24.84 mmol), PETMP (0.155 g, 0.318 mmol) were added and stirred. This corresponds to a mol % ratio of RM257/EDDET/PETMP = 100%/ 97.75%/2.25%. Finally, a solution of DPA (0.075 g, 0.74 mmol) diluted in Toluene (1:50 by volume) was added to the reaction mixture and stirred. The solution was degassed, poured in a glass mold, and left at room temperature for 24 hours. Then the loosely crosslinked LCE was placed in an oven at 85°C to completely remove the solvent. The crosslinking density is chosen such that it is just above the gel point or point of percolation of the network so that there is no flow.

5.2.3 Substrate preparation

To introduce surface roughness, 304 stainless steel spheres and rectangular strips were subjected to gritblasting using Aluminum oxide particles (24 and 100 grit for the medium and high roughness cases respectively) at a pressure of 80 psi. The roughness of the substrates was characterized using a Filmetrics Profilm 3D optical profiler by white light interferometry.

5.2.4 Lap shear testing of adhesives

We performed the Lap shear test following the ASTM D1002 test procedure, using Universal mechanical testing system (5965 Dual column testing system, Instron) with a 1-kN load cell. The adhesive (~0.95 mm thickness) was placed in between two stainless steel strips (100mmx25.4mmx1.6 mm) with an overlap area of 25.4 mmx25.4 mm. A 500g load was placed on the strips for a certain time to ensure good bonding of the adhesive and the substrate. Then the strips were placed between the grips of a tensile tester and separated at a rate of 1.3 mm/min. The shear stress was calculated by the relation F/(B*L), where F is the measured force, B and L is the

width and length of the overlap area of the adhesive respectively. The experiment was repeated for different contact times and substrate roughness (n=3-5).

5.2.5 Probe tack testing

We performed the probe tack testing of adhesives using the Instron tensile tester. The adhesives were adhered to a flat glass substrate whose position was fixed. A spherical probe (304 stainless steel, 25 mm diameter) was brought into contact with the adhesive at a rate of 0.01 mm/s until a compressive force of 0.5 N was reached. This compressive force was maintained for various contact times (1-100 mins). Then the probe was retracted at a rate of 0.01 mm/s and the peak force was recorded. This experiment was repeated for different contact times and probe roughness (n=3-5).

5.2.6 Mechanical characterization of adhesives

We performed the uniaxial tensile testing of the adhesives using rectangular samples (length: 20 mm, width: 10 mm), bonded on acrylic plates on the Instron tensile tester. Strain (ε) is defined as $\varepsilon = (LF - Lo)/Lo$, where Lo is the length of the sample in the undeformed state and LF is the height of the sample in the deformed state. The nominal stress was calculated by dividing the force by the original cross-sectional area of the sample. The experiment was performed at a strain rates of 0.05 %/s.

5.2.7 Micro-Indentation

We conducted a comparative analysis of the adhesion strength between LCE and VHB using the Bruker Hysitron BioSoft in-situ indenter, which comes with a maximum displacement capacity of 175 μm and a maximum load limit of 10 mN during indentation, and 500 μN during

debonding. To perform the indentation on the sample surfaces, we employed a flat-ended conical probe tip (Ti-0149) with a diameter of 109 microns and a cone angle of 90 degrees. Our experiment involved indenting the adhesive samples up to a load of 50 μN and maintaining this load for varying durations (10 seconds, 1 minute and 10 minutes. After the desired holding period, probe was unloaded until complete detachment from the sample occurred. During the loading and unloading of the probe, displacement control with a rate of 1μm/s was used. During the holding period, force control was used. The experiments were repeated for 3-4 times at each holding period.

5.3 Results and Discussion

Figure 5.1A shows a schematic comparing the polymer network structure of a pressure sensitive adhesive and a polydomain LCE adhesive. A traditional PSA is a viscoelastic polymer, which is loosely crosslinked to avoid creep and contains additives like plasticizer and tackifiers to modify the modulus and rheological properties[91]. Liquid crystal elastomers comprise of liquid crystal monomers known as mesogens combined in an elastomeric network using flexible polymer spacers and crosslinkers. A simple one step polymerization reaction results in a polydomain LCE network without any macroscopic alignment[38].

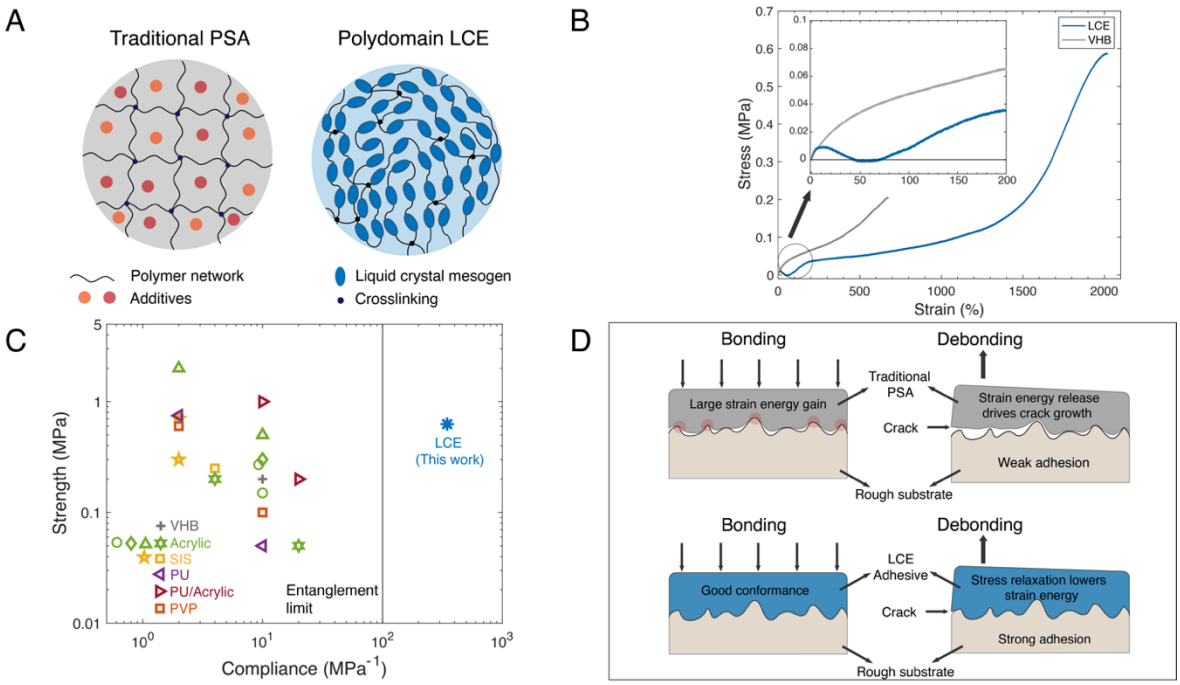

Figure 5.1: A) Schematic of the crosslinked network structures of traditional polymer adhesives (left) and liquid crystal elastomers (right). B) Uniaxial stress-strain curves of LCE and VHB adhesive obtained at a rate of 0.0005 s-1. C) Ashby chart comparing the strength and compliance of various classes of pressure sensitive adhesives from the literature. The solid vertical line at 102 MPa-1 corresponds to the limit set by chain entanglements in linear polymers. D) Schematic showing the adhesion mechanisms on rough surfaces. In traditional PSAs, the asperities of the surface can locally deform the adhesive leading to poor conformance and strain energy gain which drives crack growth on debonding. In the case of LCE, the high compliance results in good conformance under a compressive pre-load. The stress relaxation due to mesogens lowers the strain energy within LCE adhesives, leading to stronger adhesion on rough surfaces.

VHB 4910, a commercial acrylic adhesive from 3M company was used for comparison[165]. The glass transition temperature of VHB and LCE are -10°C and 0°C respectively (Figure 5.2). The nematic-isotropic transition temperature of LCE is 75°C, which ensures a liquid crystalline state at room temperature. At room temperature, the storage shear modulus of LCE is 0.3 MPa and for VHB is 0.1 MPa, both of which are under the Dahlquist criterion (0.3 MPa)[118,119]. This criterion exists due to the competition between gained surface energy on adhesion and the stored

strain energy per unit area during bonding, which makes soft elastomers good candidates for adhesives.

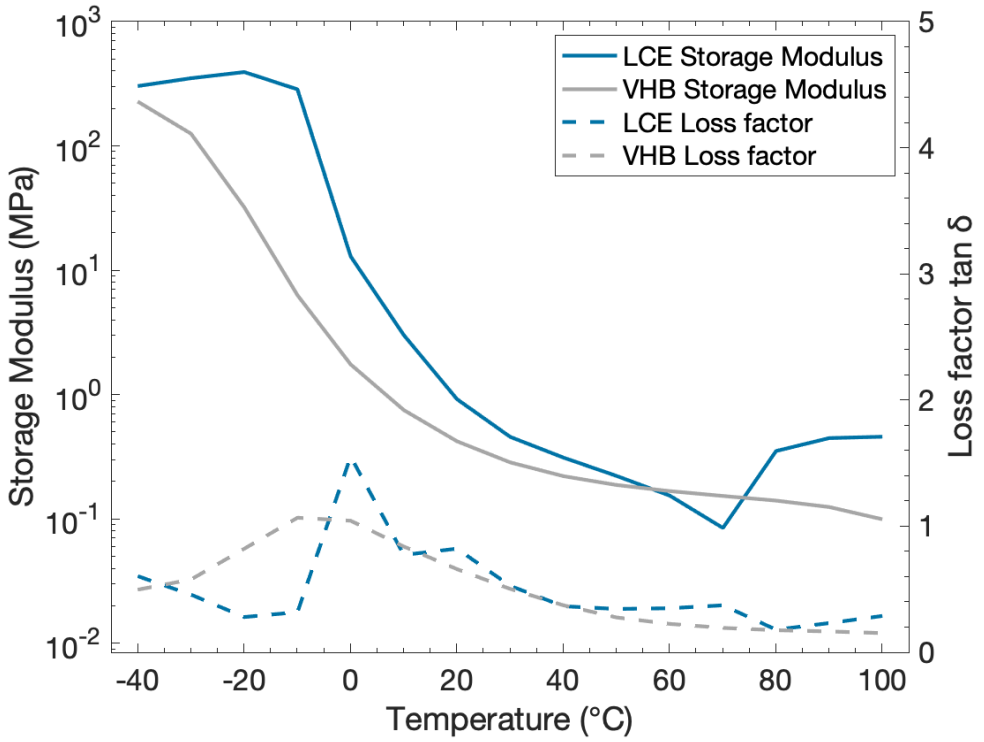

Figure 5.2: Dynamic mechanical analysis temperature sweep of LCE and VHB in uniaxial tension mode at 1 Hz, showing the curves of storage modulus (E') and loss factor (tan δ)

Under uniaxial tension (Figure 5.1B), traditional polymers typically show a monotonic stress-strain behavior. On the other hand, liquid crystal elastomers can be largely deformed by applying a very small mechanical work, due to the mesogen director rotation. This unique property known as soft elasticity, manifests as a stress plateau under uniaxial tension and an unusual in-plane liquid like behavior under biaxial tension[106]. Since this property is rate dependent, the large stress plateau due to soft elasticity has been shown to result in the unique rate-dependent adhesion energy of LCE under peeling and in impact damping applications[15,16,169]. At a very low crosslinking density, LCE shows a non-monotonic stress-strain curve with the modulus reaching

almost zero at 50% strain (Figure 5.1B inset) and possessing a tensile strength of 0.6 MPa. When it comes to adhesion, the strength and the modulus of the adhesive are two crucial parameters necessary to maintain a good balance between conformability on rough surfaces during bonding and resisting loads on debonding. If n_x is the length of the network strands between two crosslinking points in a polymer, the modulus of an elastomer is proportional to n_x^{-1} and the strength is typically proportional to the modulus[170]. Since n_x singlehandedly determines the modulus of an elastomer, the design space of a typical adhesive is limited by optimizing the crosslinking density and blending with other polymer additives to reduce the modulus[91]. Figure 5.1C is an Ashby chart, comparing the compliance (1/modulus) and the strength of various PSAs under uniaxial tension[116,133,171–177]. On the top left are the well crosslinked adhesives, which possess low compliance and high tensile strengths. By reducing the crosslink density, the compliance of the adhesive can be increased, at the cost of lowered strength. On further reduction of crosslink density, the entanglements of the polymer chains will dominate and set an upper bound of compliance (~10^2 MPa $^{-1}$). Owing to soft elasticity, LCE adhesives can achieve a higher compliance (> 10^2 MPa $^{-1}$), while maintaining good tensile strength (0.6 MPa). Note that due to the non-monotonic stress-strain behavior of LCE, the inverse of the resilience modulus at 100% strain (area under the stress-strain curve), was used to calculate the compliance. The consequence of the high compliance enabled by soft elasticity is reflected during bonding to rough surfaces, as illustrated in Figure 5.1D.

At a typical contact pressure, a crosslinked adhesive with low compliance will result in poor conforming over a rough surface with large asperities. Moreover, the deformation of the crosslinked adhesive by the asperities can lead to a gain in strain energy within the adhesive, which in turn drives debonding. By using an uncrosslinked polymer, one can increase the compliance of

the adhesive and improve the conformance, but the adhesive will be susceptible to creep flow under a constant load. Typical strategies to increase the compliance of a crosslinked adhesive is to dilute the network with large quantities of low molecular weight additives such as plasticizers and tackifiers, which introduces the risk of property drift due to segregation or leaching of volatile compounds[151]. In the case of LCE, soft elasticity results in low compliance which enables good conforming over rough surfaces, without the use of any additives. The stress relaxation of mesogens contributes to the further lowering of strain energy over long bonding time. On debonding, strain stiffening and high tensile strength under large deformation leads to improved adhesion strength. We explore the effect of surface roughness and contact time on adhesion using probe tack, indentation and lap shear experiments as follows.

Figure 5.3A, shows the schematic of the probe tack experiment. The adhesive was bonded to a glass substrate fixed at the bottom of the tensile tester. Stainless steel spheres (25 mm diameter) were used as probes and were connected to a force sensor using a gripper. Compared to cylindrical probes, spherical probes can make uniform contact with the adhesive, irrespective of minor alignment differences between the probe and the adhesive surface and do not require additional levelling tools. The stainless-steel spheres were subjected to gritblasting using aluminum oxide abrasives of 24 grit and 100 grit to produce the medium and high roughness surfaces respectively. The smooth sphere was used as received without any gritblasting (Figure 5.3B**).** The area roughness was measured using an optical profiler, which yielded root mean square height values of S_q = 0.3 µm, S_q = 2.86 µm and S_q = 20.98 µm for the smooth, medium roughness and high roughness surfaces respectively.

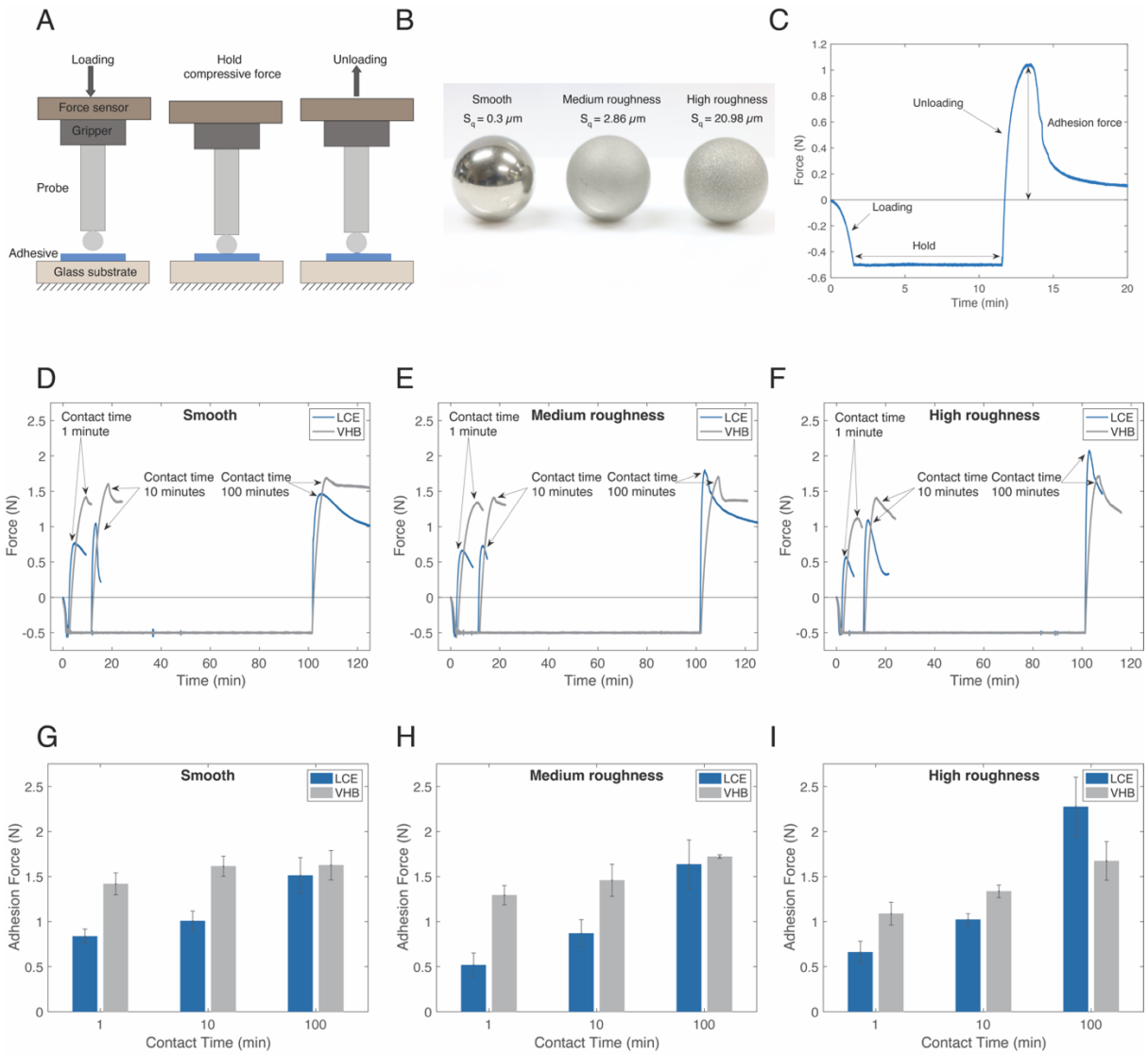

Figure 5.3: A) Schematic of the probe-tack experimental setup. A spherical probe contacts the adhesive layer and a compressive force is maintained for a contact time, after which the probe is retracted and the force is measured. B) Photographs of the spherical probes of different surface roughness. C) A typical plot of force vs time, showing various stages of loading, holding and unloading. Force vs time plots from probe-tack tests for LCE (Blue) and VHB (Grey), after different contact times (1,10 and 100 minutes) using D) Smooth probe, E) Medium roughness probe and F) High roughness probe. Bar chart showing peak adhesion force on probe retraction, measured after different contact times (1,10 and 100 minutes) for LCE (Blue) and VHB (Grey) using G) Smooth probe, H) Medium roughness probe and I) High roughness probe. The results and error bars denote mean and one standard deviation respectively (n=3-5).

The probe was allowed to approach the adhesive at a slow rate of 0.01 mm/s to avoid viscous effects, until a compressive load of 0.5 N was reached. This load was held constant for a

certain period time, which we define as “contact time”. This was followed by the retraction of the probe from the adhesive and the peak force was recorded (Figure 5.3C). This experiment was repeated for three contact times (1, 10 and 100 minutes), three probes of different roughness and two adhesives LCE and VHB (Figures 5.3D-F).In case of both LCE and VHB, the adhesion force increased with more contact time, irrespective of the probe roughness. The constant compressive force of the probe will result in increased indentation depth due to viscoelasticity, which in turn leads to improved effective contact area[126,158,178].

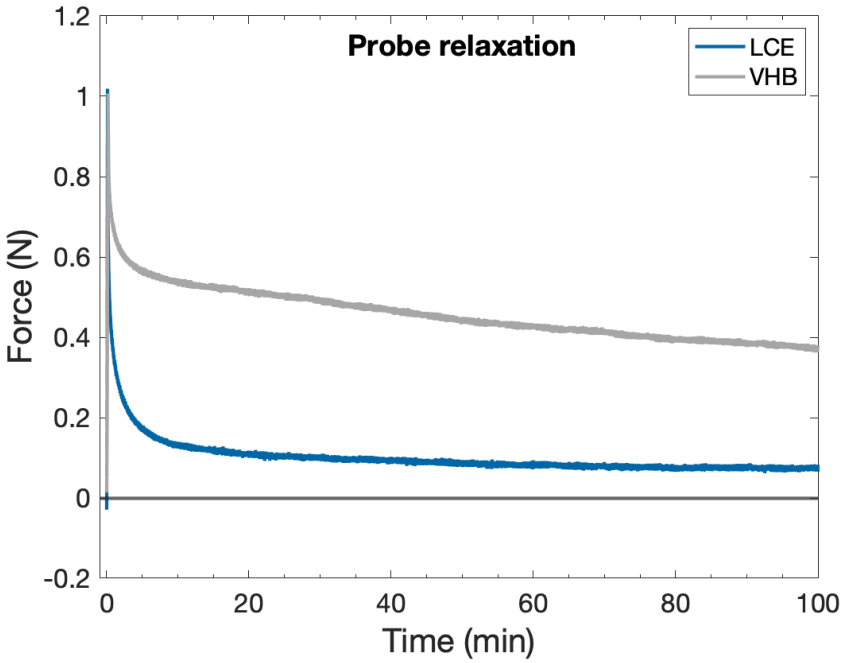

Figure 5.4: Stress relaxation of LCE and VHB under compression by a smooth spherical probe. An initial compressive force (1N) was applied at a probe approach speed of 0.1 mm/s, then the displacement was fixed and the force was measured for 100 minutes. LCE had a relaxation time of 50s while VHB had a relaxation time over 6000s.

In a recent work, Guo et al reported the increase in the adhesion energy of LCE on probe tack after a long contact time using smooth substrates. The increased adhesion strength of LCE was attributed to the enhanced stress relaxation of the nematic domains in LCE, which resulted in further lowering of free energy[115]. Performing a relaxation experiment on LCE reveals that the

stress relaxation in LCE is much drastic compared to VHB, with a relaxation time of 50s for LCE and >5000s for VHB (Figure 5.4). Polydomain LCEs have previously shown a fast relaxation at short time scales (<1000 s) and a much slower relaxation at longer time scales comparable to isotropic elastomers (>1000 s)[19]. At a short contact time of 1 minute, the adhesion force of VHB was atleast 40% higher than that of LCE for all the probe roughness. This can be understood by the lack of tackifiers in the LCE adhesive. The tack of an adhesive is defined as the ability of an adhesive to quickly wet the substrate and provide instant adhesion[179]. Commercial adhesives are blended with large weight fractions of low molecular weight additives or tackifiers, which lowers the modulus and contributes to the instant "stickiness" at a short contact time, compared to LCE which has no such additives. While an instant bonding can be desired for some applications, tackiness may not directly correlate to good adhesive performance in general, which is achieved by a subtle balance between viscous and elastic properties[91,151,155]. On comparing the contact times of 10 and 100 minutes, LCE showed a larger increase in the adhesion force compared to VHB and reached a maximum value of 2.1 N for the high roughness probe. However, the adhesion force of VHB saturated around ~1.7 N irrespective of the probe roughness, after the maximum contact time of 100 minutes. Previous studies have shown that tack of an adhesive on a rough surface with asperities is proportional to the true area of contact during bonding, which in turn is affected by both contact time and pressure[126,158,178]. Due to the high compliance of LCE, the application of a pre-load for a certain period resulted in improved contact with the substrate. As the probe was retracted from the adhesive surface, both LCE and VHB formed long adhesive necks. Due to soft elasticity LCE showed more ductility before complete detachment from the probe, which mirrors the observations of long fibrils on peeling LCE adhesives in previous studies.

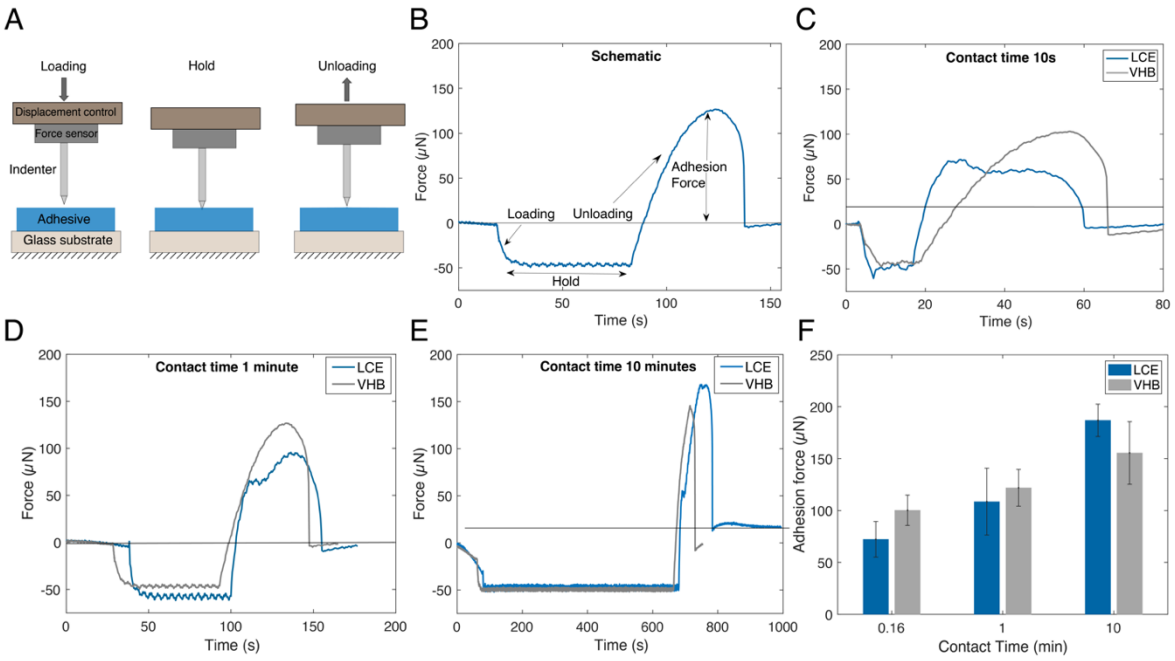

Figure 5.5: A) Schematic of the indentation experimental setup. A conical probe tip with a diameter of 109 microns indents the adhesive layer and a compressive force is maintained for a contact time, after which the probe is retracted and the peak force is measured. B) A typical plot of force vs time, showing various stages of loading, holding and unloading. Force vs time plots from Probe-tack tests for LCE (Blue) and VHB (Grey), after different contact times of C) 10 seconds, D) 1 minute and E) 100 minutes. F) Peak adhesion force on probe retraction, measured at different contact times for LCE (Blue) and VHB (Grey). The results and error bars denote mean and one standard deviation respectively (n=3-5).

The results from the probe tack experiment describe the collective interaction between thousands of asperities on the probe substrate and the adhesive layer. To simulate the interactions between one asperity and the adhesive at a smaller length scale, microindentation can be used[180]. Figure 5.5A shows the schematic of the indentation experimental setup. A flat-ended conical probe tip of diameter 109 μm penetrates the top surface of the adhesive adhered on a flat glass substrate at a rate of 1 μm/s until a force of 50 μN is reached, which is held constant for various contact times (0.16, 1 and 10 minutes). This is followed by unloading at the same rate of 1 μm/s, and the peak force during debonding is defined as the adhesion force (Figure 5.5B). The

results of the microindentation experiments follow qualitatively similar trends as the probe tack experiment. At smaller contact times of 10s and 1 minute, VHB shows a higher adhesion force compared to LCE, owing to the higher tackiness of VHB (Figure 5.5C and D). When the contact time is increased to 10 minutes, LCE shows higher adhesion strength (Figure 5.5E). At contact times longer than 10 minutes, the adhesion force of LCE exceeds the maximum debonding force of the instrument. But following the probe tack experiment, we expect the adhesion force of LCE to increase further with longer contact times before reaching a saturated value (Figure 5.5F).

During the crosslinking of LCE, it is represented by a state of quenched disorder, where the crosslinked network imposes a local field on the director of neighboring mesogens, which leads to the formation of "polydomain"[5,9]. Although the diameter of the indenter (~100 μm) is smaller compared to the spherical probe (25 mm), it is still bigger than the length scale of nematic domains in LCE (1 μm). Therefore, it is possible that the observed increase in adhesion force in both probe tack and indentation experiments comes from the stress relaxation due to collective reorientation of neighboring domains[115]. While techniques like atomic force microscopy or nanoindentation can be used to probe the effects at a scale smaller than one domain (1 μm), the adhesion force of typical PSAs diminishes at a roughness scale of few μm to hundreds of μm, which is above the size of the LCE domains. This hints that LCE adhesives hold potential for bonding to rough surfaces compared to traditional PSAs.

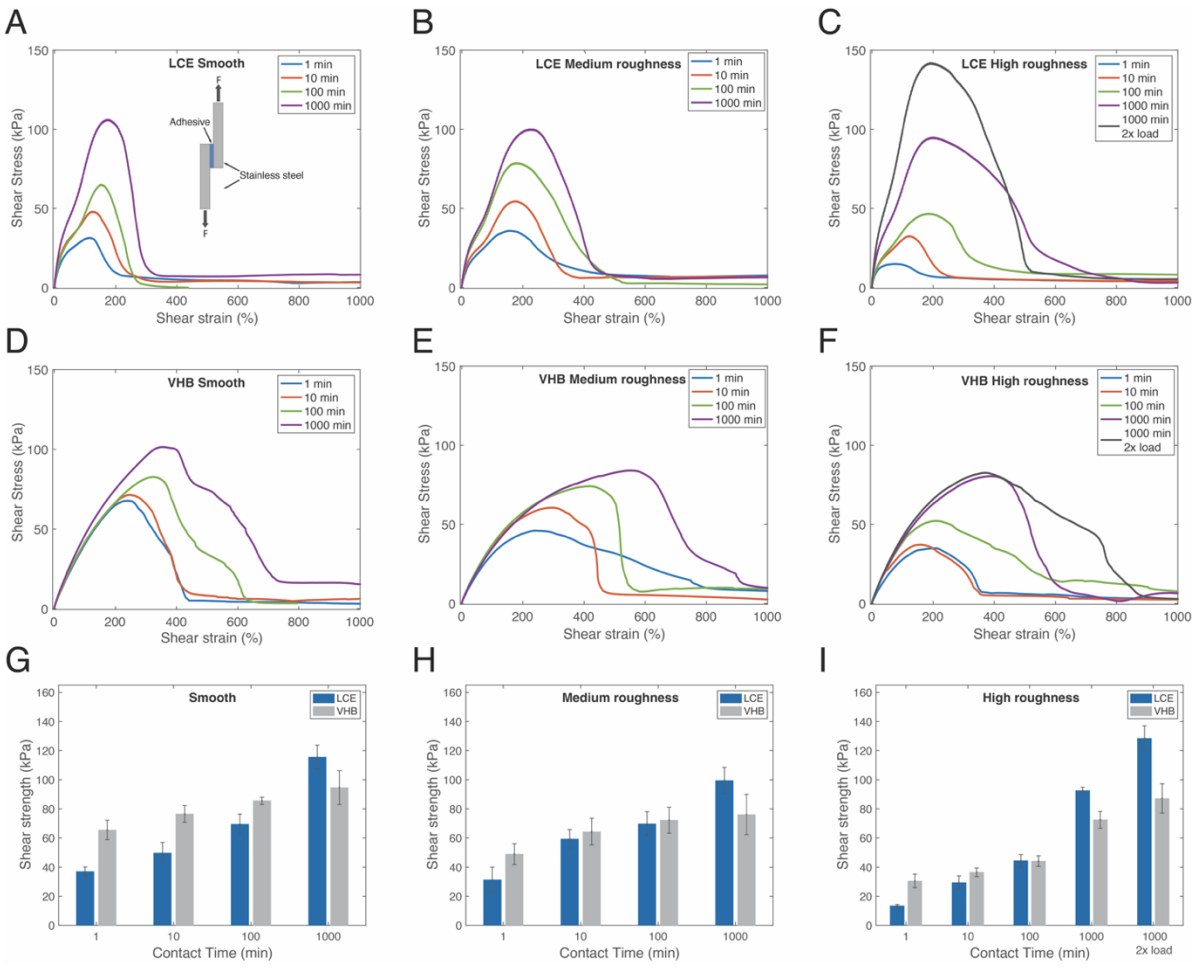

Figure 5.6: Lap shear test results of LCE using different pre-load contact times (1,10,100 and 1000 minutes), using A) Smooth substrate, B) Medium roughness substrate, C) High roughness substrate. A) Inset shows the schematic of the lap shear test, where the adhesive is bonded between two stainless steel plates with an overlap area of 25.4x25.4 mm^2. Lap shear test results of VHB using different pre-load contact times (1,10,100 and 1000 minutes), using D) Smooth substrate, E) Medium roughness substrate, F) High roughness substrate. Peak shear stress, measured at different contact times (1,10, 100 and 1000 minutes) for LCE (Blue) and VHB (Grey) using G) Smooth substrate, H) Medium roughness substrate, I) High roughness substrate. The results and error bars denote mean and one standard deviation respectively (n=3-5).

Following the industry standards (ASTM D1002), we performed lap shear tests on LCE and VHB adhesives by bonding the adhesives to substrates of various surface roughness (Figure 5.6A inset shows schematics). The adhesive was bonded between two stainless steel plates of 25.4mm width and 100 mm length. The adhesive overlap area between the plates was 25.4x25.4

mm^2. A compressive pressure of 100 kPa was applied on the overlap area for various contact times and then the shear force was measured using a tensile tester. Figure 5.6B-F shows the shear stress vs strain curves for LCE and VHB at different contact times and substrate roughness. At low contact times of 1 minute and 10 minutes VHB showed higher shear strength compared to LCE, irrespective of the substrate roughness. Comparing the same contact times, the shear strength of VHB decreased with increase in surface roughness. For the maximum contact time of 1000 minutes, the shear strength of VHB dropped from 100 kPa to 75 kPa for higher substrate roughness. On the other hand, the shear strength of LCE reached a similar value of 90-100 kPa under a contact time of 1000 minutes, irrespective of substrate roughness. Since both contact time and pressure can affect the adhesion strength, we tested the shear strength of LCE and VHB using the high roughness substrate using twice the contact pressure (200 kPa) and a contact time of 1000 minutes. Doubling the contact pressure had marginal effect on the adhesion of VHB, while it improved the shear strength of LCE to 130 kPa. This result is similar to the previous studies, which also showed that more compliant adhesives can benefit from increased contact pressure, while it does not affect the adhesion of less compliant adhesives[159,166]. Macroscopically observing the adhesive on the substrates after the lap shear test reveals further details on the failure mechanisms of LCE adhesives (Figure 5.7**)**. Polydomain LCE samples are opaque due to light scattering by randomly arranged nematic domains and becomes transparent under large deformation as the mesogens align along the direction of loading. Photographs of LCE adhesives after the tests show that under a short contact time (1-10 minutes), most of the LCE remained opaque. But for longer contact times (>100 minutes), the LCE samples became more transparent. Due to the lack of tackifiers, the initial tack of the crosslinked LCE is lower than VHB, which results in weak bonding and premature adhesive failure at short contact times. Increasing the contact time and pressure, allows LCE to

form a good contact with the substrate, which allows it to undergo large bulk deformation during the lap shear test, thereby resulting in an increased overall adhesion strength.

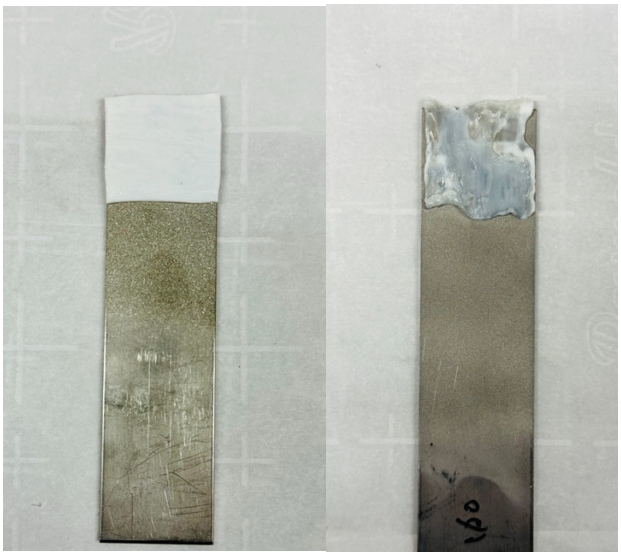

Figure 5.7: Photograph of LCE adhesives on the rough substrate after lap shear test, with a contact time of 10 minutes (left) and 1000 minutes (right). For the contact time of 1000 minutes, the sample shows changes in the transparency due to large deformation.

The effect of higher contact pressures at small contact times was not studied following the analysis from previous studies. Without sufficient time for stress relaxation, high contact pressures can result in large tensile stresses and local detachment at some of the valleys between the asperities, which can act as failure points[158]. Air pockets trapped between the valleys have been reported as a failure mechanism as well[179]. Under all the experimental conditions, both LCE and VHB did not show any cohesive failure and failed adhesively without leaving any residues.

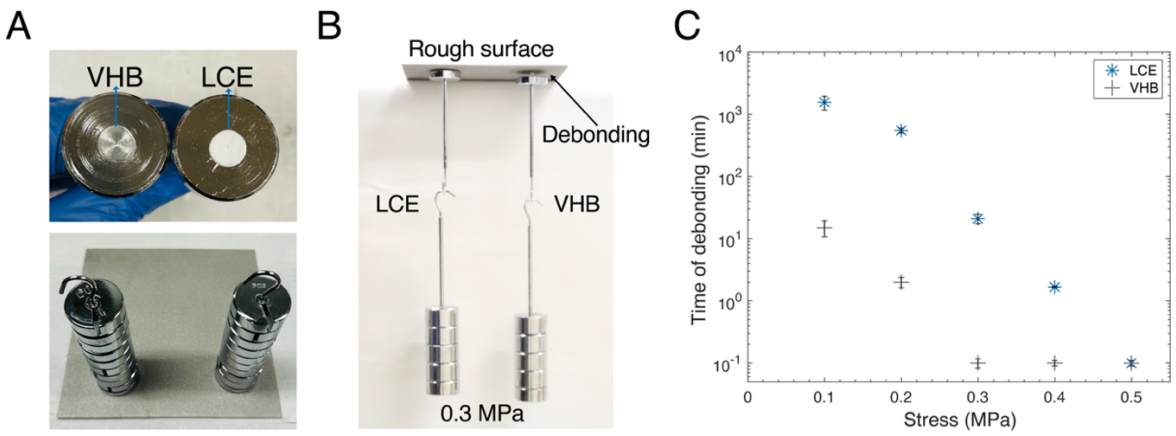

Figure 5.8: A) Photographs showing sample preparation for static loading tests. A circular piece of adhesive is bonded to the surface of a stainless-steel substrate (Top). The other surface of the adhesive is bonded to a rough substrate and a compressive pre-load is applied for 1000 minutes (Bottom). B) A static normal load is applied using slotted weights and the time of debonding from the rough surface is noted. C) The results from the static loading tests, showing the time of debonding for LCE (Blue) and VHB (Grey) and the corresponding applied stress (0.1-0.5 MPa). The results and error bars denote mean and one standard deviation respectively (n=3-5).

In addition to lap shear test, we also compared the adhesive performance of LCE and VHB from a high roughness substrate under static normal loads. One surface of the circular adhesive layers was adhered to a smooth stainless-steel cylinder (Figure 5.8A). The other surface of the adhesive was adhered to a sandblasted stainless-steel plate with high roughness (S_q > 20 µm) and a compressive load of 500 kPa was applied for a contact time of 1000 minutes. Then different static normal loads (0.1 – 0.5 MPa) were applied using hanging weights and the time of debonding was measured (Figure 5.8B). For the applied load of 0.1 MPa, VHB debonded within 15 minutes while LCE was able to withstand the load for 1500 minutes (Figure 5.8C). When an adhesive is bonded on rough surfaces, the presence of asperities will reduce the effective contact area as compared to a smooth surface and can result in the formation of cracks near the edge of the adhesive. The adhesive is also deformed by the sharp asperities, which results in a gain in strain energy[156,158,159]. When a load is applied, this release of strain energy drives the crack growth and

causes adhesive failure. In the case of LCE, the high compliance due to soft elasticity allows good conformance after sufficient contact time and pressure. The stress relaxation enabled by mesogen domain realignment, results in lowered strain energy within the adhesive. This allows LCE to sustain loads for a longer period despite the high surface roughness.

While it is possible that some commercial adhesives can sustain more loads for longer periods compared to LCE adhesive, it is important to consider the difference in their composition. For good overall performance, an adhesive should possess good adhesive and cohesive strength. A high compliance is necessary to achieve adhesion, but some crosslinking is necessary for cohesive strength and creep resistance, which will inadvertently reduce the compliance. To solve this paradox, additives such as plasticizers and tackifiers are added to the base polymer to ensure good bonding. This makes adhesive formulation a delicate balance between multiple contradicting properties[155]. To be further used as a mounting tape such as VHB 4910, the adhesive layers are coated on a crosslinked viscoelastic polymer foam which distributes stress and provides impact strength. Therefore, due to the multilayered design a mounting foam tape achieves high adhesive and cohesive strength. Despite this, many commercial products recommend the users to polish any rough surfaces, use primers and provide warning for the potential loss of adhesion. On the other hand, the LCE adhesive used in this work does not have any additives or a separate foam core. We chose a simple chemical formulation, which balances all these properties. Due to soft elasticity, the LCE adhesive can possess high compliance. The lowering of strain energy due to mesogen relaxation, leads to a good bonding in rough surfaces after a sufficient contact time (~1000 minutes), which is comparable to the time required by many commercial adhesives for achieving complete bonding strength (72 hours). The crosslinking of the LCE network provides cohesive

strength on debonding. Although in this study, we performed all the experiments at low strain rates to avoid viscoelastic effects, LCE has been reported previously to show strong rate dependent adhesion and high viscoelastic damping compared to traditional polymers. Therefore, a tape made using an LCE foam core of higher crosslinking density and LCE adhesive layers of lower crosslinking on its surface will result in a robust adhesive performance which will be our focus for future studies.

5.4 Conclusion

Despite the excellent advantages of pressure sensitive adhesives, the effect of roughness on lowered adhesion strength restricts their real-world applications. We show that liquid crystal elastomers can be designed to overcome the challenges faced by traditional adhesives on rough substrates. The asperities of a rough surface typically deform the adhesive and increase the strain energy within the material, which drives crack growth and debonding. Soft elasticity endows liquid crystal elastomers with high compliance for conforming to a rough substrate. After sufficient contact time and pressure, stress relaxation of LCE allows reduction in strain energy. The crosslinking in the network provides cohesive strength on debonding. This allows LCE adhesives to perform better than a commercial foam tape on very rough surfaces where the asperities size range from few microns to tens of microns. We hope this study opens new possibilities for roughness tolerant pressure sensitive adhesives and broaden the potential applications.

Acknowledgements

Chapter 5, in part is currently being prepared for submission for publication of the material. Annapooranan, R.; Yeerella, R.H.; Chambers, R. J.; Li, C.; Cai, S.; Enhanced adhesion of liquid crystal elastomers on rough surfaces. The dissertation author was the primary researcher and author of this material.

Chapter 6 Conclusion

6.1 Summary of the dissertation

Compared to traditional elastomers, liquid crystal elastomers hold great potential for various new applications due to their unique properties such as anisotropic elasticity, stimuli responsive actuation and energy dissipation. In this dissertation, we explore the rate and temperature dependence of these properties and use materials chemistry to improve these properties. We believe this will contribute to new engineering applications and also improve the reliability of the engineering devices and structures created using LCE. The main results of each chapter are summarized as follows.

In Chapter 2, we systematically studied the fracture properties of liquid crystal elastomers at different temperatures and loading rates. Due to the viscoelastic nature of LCE, it shows a rate and temperature dependent fracture behavior. At high loading rates and low temperatures, LCE behaves like a tough elastomer. But once it is heated above the isotropic transition temperature, the viscous dissipation effects are lost, leading to the deterioration of fracture energy. Using the fracture energy measurements, we can predict the rupture temperature under self-actuation stress for monodomain LCE actuator. We believe that the results from this article can be used in designing reliable LCE structures for various applications.

In Chapter 3, we use interpenetrating networks strategy to report a method to enhance the high temperature fracture and fatigue properties of liquid crystal elastomers. As seen in Chapter 2, LCEs in general have poor high temperature fracture properties, due to diminished viscoelastic dissipation mechanisms. We show that the overall fracture energy of LCE at high temperatures can be significantly improved, by incorporating a soft and stretchable second PU network, and tuning the crosslinking density. The entanglement of the LCE and PU networks and the covalent

bond breakage on loading can result in significant energy dissipation at various temperatures. Since the PU network doesn't show much mechanical deterioration with increasing temperature compared to the LCE network, a fracture energy of 655 Jm^{-2} is achieved for the double network LCE at 90°C. Compared to the single network LCE, the high temperature fatigue crack growth is also reduced significantly in DNLCE. The actuation properties of LCE is also retained due to the extensible PU network, which allows us to apply mechanical stretch to align the mesogens. We hope that the results of this chapter can pave way for the creation of soft thermally actuating materials that are tough and fatigue resistant at various temperatures.

In Chapter 4, we studied the properties of LCE adhesives using peel experiments and compared it with other pressure sensitive adhesives. We show that pressure sensitive adhesives fabricated using liquid crystal elastomers can exhibit an extreme temperature and rate dependence of adhesion energy, compared to traditional adhesives. The rate and temperature dependence arises from soft elasticity and strong non-linear viscoelasticity of LCE enabled by inter-mesogen interaction and polymer chain friction. Time temperature superposition was applicable for all the viscoelastic properties and adhesion energy of LCE. The unique properties of LCE can deliver functions typically inaccessible to traditional polymers, such as reversible and frequency dependent adhesion. We hope that the results from this study can lead to the development of novel PSAs and enable new applications of LCE.

In Chapter 5, we study the effect of roughness on the adhesive properties of liquid crystal elastomers. Despite the excellent properties of current pressure sensitive adhesives, the effect of roughness on lowered adhesion strength restricts their real-world applications. We show that liquid crystal elastomers can be carefully designed to overcome these challenges on rough substrates.

The asperities of a rough surface typically deforms the elastomeric adhesive and increase the strain energy, which drives crack growth and debonding of the adhesives. In case of liquid crystal elastomers, soft elasticity results in high compliance for conforming to a rough substrate. The stress relaxation of LCE allows reduction in strain energy after sufficient contact time and pressure. The crosslinking in the network provides cohesive strength on debonding and delays creep. These unique advantages allow LCE adhesives to perform better than a commercial acrylic tape on very rough surfaces with asperities range from few microns to tens of microns in size. We hope these results opens new possibilities for pressure sensitive adhesives that are more tolerant to roughness.

6.2 Outlook for future work

In our studies, we have shown the advantages of LCEs in fracture and adhesion and demonstrated some materials chemistry strategies to overcome the weaknesses. For further improvement of properties, one can use the array of polymer engineering techniques applied in other areas of soft matter such as hydrogels and dielectric elastomers. The use of functional groups which are more polar, such as amines, nitriles and fluoride, can provide more intermolecular interactions such as hydrogen bonding, which can significantly enhance the energy dissipation properties across a wider range of temperatures and frequencies. These polar groups can also lead to significant improvements in surface wetting and adhesion. To further improve adhesion, structural designs involving a more crosslinked LCE foam layer sandwiched between two adhesive layers can result in robust adhesion that are tolerant to static and dynamic loading, owing to the molecular scale dissipation of LCE combined with the macroscale dissipation from buckling.

References

(1) Gent, A. N. Engineering with Rubber. In *Engineering with Rubber (Third Edition)*; Gent, A. N., Ed.; Hanser, 2012; p I–XVIII. https://doi.org/10.3139/9783446428713.fm.

(2) Rubinstein, M.; Colby, R. H. *Polymer Physics*; Oxford university press, 2003.

(3) Tully, J. *The Devil's Milk: A Social History of Rubber*; NYU Press, 2011.

(4) Chen, D.; Pei, Q. Electronic Muscles and Skins: A Review of Soft Sensors and Actuators. *Chemical reviews* **2017**, *117* (17), 11239–11268.

(5) Warner, M.; Terentjev, E. M. *Liquid Crystal Elastomers*; Oxford university press, 2007; Vol. 120.

(6) White, T. J.; Broer, D. J. Programmable and Adaptive Mechanics with Liquid Crystal Polymer Networks and Elastomers. *Nature Materials* **2015**, *14* (11), 1087–1098. https://doi.org/10.1038/nmat4433.

(7) Li, M.; Pal, A.; Aghakhani, A.; Pena-Francesch, A.; Sitti, M. Soft Actuators for Real-World Applications. *Nature Reviews Materials* **2022**, *7* (3), 235–249.

(8) Jiang, Z.-C.; Liu, Q.; Xiao, Y.-Y.; Zhao, Y. Liquid Crystal Elastomers for Actuation: A Perspective on Structure-Property-Function Relation. *Progress in Polymer Science* **2024**, 101829.

(9) Terentjev, E. M. Liquid-Crystalline Elastomers. *Journal of Physics: Condensed Matter* **1999**, *11* (24), R239–R257. https://doi.org/10.1088/0953-8984/11/24/201.

(10) Long, R.; Hui, C.-Y.; Gong, J. P.; Bouchbinder, E. The Fracture of Highly Deformable Soft Materials: A Tale of Two Length Scales. *Annual Review of Condensed Matter Physics* **2021**, *12* (1), 71–94. https://doi.org/10.1146/annurev-conmatphys-042020-023937.

(11) Ferry, J. D. *Viscoelastic Properties of Polymers*; John Wiley & Sons, 1980.

(12) Kraus, G. Reinforcement of Elastomers by Carbon Black. *Rubber chemistry and Technology* **1978**, *51* (2), 297–321.

(13) Sun, S.; Li, M.; Liu, A. A Review on Mechanical Properties of Pressure Sensitive Adhesives. *International Journal of Adhesion and Adhesives* **2013**, *41*, 98–106.

(14) Clarke, S.; Tajbakhsh, A.; Terentjev, E.; Remillat, C.; Tomlinson, G.; House, J. Soft Elasticity and Mechanical Damping in Liquid Crystalline Elastomers. *Journal of Applied Physics* **2001**, *89* (11), 6530–6535.

(15) Merkel, D. R.; Shaha, R. K.; Yakacki, C. M.; Frick, C. P. Mechanical Energy Dissipation in Polydomain Nematic Liquid Crystal Elastomers in Response to Oscillating Loading. *Polymer* **2019**, *166*, 148–154. https://doi.org/10.1016/J.POLYMER.2019.01.042.

(16) Saed, M. O.; Elmadih, W.; Terentjev, A.; Chronopoulos, D.; Williamson, D.; Terentjev, E. M. Impact Damping and Vibration Attenuation in Nematic Liquid Crystal Elastomers. *Nature communications* **2021**, *12* (1), 6676.

(17) Mistry, D.; Traugutt, N. A.; Sanborn, B.; Volpe, R. H.; Chatham, L.; Zhou, R.; Song, B.; Yu, K.; Long, K.; Yakacki, C. M. Soft Elasticity Optimises Dissipation in 3D-Printed Liquid Crystal Elastomers. *Nature communications* **2021**, *12* (1), 6677.

(18) Luo, C.; Chung, C.; Traugutt, N. A.; Yakacki, C. M.; Long, K. N.; Yu, K. 3D Printing of Liquid Crystal Elastomer Foams for Enhanced Energy Dissipation under Mechanical Insult. *ACS Applied Materials and Interfaces* **2021**, *13* (11), 12698–12708. https://doi.org/10.1021/acsami.0c17538.

(19) Hotta, A.; Terentjev, E. M. Long-Time Stress Relaxation in Polyacrylate Nematic Liquid Crystalline Elastomers. *Journal of Physics Condensed Matter* **2001**, *13* (50), 11453–11464. https://doi.org/10.1088/0953-8984/13/50/305.
(20) Corbett, D. R.; Adams, J. M. Tack Energy and Switchable Adhesion of Liquid Crystal Elastomers. *Soft Matter* **2013**, *9* (4), 1151–1163. https://doi.org/10.1039/C2SM26868J.
(21) Ohzono, T.; Saed, M. O.; Terentjev, E. M. Enhanced Dynamic Adhesion in Nematic Liquid Crystal Elastomers. *Advanced Materials* **2019**, *31* (30), 1902642.
(22) Rus, D.; Tolley, M. T. Design, Fabrication and Control of Soft Robots. *Nature* **2015**, *521* (7553), 467–475. https://doi.org/10.1038/nature14543.
(23) Ilievski, F.; Mazzeo, A. D.; Shepherd, R. F.; Chen, X.; Whitesides, G. M. Soft Robotics for Chemists **. **2011**, 1890–1895. https://doi.org/10.1002/anie.201006464.
(24) Whitesides, G. M. Soft Robotics. *Angewandte Chemie - International Edition* **2018**, *57* (16), 4258–4273. https://doi.org/10.1002/anie.201800907.
(25) Ilami, M.; Bagheri, H.; Ahmed, R.; Skowronek, E. O.; Marvi, H. Materials, Actuators, and Sensors for Soft Bioinspired Robots. *Advanced Materials* **2021**, *33* (19), 1–47. https://doi.org/10.1002/adma.202003139.
(26) Majidi, C. Soft-Matter Engineering for Soft Robotics. *Advanced Materials Technologies* **2019**, *4* (2), 1–13. https://doi.org/10.1002/admt.201800477.
(27) Jiang, H.; Li, C.; Huang, X. Actuators Based on Liquid Crystalline Elastomer Materials. *Nanoscale* **2013**, *5* (12), 5225–5240. https://doi.org/10.1039/c3nr00037k.
(28) Wang, Z.; Wang, Z.; Zheng, Y.; He, Q.; Wang, Y.; Cai, S. Three-Dimensional Printing of Functionally Graded Liquid Crystal Elastomer. *Science Advances* **2020**, *6* (39). https://doi.org/10.1126/sciadv.abc0034.
(29) Saed, M. O.; Ambulo, C. P.; Kim, H.; De, R.; Raval, V.; Searles, K.; Siddiqui, D. A.; Cue, J. M. O.; Stefan, M. C.; Shankar, M. R.; Ware, T. H. Molecularly-Engineered, 4D-Printed Liquid Crystal Elastomer Actuators. *Advanced Functional Materials* **2019**, *29* (3), 1806412. https://doi.org/10.1002/adfm.201806412.
(30) Wang, Z.; Tian, H.; He, Q.; Cai, S. Reprogrammable, Reprocessible, and Self-Healable Liquid Crystal Elastomer with Exchangeable Disulfide Bonds. *ACS Applied Materials and Interfaces* **2017**, *9* (38), 33119–33128. https://doi.org/10.1021/acsami.7b09246.
(31) Wang, Z.; Cai, S. Recent Progress in Dynamic Covalent Chemistries for Liquid Crystal Elastomers. *Journal of Materials Chemistry B* **2020**, *8* (31), 6610–6623. https://doi.org/10.1039/d0tb00754d.
(32) Pei, Z.; Yang, Y.; Chen, Q.; Terentjev, E. M.; Wei, Y.; Ji, Y. Mouldable Liquid-Crystalline Elastomer Actuators with Exchangeable Covalent Bonds. *Nature Materials* **2014**, *13* (1), 36–41. https://doi.org/10.1038/nmat3812.
(33) Wang, Z.; He, Q.; Wang, Y.; Cai, S. Programmable Actuation of Liquid Crystal Elastomers: Via "Living" Exchange Reaction. *Soft Matter* **2019**, *15* (13), 2811–2816. https://doi.org/10.1039/c9sm00322c.
(34) He, Q.; Wang, Z.; Song, Z.; Cai, S. Bioinspired Design of Vascular Artificial Muscle. *Advanced Materials Technologies* **2019**, *4* (1), 1–7. https://doi.org/10.1002/admt.201800244.
(35) He, Q.; Wang, Z.; Wang, Y.; Minori, A.; Tolley, M. T.; Cai, S. Electrically Controlled Liquid Crystal Elastomer-Based Soft Tubular Actuator with Multimodal Actuation. *Science Advances* **2019**, *5* (10), 1–8. https://doi.org/10.1126/sciadv.aax5746.

(36) Ula, S. W.; Traugutt, N. A.; Volpe, R. H.; Patel, R. R.; Yu, K.; Yakacki, C. M. Liquid Crystal Elastomers: An Introduction and Review of Emerging Technologies. *Liquid Crystals Reviews* **2018**, *6* (1), 78–107. https://doi.org/10.1080/21680396.2018.1530155.
(37) Wang, Z.; Li, K.; He, Q.; Cai, S. A Light-Powered Ultralight Tensegrity Robot with High Deformability and Load Capacity. *Advanced Materials* **2019**, *31* (7), 1–8. https://doi.org/10.1002/adma.201806849.
(38) Yakacki, C. M.; Saed, M.; Nair, D. P.; Gong, T.; Reed, S. M.; Bowman, C. N. Tailorable and Programmable Liquid-Crystalline Elastomers Using a Two-Stage Thiol-Acrylate Reaction. *RSC Advances* **2015**, *5* (25), 18997–19001. https://doi.org/10.1039/c5ra01039j.
(39) Donnio, B.; Wermter, H.; Finkelmann, H. A Simple and Versatile Synthetic Route for the Preparation of Main-Chain, Liquid-Crystalline Elastomers. *Macromolecules* **2000**, *33* (21), 7724–7729. https://doi.org/10.1021/ma0002850.
(40) Thomsen, D. L.; Keller, P.; Naciri, J.; Pink, R.; Jeon, H.; Shenoy, D.; Ratna, B. R. Liquid Crystal Elastomers with Mechanical Properties of a Muscle. *Macromolecules* **2001**, *34* (17), 5868–5875. https://doi.org/10.1021/ma001639q.
(41) Herbert, K. M.; Fowler, H. E.; McCracken, J. M.; Schlafmann, K. R.; Koch, J. A.; White, T. J. Synthesis and Alignment of Liquid Crystalline Elastomers. *Nature Reviews Materials* **2022**, *7* (1), 23–38. https://doi.org/10.1038/s41578-021-00359-z.
(42) *Liquid Crystal Elastomers: Materials and Applications*; Springer Berlin Heidelberg: Berlin, Heidelberg, 2012; Vol. 250.
(43) Ohm, C.; Brehmer, M.; Zentel, R. Liquid Crystalline Elastomers as Actuators and Sensors. *Advanced Materials* **2010**, *22* (31), 3366–3387. https://doi.org/10.1002/adma.200904059.
(44) Zhang, W.; Liu, X.; Wang, J.; Tang, J.; Hu, J.; Lu, T.; Suo, Z. Fatigue of Double-Network Hydrogels. *Engineering Fracture Mechanics* **2018**, *187*, 74–93. https://doi.org/10.1016/j.engfracmech.2017.10.018.
(45) Sun, J. Y.; Zhao, X.; Illeperuma, W. R. K.; Chaudhuri, O.; Oh, K. H.; Mooney, D. J.; Vlassak, J. J.; Suo, Z. Highly Stretchable and Tough Hydrogels. *Nature* **2012**, *489* (7414), 133–136. https://doi.org/10.1038/nature11409.
(46) Pharr, M.; Sun, J. Y.; Suo, Z. Rupture of a Highly Stretchable Acrylic Dielectric Elastomer. *Journal of Applied Physics* **2012**, *111* (10). https://doi.org/10.1063/1.4721777.
(47) Lake, G. J.; Thomas, A. G.; Tabor, D. The Strength of Highly Elastic Materials. *Proceedings of the Royal Society of London. Series A. Mathematical and Physical Sciences* **1967**, *300* (1460), 108–119. https://doi.org/10.1098/rspa.1967.0160.
(48) Creton, C.; Ciccotti, M. Fracture and Adhesion of Soft Materials: A Review. *Reports on Progress in Physics* **2016**, *79* (4). https://doi.org/10.1088/0034-4885/79/4/046601.
(49) Lake, G. J. Fatigue and Fracture of Elastomers. *Rubber Chemistry and Technology* **1995**, *68* (3), 435–460. https://doi.org/10.5254/1.3538750.
(50) Long, R.; Hui, C. Y. Fracture Toughness of Hydrogels: Measurement and Interpretation. *Soft Matter* **2016**, *12* (39), 8069–8086. https://doi.org/10.1039/c6sm01694d.
(51) Rivlin, R. S.; Thomas, A. G. Rupture of Rubber. I. Characteristic Energy for Tearing. *Journal of Polymer Science* **1953**, *10* (3), 291–318. https://doi.org/10.1002/pol.1953.120100303.
(52) Ahagon, A.; Gent, A. N. Threshold Fracture Energies for Elastomers. *Journal of Polymer Science: Polymer Physics Edition* **1975**, *13* (10), 1903–1911. https://doi.org/10.1002/pol.1975.180131005.

(53) Persson, B. N. J.; Albohr, O.; Heinrich, G.; Ueba, H. Crack Propagation in Rubber-like Materials. *Journal of Physics: Condensed Matter* **2005**, *17* (44), R1071–R1142. https://doi.org/10.1088/0953-8984/17/44/r01.
(54) Azoug, A.; Vasconcellos, V.; Dooling, J.; Saed, M.; Yakacki, C. M.; Nguyen, T. D. Viscoelasticity of the Polydomain-Monodomain Transition in Main-Chain Liquid Crystal Elastomers. *Polymer* **2016**, *98*, 165–171. https://doi.org/10.1016/j.polymer.2016.06.022.
(55) Wang, Z.; El Hajj Chehade, A.; Govindjee, S.; Nguyen, T. D. A Nonlinear Viscoelasticity Theory for Nematic Liquid Crystal Elastomers. *Journal of the Mechanics and Physics of Solids* **2022**, *163*, 104829. https://doi.org/10.1016/j.jmps.2022.104829.
(56) Ahagon, A.; Gent, A. N. Threshold Fracture Energies for Elastomers. *Journal of Polymer Science: Polymer Physics Edition* **1975**, *13* (10), 1903–1911. https://doi.org/10.1002/pol.1975.180131005.
(57) Zhao, X.; Chen, X.; Yuk, H.; Lin, S.; Liu, X.; Parada, G. Soft Materials by Design: Unconventional Polymer Networks Give Extreme Properties. *Chemical Reviews* **2021**, *121* (8), 4309–4372. https://doi.org/10.1021/acs.chemrev.0c01088.
(58) Bisoyi, H. K.; Li, Q. Light-Driven Liquid Crystalline Materials: From Photo-Induced Phase Transitions and Property Modulations to Applications. *Chemical Reviews* **2016**, *116* (24), 15089–15166. https://doi.org/10.1021/acs.chemrev.6b00415.
(59) Ware, T. H.; McConney, M. E.; Wie, J. J.; Tondiglia, V. P.; White, T. J. Voxelated Liquid Crystal Elastomers. *Science* **2015**, *347* (6225), 982–984. https://doi.org/10.1126/science.1261019.
(60) Kotikian, A.; Truby, R. L.; Boley, J. W.; White, T. J.; Lewis, J. A. 3D Printing of Liquid Crystal Elastomeric Actuators with Spatially Programed Nematic Order. *Advanced Materials* **2018**, *30* (10), 1706164. https://doi.org/10.1002/adma.201706164.
(61) Saed, M. O.; Ambulo, C. P.; Kim, H.; De, R.; Raval, V.; Searles, K.; Siddiqui, D. A.; Cue, J. M. O.; Stefan, M. C.; Shankar, M. R.; Ware, T. H. Molecularly-Engineered, 4D-Printed Liquid Crystal Elastomer Actuators. *Advanced Functional Materials* **2019**, *29* (3), 1–9. https://doi.org/10.1002/adfm.201806412.
(62) Chen, L.; Bisoyi, H. K.; Huang, Y.; Huang, S.; Wang, M.; Yang, H.; Li, Q. Healable and Rearrangeable Networks of Liquid Crystal Elastomers Enabled by Diselenide Bonds. *Angewandte Chemie* **2021**, *133* (30), 16530–16534. https://doi.org/10.1002/ange.202105278.
(63) He, Q.; Wang, Z.; Wang, Y.; Wang, Z.; Li, C.; Annapooranan, R.; Zeng, J.; Chen, R.; Cai, S. Electrospun Liquid Crystal Elastomer Microfiber Actuator. *Science Robotics* **2021**, *6* (57). https://doi.org/10.1126/scirobotics.abi9704.
(64) Buguin, A.; Li, M. H.; Silberzan, P.; Ladoux, B.; Keller, P. Micro-Actuators: When Artificial Muscles Made of Nematic Liquid Crystal Elastomers Meet Soft Lithography. *Journal of the American Chemical Society* **2006**, *128* (4), 1088–1089. https://doi.org/10.1021/ja0575070.
(65) Roach, D. J.; Yuan, C.; Kuang, X.; Li, V. C.-F.; Blake, P.; Romero, M. L.; Hammel, I.; Yu, K.; Qi, H. J. Long Liquid Crystal Elastomer Fibers with Large Reversible Actuation Strains for Smart Textiles and Artificial Muscles. *ACS Applied Materials & Interfaces* **2019**, *11* (21), 19514–19521. https://doi.org/10.1021/acsami.9b04401.
(66) Annapooranan, R.; Cai, S. Thermally Induced Self-Rupture of a Constrained Liquid Crystal Elastomer. **2021**.

(67) Zhao, X.; Chen, X.; Yuk, H.; Lin, S.; Liu, X.; Parada, G. Soft Materials by Design: Unconventional Polymer Networks Give Extreme Properties. *Chemical Reviews* **2021**, *121* (8), 4309–4372. https://doi.org/10.1021/acs.chemrev.0c01088.
(68) Creton, C. 50th Anniversary Perspective: Networks and Gels: Soft but Dynamic and Tough. *Macromolecules* **2017**, *50* (21), 8297–8316. https://doi.org/10.1021/acs.macromol.7b01698.
(69) He, Q.; Wang, Z.; Yan, Y.; Zheng, J.; Cai, S. Polymer Nanofiber Reinforced Double Network Gel Composite: Strong, Tough and Transparent. *Extreme Mechanics Letters* **2016**, *9*, 165–170. https://doi.org/10.1016/j.eml.2016.06.004.
(70) Shaoting, L.; Xinyue, L.; Ji, L.; Hyunwoo, Y.; Hyun-Chae, L.; A., P. G.; Charles, S.; Jake, S.; Admir, M.; H., M. G.; Xuanhe, Z. Anti-Fatigue-Fracture Hydrogels. *Science Advances* **2021**, *5* (1), eaau8528. https://doi.org/10.1126/sciadv.aau8528.
(71) Junsoo, K.; Guogao, Z.; Meixuanzi, S.; Zhigang, S. Fracture, Fatigue, and Friction of Polymers in Which Entanglements Greatly Outnumber Cross-Links. *Science* **2021**, *374* (6564), 212–216. https://doi.org/10.1126/science.abg6320.
(72) Gong, J. P.; Katsuyama, Y.; Kurokawa, T.; Osada, Y. Double-Network Hydrogels with Extremely High Mechanical Strength. *Advanced Materials* **2003**, *15* (14), 1155–1158. https://doi.org/10.1002/adma.200304907.
(73) Etienne, D.; Yulan, C.; Markus, B.; P., S. R.; Costantino, C. Toughening Elastomers with Sacrificial Bonds and Watching Them Break. *Science* **2014**, *344* (6180), 186–189. https://doi.org/10.1126/science.1248494.
(74) Lu, H.-F.; Wang, M.; Chen, X.-M.; Lin, B.-P.; Yang, H. Interpenetrating Liquid-Crystal Polyurethane/Polyacrylate Elastomer with Ultrastrong Mechanical Property. *Journal of the American Chemical Society* **2019**, *141* (36), 14364–14369. https://doi.org/10.1021/jacs.9b06757.
(75) Fan, W.; Wang, Y.; Cai, S. Fatigue Fracture of a Highly Stretchable Acrylic Elastomer. *Polymer Testing* **2017**, *61*, 373–377. https://doi.org/10.1016/j.polymertesting.2017.06.005.
(76) Gong, J. P. Why Are Double Network Hydrogels so Tough? *Soft Matter* **2010**, *6* (12), 2583–2590. https://doi.org/10.1039/B924290B.
(77) Reading, Mike.; Hourston, D. J. *Modulated Temperature Differential Scanning Calorimetry Theoretical and Practical Applications in Polymer Characterisation*; Hot Topics in Thermal Analysis and Calorimetry, 6; Springer Netherlands: Dordrecht, 2006. https://doi.org/10.1007/1-4020-3750-3.
(78) Traugutt, N. A.; Volpe, R. H.; Bollinger, M. S.; Saed, M. O.; Torbati, A. H.; Yu, K.; Dadivanyan, N.; Yakacki, C. M. Liquid-Crystal Order during Synthesis Affects Main-Chain Liquid-Crystal Elastomer Behavior. *Soft Matter* **2017**, *13* (39), 7013–7025. https://doi.org/10.1039/C7SM01405H.
(79) Cao, S.; Li, S.; Li, M.; Xu, L.; Ding, H.; Xia, J.; Zhang, M.; Huang, K. A Thermal Self-Healing Polyurethane Thermoset Based on Phenolic Urethane. *Polymer Journal* **2017**, *49* (11), 775–781. https://doi.org/10.1038/pj.2017.48.
(80) Król, P. Synthesis Methods, Chemical Structures and Phase Structures of Linear Polyurethanes. Properties and Applications of Linear Polyurethanes in Polyurethane Elastomers, Copolymers and Ionomers. *Progress in Materials Science* **2007**, *52* (6), 915–1015. https://doi.org/10.1016/j.pmatsci.2006.11.001.

(81) Webber, R. E.; Creton, C.; Brown, H. R.; Gong, J. P. Large Strain Hysteresis and Mullins Effect of Tough Double-Network Hydrogels. *Macromolecules* **2007**, *40* (8), 2919–2927. https://doi.org/10.1021/ma062924y.
(82) Eom, Y.; Kim, S.-M.; Lee, M.; Jeon, H.; Park, J.; Lee, E. S.; Hwang, S. Y.; Park, J.; Oh, D. X. Mechano-Responsive Hydrogen-Bonding Array of Thermoplastic Polyurethane Elastomer Captures Both Strength and Self-Healing. *Nature Communications* **2021**, *12* (1), 621. https://doi.org/10.1038/s41467-021-20931-z.
(83) Lin, Y.; Li, G. An Intermolecular Quadruple Hydrogen-Bonding Strategy to Fabricate Self-Healing and Highly Deformable Polyurethane Hydrogels. *Journal of Materials Chemistry B* **2014**, *2* (39), 6878–6885. https://doi.org/10.1039/C4TB00862F.
(84) Bai, R.; Yang, Q.; Tang, J.; Morelle, X. P.; Vlassak, J.; Suo, Z. Fatigue Fracture of Tough Hydrogels. *Extreme Mechanics Letters* **2017**, *15*, 91–96. https://doi.org/10.1016/j.eml.2017.07.002.
(85) Bai, R.; Yang, J.; Suo, Z. Fatigue of Hydrogels. *European Journal of Mechanics - A/Solids* **2019**, *74*, 337–370. https://doi.org/10.1016/j.euromechsol.2018.12.001.
(86) Zhang, W.; Hu, J.; Tang, J.; Wang, Z.; Wang, J.; Lu, T.; Suo, Z. Fracture Toughness and Fatigue Threshold of Tough Hydrogels. *ACS Macro Letters* **2019**, *8* (1), 17–23. https://doi.org/10.1021/acsmacrolett.8b00788.
(87) Bai, R.; Yang, J.; Morelle, X. P.; Yang, C.; Suo, Z. Fatigue Fracture of Self-Recovery Hydrogels. *ACS Macro Letters* **2018**, *7* (3), 312–317. https://doi.org/10.1021/acsmacrolett.8b00045.
(88) Lin, S.; Ni, J.; Zheng, D.; Zhao, X. Fracture and Fatigue of Ideal Polymer Networks. *Extreme Mechanics Letters* **2021**, *48*, 101399. https://doi.org/10.1016/j.eml.2021.101399.
(89) E., S. G.; P., M. X.; Jean, C.; Joshua, Y. C.; Matteo, C.; Costantino, C. Why Is Mechanical Fatigue Different from Toughness in Elastomers? The Role of Damage by Polymer Chain Scission. *Science Advances* **2021**, *7* (42), eabg9410. https://doi.org/10.1126/sciadv.abg9410.
(90) Wang, S.; Urban, M. W. Self-Healing Polymers. *Nature Reviews Materials* **2020**, *5* (8), 562–583. https://doi.org/10.1038/s41578-020-0202-4.
(91) *Fundamentals of Pressure Sensitivity*, 0 ed.; Benedek, I., Feldstein, M. M., Eds.; CRC Press, 2008.
(92) Creton, C. Pressure-Sensitive Adhesives: An Introductory Course. *MRS Bulletin* **2003**, *28* (6), 434–439. https://doi.org/10.1557/mrs2003.124.
(93) Pocius, A. V. The Chemistry and Physical Properties of Structural Adhesives. In *Adhesion and Adhesives Technology (Third Edition)*; Pocius, A. V., Ed.; Hanser, 2012; pp 219–258.
(94) Zentel, R.; Reckert, G. Liquid Crystalline Elastomers Based on Liquid Crystalline Side Group, Main Chain and Combined Polymers. *Die Makromolekulare Chemie* **1986**, *187* (8), 1915–1926. https://doi.org/10.1002/macp.1986.021870811.
(95) Küpfer, J.; Finkelmann, H. Nematic Liquid Single Crystal Elastomers. *Die Makromolekulare Chemie, Rapid Communications* **1991**, *12* (12), 717–726.
(96) Thomsen, D. L.; Keller, P.; Naciri, J.; Pink, R.; Jeon, H.; Shenoy, D.; Ratna, B. R. Liquid Crystal Elastomers with Mechanical Properties of a Muscle. *Macromolecules* **2001**, *34* (17), 5868–5875. https://doi.org/10.1021/ma001639q.
(97) Tajbakhsh, A. R.; Terentjev, E. M. Spontaneous Thermal Expansion of Nematic Elastomers. *The European Physical Journal E* **2001**, *6* (2), 181–188. https://doi.org/10.1007/s101890170020.

(98) Li, M.-H.; Keller, P. Artificial Muscles Based on Liquid Crystal Elastomers. *Philosophical Transactions of the Royal Society A: Mathematical, Physical and Engineering Sciences* **2006**, *364* (1847), 2763–2777. https://doi.org/10.1098/rsta.2006.1853.
(99) *Liquid Crystal Elastomers: Materials and Applications*; de Jeu, W. H., Ed.; Advances in Polymer Science; Springer Berlin Heidelberg: Berlin, Heidelberg, 2012; Vol. 250.
(100) White, T. J.; Broer, D. J. Programmable and Adaptive Mechanics with Liquid Crystal Polymer Networks and Elastomers. *Nature Mater* **2015**, *14* (11), 1087–1098. https://doi.org/10.1038/nmat4433.
(101) McCracken, J. M.; Donovan, B. R.; White, T. J. Materials as Machines. *Advanced Materials* **2020**, *32* (20), 1906564. https://doi.org/10.1002/adma.201906564.
(102) Fowler, H. E.; Rothemund, P.; Keplinger, C.; White, T. J. Liquid Crystal Elastomers with Enhanced Directional Actuation to Electric Fields. *Advanced Materials* **2021**, *33* (43), 2103806. https://doi.org/10.1002/adma.202103806.
(103) Annapooranan, R.; Wang, Y.; Cai, S. Harnessing Soft Elasticity of Liquid Crystal Elastomers to Achieve Low Voltage Driven Actuation. *Advanced Materials Technologies* **2023**, *8* (9), 2201969. https://doi.org/10.1002/admt.202201969.
(104) Warner, M.; Bladon, P.; Terentjev, E. "Soft Elasticity"—Deformation without Resistance in Liquid Crystal Elastomers. *Journal de Physique II* **1994**, *4* (1), 93–102.
(105) Clarke, S.; Terentjev, E.; Kundler, I.; Finkelmann, H. Texture Evolution during the Polydomain-Monodomain Transition in Nematic Elastomers. *Macromolecules* **1998**, *31* (15), 4862–4872.
(106) Tokumoto, H.; Zhou, H.; Takebe, A.; Kamitani, K.; Kojio, K.; Takahara, A.; Bhattacharya, K.; Urayama, K. Probing the In-Plane Liquid-like Behavior of Liquid Crystal Elastomers. *Science Advances* **2022**, *7* (25), eabe9495. https://doi.org/10.1126/sciadv.abe9495.
(107) Annapooranan, R.; Cai, S. Thermally Induced Self-Rupture of a Constrained Liquid Crystal Elastomer. *Engineering Fracture Mechanics* **2022**, *269*, 108584. https://doi.org/10.1016/j.engfracmech.2022.108584.
(108) Annapooranan, R.; Wang, Y.; Cai, S. Highly Durable and Tough Liquid Crystal Elastomers. *ACS Applied Materials & Interfaces* **2022**, *14* (1), 2006–2014. https://doi.org/10.1021/acsami.1c20707.
(109) Cui, J.; Drotlef, D.-M.; Larraza, I.; Fernández-Blázquez, J. P.; Boesel, L. F.; Ohm, C.; Mezger, M.; Zentel, R.; del Campo, A. Bioinspired Actuated Adhesive Patterns of Liquid Crystalline Elastomers. *Advanced Materials* **2012**, *24* (34), 4601–4604. https://doi.org/10.1002/adma.201200895.
(110) Farre-Kaga, H. J.; Saed, M. O.; Terentjev, E. M. Dynamic Pressure Sensitive Adhesion in Nematic Phase of Liquid Crystal Elastomers. *Advanced Functional Materials* **2022**, *32* (12), 2110190.
(111) Ohzono, T.; Norikane, Y.; Saed, M. O.; Terentjev, E. M. Light-Driven Dynamic Adhesion on Photosensitized Nematic Liquid Crystalline Elastomers. *ACS applied materials & interfaces* **2020**, *12* (28), 31992–31997.
(112) Ohzono, T.; Minamikawa, H.; Koyama, E.; Norikane, Y. Unlocking Entropic Elasticity of Nematic Elastomers Through Light and Dynamic Adhesion. *Advanced Materials Interfaces* **2021**, *8* (14), 2100672. https://doi.org/10.1002/admi.202100672.
(113) Ohzono, T.; Koyama, E. Enhanced Photocontrollable Dynamic Adhesion of Nematic Elastomers on Rough Surfaces. *Polymer* **2022**, *260*, 125377.

(114) Bartlett, M. D.; Case, S. W.; Kinloch, A. J.; Dillard, D. A. Peel Tests for Quantifying Adhesion and Toughness: A Review. *Progress in Materials Science* **2023**, 101086. https://doi.org/10.1016/j.pmatsci.2023.101086.
(115) Guo, H.; Saed, M. O.; Terentjev, E. M. Mechanism of Pressure-Sensitive Adhesion in Nematic Elastomers. *Macromolecules* **2023**, *56* (16), 6247–6255. https://doi.org/10.1021/acs.macromol.3c01038.
(116) Chopin, J.; Villey, R.; Yarusso, D.; Barthel, E.; Creton, C.; Ciccotti, M. Nonlinear Viscoelastic Modeling of Adhesive Failure for Polyacrylate Pressure-Sensitive Adhesives. *Macromolecules* **2018**, *51* (21), 8605–8610. https://doi.org/10.1021/acs.macromol.8b01374.
(117) Gent, A.; Petrich, R. Adhesion of Viscoelastic Materials to Rigid Substrates. *Proceedings of the Royal Society of London. A. Mathematical and Physical Sciences* **1969**, *310* (1502), 433–448.
(118) Chang, E. Viscoelastic Windows of Pressure-Sensitive Adhesives. *The Journal of Adhesion* **1991**, *34* (1–4), 189–200.
(119) Chang, E. P. Viscoelastic Properties of Pressure-Sensitive Adhesives. *The Journal of Adhesion* **1997**, *60* (1–4), 233–248.
(120) Cox, W.; Merz, E. Correlation of Dynamic and Steady Flow Viscosities. *Journal of Polymer Science* **1958**, *28* (118), 619–622.
(121) Lake, G. J.; Thomas, A. G. Strength; Gent, A. N. B. T.-E. with R., Ed.; Hanser, 2012; pp 119–158. https://doi.org/10.3139/9783446428713.005.
(122) Villey, R.; Creton, C.; Cortet, P.-P.; Dalbe, M.-J.; Jet, T.; Saintyves, B.; Santucci, S.; Vanel, L.; Yarusso, D. J.; Ciccotti, M. Rate-Dependent Elastic Hysteresis during the Peeling of Pressure Sensitive Adhesives. *Soft Matter* **2015**, *11* (17), 3480–3491.
(123) Derail, C.; Allal, A.; Marin, G.; Tordjeman, P. Relationship between Viscoelastic and Peeling Properties of Model Adhesives. Part 1. Cohesive Fracture. *The Journal of Adhesion* **1997**, *61* (1–4), 123–157.
(124) Yarusso, D. J. Quantifying the Relationship Between Peel and Rheology for Pressure Sensitive Adhesives. *The Journal of Adhesion* **1999**, *70* (3–4), 299–320. https://doi.org/10.1080/00218469908009561.
(125) Gower, M.; Shanks, R. Acrylic Acid Level and Adhesive Performance and Peel Master-curves of Acrylic Pressure-sensitive Adhesives. *Journal of Polymer Science Part B: Polymer Physics* **2006**, *44* (8), 1237–1252.
(126) Creton, C.; Leibler, L. How Does Tack Depend on Time of Contact and Contact Pressure? *Journal of Polymer Science Part B: Polymer Physics* **1996**, *34* (3), 545–554.
(127) Lee, J. H.; Lee, D. W. Contact-Induced Molecular Rearrangement of Acrylic Acid-Incorporated Pressure Sensitive Adhesives. *Applied Surface Science* **2020**, *500*, 144246.
(128) de Gennes, P.-G. Soft Adhesives. *Langmuir* **1996**, *12* (19), 4497–4500.
(129) Saulnier, F.; Ondarçuhu, T.; Aradian, A.; Raphaël, E. Adhesion between a Viscoelastic Material and a Solid Surface. *Macromolecules* **2004**, *37* (3), 1067–1075.
(130) Yamaguchi, T.; Creton, C.; Doi, M. Simple Model on Debonding of Soft Adhesives. *Soft matter* **2018**, *14* (30), 6206–6213.
(131) Bellamine, A.; Degrandi, E.; Gerst, M.; Stark, R.; Beyers, C.; Creton, C. Design of Nanostructured Waterborne Adhesives with Improved Shear Resistance. *Macromolecular Materials and Engineering* **2011**, *296* (1), 31–41.

(132) Degrandi-Contraires, E.; Lopez, A.; Reyes, Y.; Asua, J. M.; Creton, C. High-Shear-Strength Waterborne Polyurethane/Acrylic Soft Adhesives. *Macromolecular Materials and Engineering* **2013**, *298* (6), 612–623.
(133) Deplace, F.; Carelli, C.; Mariot, S.; Retsos, H.; Chateauminois, A.; Ouzineb, K.; Creton, C. Fine Tuning the Adhesive Properties of a Soft Nanostructured Adhesive with Rheological Measurements. *The Journal of Adhesion* **2009**, *85* (1), 18–54.
(134) Dalbe, M.-J.; Villey, R.; Ciccotti, M.; Santucci, S.; Cortet, P.-P.; Vanel, L. Inertial and Stick-Slip Regimes of Unstable Adhesive Tape Peeling. *Soft Matter* **2016**, *12* (20), 4537–4548. https://doi.org/10.1039/C6SM00119J.
(135) Verdier, C.; Ravilly, G. Peeling of Polydimethylsiloxane Adhesives: The Case of Adhesive Failure. *Journal of Polymer Science Part B: Polymer Physics* **2007**, *45* (16), 2113–2122. https://doi.org/10.1002/polb.21045.
(136) Kovalchick, C.; Molinari, A.; Ravichandran, G. Rate Dependent Adhesion Energy and Nonsteady Peeling of Inextensible Tapes. *Journal of Applied Mechanics* **2013**, *81* (4). https://doi.org/10.1115/1.4025273.
(137) Benyahia, L.; Verdier, C.; Piau, J.-M. The Mechanisms of Peeling of Uncross-Linked Pressure Sensitive Adhesives. *The Journal of Adhesion* **1997**, *62* (1–4), 45–73. https://doi.org/10.1080/00218469708014562.
(138) Kaelble, D. H. Peel Adhesion: Influence of Surface Energies and Adhesive Rheology. *The Journal of Adhesion* **1969**, *1* (2), 102–123. https://doi.org/10.1080/00218466908078882.
(139) Maugis, D.; Barquins, M. Fracture Mechanics and the Adherence of Viscoelastic Bodies. *Journal of Physics D: Applied Physics* **1978**, *11* (14), 1989.
(140) Villey, R.; Cortet, P.-P.; Creton, C.; Ciccotti, M. In-Situ Measurement of the Large Strain Response of the Fibrillar Debonding Region during the Steady Peeling of Pressure Sensitive Adhesives. *International Journal of Fracture* **2017**, *204* (2), 175–190. https://doi.org/10.1007/s10704-016-0171-1.
(141) Pandey, V.; Fleury, A.; Villey, R.; Creton, C.; Ciccotti, M. Linking Peel and Tack Performances of Pressure Sensitive Adhesives. *Soft Matter* **2020**, *16* (13), 3267–3275. https://doi.org/10.1039/C9SM02172H.
(142) Meitl, M. A.; Zhu, Z.-T.; Kumar, V.; Lee, K. J.; Feng, X.; Huang, Y. Y.; Adesida, I.; Nuzzo, R. G.; Rogers, J. A. Transfer Printing by Kinetic Control of Adhesion to an Elastomeric Stamp. *Nature Materials* **2006**, *5* (1), 33–38. https://doi.org/10.1038/nmat1532.
(143) Carlson, A.; Bowen, A. M.; Huang, Y.; Nuzzo, R. G.; Rogers, J. A. Transfer Printing Techniques for Materials Assembly and Micro/Nanodevice Fabrication. *Advanced Materials* **2012**, *24* (39), 5284–5318. https://doi.org/10.1002/adma.201201386.
(144) Li, Y.; Liu, T.; Ambrogi, V.; Rios, O.; Xia, M.; He, W.; Yang, Z. Liquid Crystalline Elastomers Based on Click Chemistry. *ACS Applied Materials & Interfaces* **2022**, *14* (13), 14842–14858.
(145) Saed, M. O.; Gablier, A.; Terentjev, E. M. Exchangeable Liquid Crystalline Elastomers and Their Applications. *Chem. Rev.* **2022**, *122* (5), 4927–4945. https://doi.org/10.1021/acs.chemrev.0c01057.
(146) Ohzono, T.; Minamikawa, H.; Koyama, E.; Norikane, Y. Impact of Crystallites in Nematic Elastomers on Dynamic Mechanical Properties and Adhesion. *Macromolecules* **2021**, *54* (19), 8987–8995. https://doi.org/10.1021/acs.macromol.1c01160.

(147) Xia, S.; Ponson, L.; Ravichandran, G.; Bhattacharya, K. Toughening and Asymmetry in Peeling of Heterogeneous Adhesives. *Physical review letters* **2012**, *108* (19), 196101.
(148) Chung, H. U.; Kim, B. H.; Lee, J. Y.; Lee, J.; Xie, Z.; Ibler, E. M.; Lee, K.; Banks, A.; Jeong, J. Y.; Kim, J.; Ogle, C.; Grande, D.; Yu, Y.; Jang, H.; Assem, P.; Ryu, D.; Kwak, J. W.; Namkoong, M.; Park, J. B.; Lee, Y.; Kim, D. H.; Ryu, A.; Jeong, J.; You, K.; Ji, B.; Liu, Z.; Huo, Q.; Feng, X.; Deng, Y.; Xu, Y.; Jang, K.-I.; Kim, J.; Zhang, Y.; Ghaffari, R.; Rand, C. M.; Schau, M.; Hamvas, A.; Weese-Mayer, D. E.; Huang, Y.; Lee, S. M.; Lee, C. H.; Shanbhag, N. R.; Paller, A. S.; Xu, S.; Rogers, J. A. Binodal, Wireless Epidermal Electronic Systems with in-Sensor Analytics for Neonatal Intensive Care. *Science* **2019**, *363* (6430), eaau0780. https://doi.org/10.1126/science.aau0780.
(149) Jinkins, K. R.; Li, S.; Arafa, H.; Jeong, H.; Lee, Y. J.; Wu, C.; Campisi, E.; Ni, X.; Cho, D.; Huang, Y.; Rogers, J. A. Thermally Switchable, Crystallizable Oil and Silicone Composite Adhesives for Skin-Interfaced Wearable Devices. *Science Advances 8* (23), eabo0537. https://doi.org/10.1126/sciadv.abo0537.
(150) Gao, Y.; Wu, K.; Suo, Z. Photodetachable Adhesion. *Advanced Materials* **2019**, *31* (6), 1806948.
(151) Abbott, S. *Adhesion Science: Principles and Practice*; DEStech Publications, Inc, 2015.
(152) Greenwood, J. A.; Williamson, J. P. Contact of Nominally Flat Surfaces. *Proceedings of the royal society of London. Series A. Mathematical and physical sciences* **1966**, *295* (1442), 300–319.
(153) Persson, B. N.; Albohr, O.; Tartaglino, U.; Volokitin, A.; Tosatti, E. On the Nature of Surface Roughness with Application to Contact Mechanics, Sealing, Rubber Friction and Adhesion. *Journal of physics: Condensed matter* **2004**, *17* (1), R1.
(154) Fuller, K.; Tabor, D. The Effect of Surface Roughness on the Adhesion of Elastic Solids. *Proceedings of the Royal Society of London. A. Mathematical and Physical Sciences* **1975**, *345* (1642), 327–342.
(155) Kendall, K. *Molecular Adhesion and Its Applications: The Sticky Universe*; Springer Science & Business Media, 2001.
(156) Persson, B. N.; Scaraggi, M. Theory of Adhesion: Role of Surface Roughness. *The Journal of chemical physics* **2014**, *141* (12).
(157) Pastewka, L.; Robbins, M. O. Contact between Rough Surfaces and a Criterion for Macroscopic Adhesion. *Proceedings of the National Academy of Sciences* **2014**, *111* (9), 3298–3303.
(158) Persson, B.; Albohr, O.; Creton, C.; Peveri, V. Contact Area between a Viscoelastic Solid and a Hard, Randomly Rough, Substrate. *The Journal of chemical physics* **2004**, *120* (18), 8779–8793.
(159) Tiwari, A.; Dorogin, L.; Bennett, A.; Schulze, K.; Sawyer, W.; Tahir, M.; Heinrich, G.; Persson, B. The Effect of Surface Roughness and Viscoelasticity on Rubber Adhesion. *Soft matter* **2017**, *13* (19), 3602–3621.
(160) Tiwari, A.; Wang, J.; Persson, B. Adhesion Paradox: Why Adhesion Is Usually Not Observed for Macroscopic Solids. *Physical Review E* **2020**, *102* (4), 042803.
(161) Arrington, K. J.; Radzinski, S. C.; Drummey, K. J.; Long, T. E.; Matson, J. B. Reversibly Cross-Linkable Bottlebrush Polymers as Pressure-Sensitive Adhesives. *ACS applied materials & interfaces* **2018**, *10* (31), 26662–26668.
(162) Kim, H.; Watkins, J. J.; Crosby, A. J. Adhesion and Mechanical Properties of Poly (Dimethylsiloxane) Bottlebrush Elastomers. *Soft Matter* **2023**, *19* (28), 5311–5317.

(163) Arzt, E.; Quan, H.; McMeeking, R. M.; Hensel, R. Functional Surface Microstructures Inspired by Nature–From Adhesion and Wetting Principles to Sustainable New Devices. *Progress in Materials Science* **2021**, *120*, 100823.
(164) Ina, M.; Cao, Z.; Vatankhah-Varnoosfaderani, M.; Everhart, M. H.; Daniel, W. F.; Dobrynin, A. V.; Sheiko, S. S. From Adhesion to Wetting: Contact Mechanics at the Surfaces of Super-Soft Brush-like Elastomers. *ACS Macro Letters* **2017**, *6* (8), 854–858.
(165) Shi, Y.; Wu, B.; Sun, S.; Wu, P. Peeling–Stiffening Self-Adhesive Ionogel with Superhigh Interfacial Toughness. *Advanced Materials* **2024**, *36* (11), 2310576.
(166) Linghu, C.; Liu, Y.; Tan, Y. Y.; Sing, J. H. M.; Tang, Y.; Zhou, A.; Wang, X.; Li, D.; Gao, H.; Hsia, K. J. Overcoming the Adhesion Paradox and Switchability Conflict on Rough Surfaces with Shape-Memory Polymers. *Proceedings of the National Academy of Sciences* **2023**, *120* (13), e2221049120.
(167) Annapooranan, R.; Wang, Y.; Cai, S. Harnessing Soft Elasticity of Liquid Crystal Elastomers to Achieve Low Voltage Driven Actuation. *Advanced Materials Technologies* **2023**, *n/a* (n/a), 2201969. https://doi.org/10.1002/admt.202201969.
(168) Qiguang, H.; Zhijian, W.; Yang, W.; Zijun, W.; Chenghai, L.; Raja, A.; Jian, Z.; Renkun, C.; Shengqiang, C. Electrospun Liquid Crystal Elastomer Microfiber Actuator. *Science Robotics* **2021**, *6* (57), eabi9704. https://doi.org/10.1126/scirobotics.abi9704.
(169) Annapooranan, R.; Suresh Jeyakumar, S.; J. Chambers, R.; Long, R.; Cai, S. Ultra Rate-Dependent Pressure Sensitive Adhesives Enabled by Soft Elasticity of Liquid Crystal Elastomers. *Advanced Functional Materials* **2024**, *34* (1), 2309123. https://doi.org/10.1002/adfm.202309123.
(170) Treloar, L. G. The Physics of Rubber Elasticity. **1975**.
(171) Roos, A.; Creton, C. Effect of the Presence of Diblock Copolymer on the Nonlinear Elastic and Viscoelastic Properties of Elastomeric Triblock Copolymers. *Macromolecules* **2005**, *38* (18), 7807–7818.
(172) Lopez, A.; Reyes, Y.; Degrandi-Contraires, E.; Canetta, E.; Creton, C.; Keddie, J. L.; Asua, J. M. Simultaneous Free-Radical and Addition Miniemulsion Polymerization: Effect of the Chain Transfer Agent on the Microstructure of Polyurethane-Acrylic Pressure-Sensitive Adhesives. *Macromolecular Materials and Engineering* **2013**, *298* (1), 53–66.
(173) Roos, A.; Creton, C.; Novikov, M. B.; Feldstein, M. M. Viscoelasticity and Tack of Poly (Vinyl Pyrrolidone)–Poly (Ethylene Glycol) Blends. *Journal of Polymer Science Part B: Polymer Physics* **2002**, *40* (20), 2395–2409.
(174) Tanguy, F.; Nicoli, M.; Lindner, A.; Creton, C. Quantitative Analysis of the Debonding Structure of Soft Adhesives. *The European Physical Journal E* **2014**, *37*, 1–12.
(175) Creton, C.; Hu, G.; Deplace, F.; Morgret, L.; Shull, K. R. Large-Strain Mechanical Behavior of Model Block Copolymer Adhesives. *Macromolecules* **2009**, *42* (20), 7605–7615.
(176) Deplace, F.; Rabjohns, M. A.; Yamaguchi, T.; Foster, A. B.; Carelli, C.; Lei, C.-H.; Ouzineb, K.; Keddie, J. L.; Lovell, P. A.; Creton, C. Deformation and Adhesion of a Periodic Soft–Soft Nanocomposite Designed with Structured Polymer Colloid Particles. *Soft Matter* **2009**, *5* (7), 1440–1447. https://doi.org/10.1039/B815292F.
(177) Degrandi-Contraires, E.; Udagama, R.; McKenna, T.; Bourgeat-Lami, E.; Plummer, C. J. G.; Creton, C. Influence of Composition on the Morphology of Polyurethane/Acrylic Latex Particles and Adhesive Films. *International Journal of Adhesion and Adhesives* **2014**, *50*, 176–182. https://doi.org/10.1016/j.ijadhadh.2014.01.025.

(178) Hui, C.; Lin, Y.; Baney, J. The Mechanics of Tack: Viscoelastic Contact on a Rough Surface. *Journal of Polymer Science Part B: Polymer Physics* **2000**, *38* (11), 1485–1495.
(179) Gay, C.; Leibler, L. Theory of Tackiness. *Physical review letters* **1999**, *82* (5), 936.
(180) Paiva, A.; Sheller, N.; Foster, M. D.; Crosby, A. J.; Shull, K. R. Microindentation and Nanoindentation Studies of Aging in Pressure-Sensitive Adhesives. *Macromolecules* **2001**, *34* (7), 2269–2276.